THE UNIVERSITY OF ALBERTA

RELEASE FORM

NAME OF AUTHOR   Ronald Goodson

TITLE OF THESIS   Precipitation Measurements From Satellites

DEGREE FOR WHICH THESIS WAS PRESENTED   Master of Science

YEAR THIS DEGREE GRANTED   Spring 1984

Permission is hereby granted to THE UNIVERSITY OF ALBERTA LIBRARY to reproduce single copies of this thesis and to lend or sell such copies for private, scholarly or scientific research purposes only.

The author reserves other publication rights, and neither the thesis nor extensive extracts from it may be printed or otherwise reproduced without the author's written permission.

THE UNIVERSITY OF ALBERTA

Precipitation Measurements From Satellites

by

Ronald Goodson

A THESIS

SUBMITTED TO THE FACULTY OF GRADUATE STUDIES AND RESEARCH

IN PARTIAL FULFILMENT OF THE REQUIREMENTS FOR THE DEGREE

OF Master of Science

IN

Meteorology

Department of Geography

EDMONTON, ALBERTA

Spring 1984

THE UNIVERSITY OF ALBERTA

FACULTY OF GRADUATE STUDIES AND RESEARCH

The undersigned certify that they have read, and recommend to the Faculty of Graduate Studies and Research, for acceptance, a thesis entitled Precipitation Measurements From Satellites submitted by Ronald Goodson in partial fulfilment of the requirements for the degree of Master in Meteorology.

Abstract

Data from the Automatic Picture Transmissions (APT) of the TIROS-N and NOAA-7 polar-orbiting satellites has been used to determine cloud-top temperatures and brightness for convective storms that produced heavy rain. The study is restricted to the period May to September 1979 and 1982 over Alberta and Saskatchewan.

As a storm passes over a point on the ground, the rain accumulation is a result of the combination of the cloud's speed, size of the rain area, and the rain rate. The results presented here suggest that rain accumulation is inversely proportional to temperature, due mainly to enhanced rain rates at lower temperatures or a greater temperature difference between the cloud top and the tropopause. No correlation was found between rainfall and brightness (other than a threshold value of brightness indicative of heavy rain), but this was not unexpected as the satellite-measured brightness was not corrected for sun or viewing angle.

Based on the above, a simple rain-estimation technique has been developed. This was tested against an independent data set of storms chosen only on the basis of their appearance on the infrared satellite imagery, without any knowledge of the associated precipitation. The scheme performed well for isolated convective storms. but gave poor results for more complicated situations such as merging cells, due mainly to the large amount of obscuring cirrus debris.

The technique presented here can be used as a simple "now-casting" tool for isolated storms and should serve well as the basis for a more complicated, and accurate, satellite-based, rain-estimation scheme.

Acknowldegments

Table of Contents

List of Tables

Table

xi

Page

List of Figures

1. Review and Preview

1.1 Introduction

Rainfall is vital to sustain life but too much too quickly can bring floods, destruction and death. Precipitation measurements are therefore important for a number of endeavors which affect the well-being of mankind. Some of these, discussed by Barrett and Martin (1981) in their book "The Use of Satellite Data in Rainfall Monitoring" include: rainfall inventories, moisture budgets, water resource monitoring, river monitoring and control, flash flood warnings, pest and plague control and crop growth programs. Unfortunately, the distribution of rainfall is often not well known due to a combination of its large fluctuations over short intervals of space and time and a deficient observing network.

There are currently three methods by which rainfall is measured. Most simply, rain is collected in a graduated cylinder or bucket, although the design of the bucket may be quite sophisticated. These devices (known as rain gauges) are often placed hundreds of kilometers apart and inspected only once per day, so that small scale variations of rainfall are poorly represented. Near-continuous monitoring of rainfall, in both space and time, is possible with the use of radars capable of detecting precipitation-sized water drops. However, only a relatively small area can be covered in this way and, as radars are expensive, they are usually located only near population centres. Much effort has therefore been directed in recent years to the devising of schemes whereby rain amounts can be deduced from satellite imagery of the infared and visible energy from cloud tops. Satellites offer the advantage of repeatedly viewing large areas in a relatively short period of time (ranging from five minutes to several days). Considerable success has been achieved estimating precipitation from convective storms. Synoptic-scale rainfall has proved more troublesome, however work in this area continues to progress. An excellent review of techniques for inferring rain from satellite images is given in Barrett and Martin's 1981 book. Accordingly, only the highlights are presented here.

1.2 Review

1.2.1 Basic Relationships

The first investigators to relate satellite measured cloud top brightness to precipitation were Whitney and Fritz (1961). They were able to show that a small, isolated, bright cloud seen on a TIROS-I image was related to precipitation on the ground and reasoned that brightness was indicative of heavy convective activity. The major conclusion over the next 10 years of study was that the brightest convective clouds were the most likely to contain precipitation (Woodley and Sancho, 1971). However, while strong radar echoes are associated with bright clouds, the reverse is not always true, and the echo area is often much less than the cloud area (Martin and Suomi, 1972).

Cloud-top temperatures can be evaluated by measuring their infrared radiance and assuming black body radiation. Lethbridge (1967), for late spring, found that the probability of precipitation within 3 hours after the passage of a cloud increased with decreasing cloud-top temperature but was only 50% for temperatures less than -24°C. More importantly, this study marked the first time that temperature and brightness measurements were combined, which improved results considerably. The 3-hour probabilty of rain was only 5% for warm, dark clouds, but rose to 75% for cold, bright clouds. It was concluded that brightness was important, as it distinguished between thin and thick clouds for low temperatures. A cumulonimbus cell (Cb) could, therefore, be identified on a satellite photograph as a cold, bright cloud.

Cumulonimbus clouds can also be identified by their explosive growth, seen on a sequence of satellite images as a rapid increase in the anvil area. Rain-estimation techniques which employ this time element are called "life-history" methods by Barrett and Martin.

1.2.2 Life History Methods

The simplest life-history method is that of Stout et al. (1979). Volumetric rain rate is correlated to cloud area and its rate of expansion, cloud area being defined as the area enclosed by the 245°K (-28°C) or 200W/m² temperature and brightness contours respectively. Coefficents to convert cloud area and its rate of change to rain rates are

determined from correlation to radar-derived rain rates. In a test over the southern Atlantic, the correlation between radar and satellite estimates of one hour rain amounts was 0.84.

Griffith and Woodley developed a similar technique (described in Griffith et al., 1978) except that rain intensity is also taken to be a function of the Cb's stage of development. Cloud areas are tracked, classified as being in their growing or shrinking stage and correlated to echo area. As radar echoes can be used to infer rain rates, a relation can be established between cloud area and rainfall. A different relation exists for the growing and shrinking phase, with more rain inferred while the cloud is growing. Also, the amount of predicted rain is distributed through the cloud depending on temperature, with most of the rain assigned to the coldest areas. The correlation coefficients for satellite-estimated to gauge-rain amounts over Florida were as high as 0.80 for one hour amounts and 0.93 for 6-9 hour amounts. When applied to convective storms over the High Plains States (Griffith et al., 1981) rain estimates had to be adjusted downward to account for the lower precipitable water content of the air, but otherwise the technique worked well. In their 1981 paper, four empirical relationships were outlined:

1. "Rain clouds are those which are as cold or colder than $-20^{\circ}C$.

2. Rainfall is directly proportional to cloud area on any given picture.

3. Rainfall is inversely proportional to cloud-top temperature.

4. Rainfall is a function of cloud life cycle, that is, more rain is inferred in the early stages of a cloud's history than in the later stages."

Augustine et al. (1981) evaluated the Griffith and Woodley technique over southern Florida and found that the correlation of satellite versus gauge rain amounts varied drastically for changes in study area and duration. For example, the correlation coefficient for an area of 500 km^2 and one hour was only 0.2, while the maximum correlation of 0.9 was obtained for 9350 km^2 and 6 hours.

Scofield and Oliver (1977) devised a method by which rainfall estimates could be made directly from half-hourly GOES satellite images. Cloud-top temperature is used to determine base 30-minute rain rates. Enhanced rain fall is assigned to clouds according to features seen on the satellite photographs, such as: rapidly expanding anvils, merging

clouds, merging cloud lines and "overshooting tops", ie. tops of cells that appear highly textured on the visible image and which have likely penetrated the tropopause. This technique was developed to assist in the estimation of rain amounts associated with extreme weather events. It has been succesfully applied to storms which caused flash floods over eastern United States (Schneider and Scofield, 1980; Scofield, 1981). However, similar to the Griffith and Woodley method, additional factors needed to be introduced when the technique was applied to different geographical regions. For example, a precipitable water factor was required so that rain amounts over the Plain States would not be over-estimated. The opposite problem was encountered over the southern states where slow-moving, steady-state storms gave more rain than expected (Scofield and Oliver, 1980).

1.2.3 Bi-Spectral Methods

Lovejoy and Austin (1979a) introduced a bi-spectral method, that is, one which combines infrared and visible-range information. Satellite-measured cloud-top brightness and temperature values are assigned to grid points at which the occurrence of rain or no-rain is deduced from radar data. Threshold values of temperature and brightness are then used to infer rain or no-rain, and varied in order to minimize a "loss function" involving the incorrect inferences of:

1.   no rain assigned, rain observed, and

2.   rain assigned, no rain observed.

In this manner optimum values of temperature and brightness which lead to the best estimate of rain areas are determined.

The next step taken by Lovejoy and Austin (1979b) was to estimate rain amounts. They found that rain areas were highly correlated to rain amounts, but weakly correlated to rain rates. An average rain rate (as determined by radar) was used to estimate rain amounts for convective storms over Montreal and the Global Atmospheric Research Programme (GARP) - Atlantic Tropical Experiment (GATE) area. The RMS difference between radar and satellite-inferred one-hour amounts were 40% and 20% respectively. Using a single image and a single rain rate, it was estimated that the RMS difference for one hour convective rain amounts over Montreal would be 49% for satellite versus gauge.

It was concluded that the most revealing information concerning rain amount is contained in the area of cloud cover, and that a single image provides little information on rain intensity. As noted by Barrett and Martin, this runs counter to the claims of the Griffith and Woodley or Scofield and Oliver technique.

1.2.4 Other Work

Wiley and Laitsch (1983) investigated the effect of varying the amount of satellite data on the accuracy of rain estimates. Rain accumulations were estimated for the month of August 1979, over the Great Plains, using various frequencies of the number of satellite pictures per day (ranging from 2 to 24). Rain rates of 2.5mm/6hr were assigned to cloud areas deemed to be raining by a meteorologist, with additional rainfall ascribed to storms that appeared more intense. It was found that the correlation of monthly rain amounts for satellite versus gauge was 0.51 for 2 pictures/day and 0.59 for 24 pictures/day.

Adler and Fenn (1979) used the rate of change of cloud-top temperature (dT/dt), measured at 5 minute intervals, to infer updraft velocities. They showed that larger updrafts are associated with more severe storms. In 1981, Negri and Adler presented examples which showed that the clouds with the coldest tops (Tmin) had both the highest radar reflectivity and rainfall rate. They concluded that dT/dt and Tmin were correlated to precipitation rate for well-defined Cb's, as seen on satellite imagery. Adler et al. (1981) presented a physical model that related rain rate to Tmin, along with supporting case-studies. Using much of the information contained in the above work, Adler and Markus (1983) introduced an index, based on rate of change of cloud area and temperature, that could be used to predict severe weather. In hind-casting examples, tornadic outbreaks could be predicted as much as 30 minutes in advance.

Temperature structure, rather than absolute values, may also be used to infer severe weather. Recent work (see Hymsfield et al., 1983, for example) has shown that a "V" shaped structure is often associated with severe weather, and indicative of a storm that has penetrated well into the stratosphere.

1.2.5 Physical Relationships

The rain-estimation techniques described above give only empirical relationships. The underlying physical basis is that a cold, bright cloud implies a thick cloud, and that the probability and intensity of precipitation increases as thickness increases. That precipitation is related to cloud thickness is well known. Rain is usually present in clouds thicker than 3,000 meters or those with temperatures below -10°C to -20°C, and rarely falls from clouds less than 700 metres thick. It is necessary, then, to relate temperature and brightness to thickness. Temperature is considered first.

Absorption (and re-emittance) of infrared radiation in the 8 to 12 μm range is strong for liquid water drops but weak for water vapour. The cloud top is, therefore, assumed to be a black body so that its radiation is proportional to the fourth power of temperature. Measurements from space can then be used to determine the cloud-top radiation temperature which is usually equated to the actual cloud-top temperature. From knowledge of the atmospheric lapse rate, the height of the cloud top can be calculated. For thin clouds, the radiation measured by the satellite's radiometer is a result of some layer through the cloud (or possibly even some radiation from the ground) so that the radiation temperature is higher than the actual temperature. However, in these cases the clouds are usually so thin that precipitation is highly unlikely. More difficult, and of more concern here, is the problem of differentiating between a precipitating deep convective cell and its associated cirrus anvil, both of which may be radiometrically thick and therefore have the same cloud-top temperature. This can sometimes be done using brightness in conjuction with temperature. There is little doubt, however, that the occurrence of precipitation can be correlated to cloud-top temperatures. This is the principal hypothesis on which are built many of the rain-estimation techniques described above.

The interpretation of brightness measurements is much more difficult than that for temperature and only a brief over-view is given here. The following discussion is taken from Chapter 7 in Barrett and Martin (1981).

Studies have shown that brightness is highly correlated to thickness, especially for stratus clouds over water. However, clouds become optically thick at approximately 1km, so the association weakens as depth increases. Brightness from various cloud

shapes have been modelled, such as infinite planes, cubes or cuboids, and towers rising out of slabs. As well as thickness, the width of the cloud is very important. Reflectance from the top of a cube is only one-half that of a plane, but increases as width increases. This suggests that the observed increase in brightness of a growing Cb is caused mainly by the increase in width. Unexpectedly, turrets act to decrease brightness, as viewed from above. The fractional light reflected from the top decreases, but is compensated by an increase in radiation from the sides of the turret.

Generally, brightness decreases as the angle of illumination increases (using 0^c as overhead illumination). However, the rate of decrease depends upon the cloud's optical depth and shape. Also, the brightness, as measured by the satellite's radiometer (radiance), depends upon the angle of view. Radiance may increase when the satellite is in the anti-solar direction and the angle of illumination is small.

At any time, then, the brightness depends on a combination of cloud thickness and geometry, angle of illumination and angle of view.

1.3 Purpose of Present Study

Rain estimation from satellite data for the Prairie Provinces is in its infancy. The only investigation to date was that of Wieler (1981) who, based on comparison with radar data, determined threshold values of temperature and brightness (-50°C, 145) that would delineate areas of heavy rain. As this study represents only the first small steps, the present goals are rather modest. They are: to determine whether precipitation amounts or intensities from convective storms are correlated to cloud-top temperature and brightness and, if so, is the relationship strong enough to become the basis of a rain-estimation technique.

To this end, storms which gave heavy rainfall (>10mm) over Alberta and Saskatchewan have been investigated. Cloud-top temperatures and brightness were obtained from measurements made by the radiometer on-board the TIROS-N and NOAA-7 polar-orbiting satellites and recorded at the University of Alberta satellite receiving station. Data are recorded for two "passes" per day when the satellite is over Western Canada. Passes are separated by about 100 minutes. Rain data consist of amounts and intensities supplied by the surface observation network of the Atmospheric Environment Service of

Canada (AES).

Except on a few rare occasions, radar data have not been employed. As this is a preliminary investigation, it was thought preferable to keep the analysis of data as simple as possible. Also, the study is designed so that case-studies can be quickly and easily added at some future date. Radar data do not allow either of the above. Firstly, the conversion from radar echoes to rain accumulation maps is very time consuming-almost an order of magnitude greater than real time at its worst. Secondly, the rain amounts are given only in large ranges (eg 10-25mm) too coarse for use here. Admittedly, this difficulty can be overcome, but the data and computer programs are owned by the Alberta Research Council, and changes to programs are not always feasible. In fact, at the time this report was written, the rain-accumulation program was not completely operational. Also, the radar data would have to be re-mapped onto the satellite image (or vice-versa) and this is not a trivial task. Finally, and most important, an empirical relationship is used to convert radar echoes to rainfall, and the conversion is not necessarily adequate under all conditions. The consideration of all possible errors in the radar-derived rain amounts is beyond the scope of the present study.

However, it is undeniable that the inclusion of radar data would be highly desirable, and is the next logical step to take. As will be seen, some problems were encountered which would not have occurred had radar data been used. Since the number of ground observing sites is quite small, the sample size is also small. Moreover, confusion can arise if the time of the satellite pass is much different than the time rain was observed. As always, when simplifications are made, some compromises are inevitable.

Chapter 2 presents a description of the satellite and its radiometer. The method by which storms were selected and analyzed is given in chapter 3, followed by a discussion of each storm in chapter 4. This information is used to construct the rain-estimation scheme presented in chapter 5. The application of this scheme to infer rain amounts from satellite images is given in chapter 6. Finally, conclusions and suggested future work is discussed in chapter 7.

2. The Satellite

2.1 Orbit and Sensors

2.1.1 Description

Cloud-top temperature and brightness was obtained from the Automatic Picture Transmissions (APT) data recorded at the University of Alberta from the TIROS-N and NOAA-7 polar orbiting satellites. Both satellites are part of the TIROS series and differ only in the calibration constants required to convert radiance to temperature (as will be discussed shortly). A complete discussion of the satellite and its components is given by Schwalb (1978). Consequently, only a brief description is given here.

The satellite is placed in a sun-synchronous orbit at an altitude of approximately 865 km. Sun synchronous means that the satellite passes over any given latitude at the same solar time each day. The orbital parameters are given in figure 2.1 which also displays a typical path of the satellite. The Earth is viewed by an on-board scanning radiometer, known as a Advanced Very High Resolution Radiometer (AVHRR), by means of a mirror rotating at 360 RPM perpendicular to the satellite's path. Data is obtained across the entire horizon but retained only for 55^0 on either side of the mirror's nadir. Beyond this range, limb darkening and foreshortening limit the usefulness of the data. This coverage corresponds to 2997 km on the ground at the equator and extends to approximately 55^0 of latitude at 50^0 north. As the satellite regresses 25^0 per orbit, there is a large amount of overlap between two successive images. In this manner, Alberta is in the satellite's field of view for at least two passes in the afternoon. As the mirror scans the Earth data are collected at the rate of 66.5K words per second. However, of this, only every third scan line and only two of five frequency bands (one visible and one infrared) are fed to the APT transmitter. Furthermore, the data along a scan line are averaged to give a near constant resolution of 4km. As only every third scan line is sent, the between-line resolution is:

$$(6368 \text{ Km})(2\pi)/(102 \text{ min})(120 \text{ scans min}^{-1}) = 3.3 \text{ Km}$$

PM ASCENDING NODE ORBIT
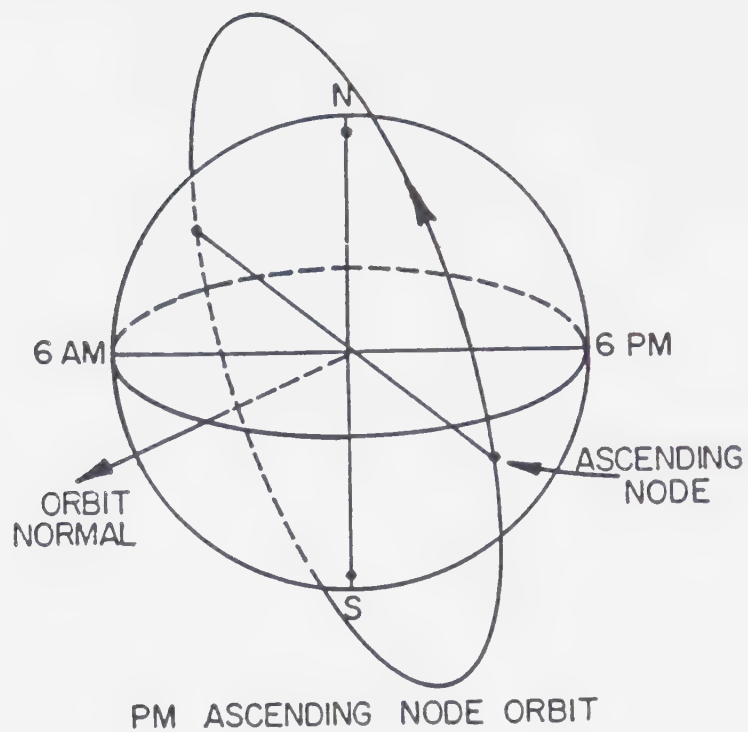
Orbital Period	102 minutes
Regression	25.5°/orbit west
Inclination Angle	99°
Height Above Ground	865 km

Figure 2.1   Orbital parameters for the Tiros-N and NOAA-7 satellites.

The APT signal is amplitude modulated at an equivalent digital rate of 4160 words/sec (or 2080 words/line at 2 lines/sec). The information consists of 909 words each of visible and infrared data with the remaining 262 word consisting of synchronization pulses and calibration data. This is digitized at the University of Alberta at 3200 Hz (1600 words/line) so that the 909 words are "squeezed" into only 700 words. This reduces the 4km resolution along a scan line to 5.2 km. However, the distance between these "new" pixels is only 4.2km. Consequently, some information is smeared from one pixel to the next.

The infrared and visible radiation measured by the radiometer are represented by digital counts between 0-255. High counts correspond to high reflectivity and low temperature for the visible and infrared bands respectively. Using calibration data from the radiometer and the fact that the radiometer output (in digital counts) is very close to linear makes it possible to construct a calibration curve which converts counts, as recorded by a ground receiving station, to temperature. Brightness counts can be converted to reflectance values measured in watts/m^2. However, as outlined in section 1.2.5, the interpretation of these values is more difficult than for the infrared. As no attempt was made to normalize the brightness for angle of illumination or viewing angle, the values were left as digital counts.

2.1.2 Calibration of Infrared Data

Calibration data are sent from the satellite with each scan line. There are 16 pieces of calibration data, each repeated over 8 lines, so that a total of 128 lines are needed to receive all the information. This is known as a telemetry frame, as is shown in figure 2.2. Of these, only boxes 1-13 and 15 are of concern here.

The first 9 boxes consist of "wedge" values. Each wedge is assigned a known digital count before the satellite is launched. By comparing digital wedge values received on the ground to the expected values, it is possible to relate ground-received digital counts for cloud temperature and brightness to satellite measured counts. The two can differ slightly because of the digital-to-analogue and back to digital conversion of the APT signal. Boxes 10-13 are digital counts from the radiometer viewing four platinum resistance thermometers (PRTs) embedded in its housing, which is designed to be a black
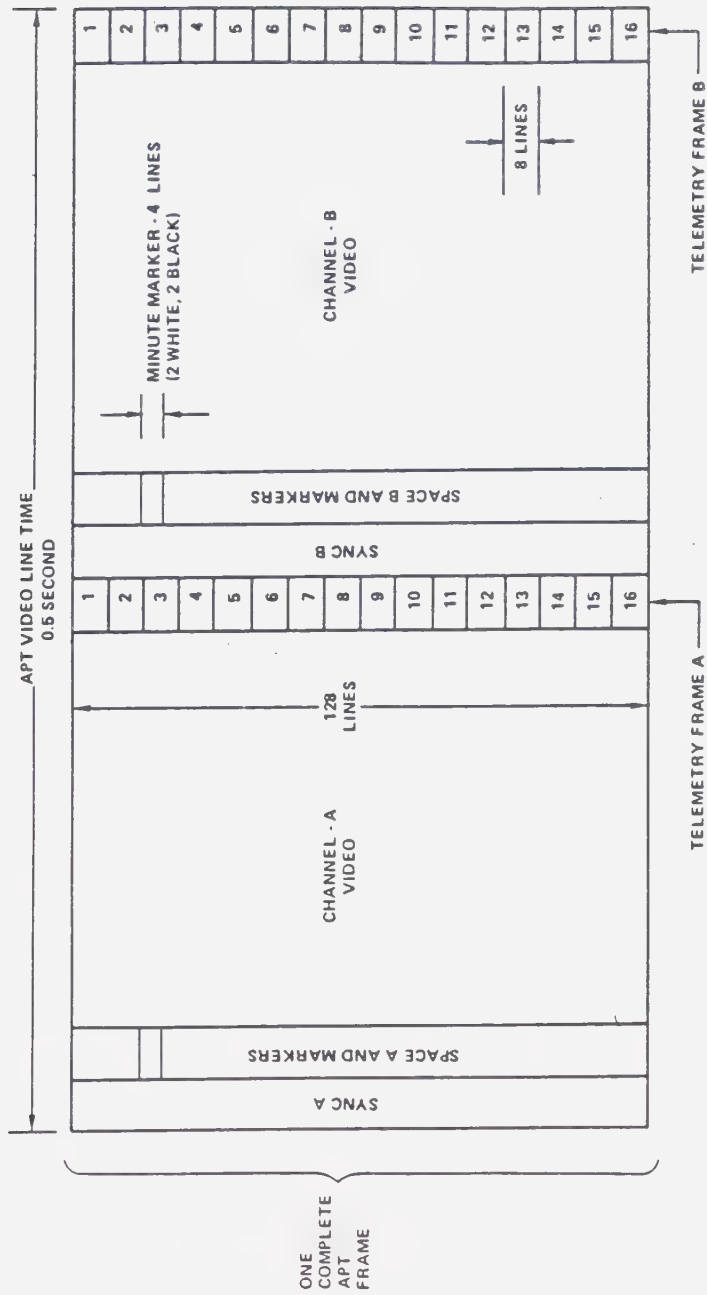
Figure 2.2   Data stream from satellites.   See text for
explanation of telemetry frame.
(from Schwalb, 1978)

body. Box 15 contains counts for the sensor viewing outer space. To obtain a relationship between received digital counts and temperature (for the infrared information, of course) the following procedure is employed:

1.   A relationship is obtained between known wedge values and received wedge values, using a curve-fitting routine from the Interactive Michigan Statistical Library (IMSL) computer package.

2.   Using the curve established above, PRT received counts are converted to satellite counts.

3.   Using expressions given by Lauritson et al. (1979) and listed in appendix A, satellite PRT counts are converted to temperature. The four temperature estimates are then averaged.

4.   The black-body radiation associated with the above temperature is calculated using an approximation of the integral of the Planck function and the spectral response of the radiometer (see appendix A). This gives one point for the radiance versus digital count calibration curve.

5.   The above point and the counts associated with the radiance of space (box 15) are used to construct a straight line graph relating radiance to digital counts. As the response of the radiometer is not exactly linear, a small correction is applied (see Appendix A).

6.   Radiance values for each temperature, in $2^{\circ}C$ increments from $27^{\circ}C$ to $-73^{\circ}C$, are then calculated using the same routine as in step 4.

7.   Combining (5) and (6), a curve of temperature versus satellite digital counts is constructed.

8.   Using curves from (1) and (7), a calibration curve of temperature versus received digital counts is made.

9.   Finally, received digital counts are converted to temperature, using the curve established above and interpolating as necessary between the $2^{\circ}C$-interval temperature values.

2.1.3 Accuracy of Temperature Calibration

Two different satellites, both of the TIROS series, are used in this study, each having its own calibration curve. These curves, derived as in step (8) above, and averaged over 12 passes for NOAA-7, and 18 passes for TIROS-N, are given in Table 2.1. The uncertainty quoted is ±1 standard deviation and is seen to be of order one 1 count. This suggests an uncertainty of ±1 count in the digitizing process. Using this, columns 3 and 5 of Table 2.1 give the uncertainty in temperature, which ranges from 2-3°C at low temperatures to 0.5° at high temperatures. It is still necessary, however, to compute a separate calibration curve for each orbit. Variations of up to 10°C, for a given count, are possible from one pass to the next.

There are other factors which can contribute to uncertainties in the temperature. Even with the non-linearity correction introduced in step (5) above, errors of +1°C at 300°K (22°C) and -1°K at 200°K (-73°C) can still occur (Lauritson et al., 1979). The sign of the error is for actual temperature minus derived temperature.

Errors can also be introduced if clouds are thin, in which case the radiation received by the satellite is from some other layer of the atmosphere, and not from the cloud top itself. The derived temperature would be an average temperature through the layer. As mentioned in section 1.2.5 this should not be a problem here, as thin clouds will likely not be precipitating. A similar condition may exist in a moist, but cloud-free atmosphere. Here, some radiation is emitted by the atmosphere as well as the Earth's surface. The derived surface temperature will therefore be less than the true temperature. As noted by Wieler (1981), Curtis and Rao (1969) estimate that, in the Tropics, the magnitude of this effect can be as large as 4°C. As the atmosphere in Alberta is drier than that of the Tropics a realistic estimate of the error would be approximately 2°C. Again, this is not of great importance here, as cloud-free areas are of little interest in the present work.

Combining the various errors, then, the uncertainty in cloud-top temperatures is likely to be ±3 - 3.5°K.

Table 2.1   Temperature Calibration Curves for NOAA-7 and TIROS-N

Temperature (°K)	NOAA-7 (average of 12 passes)		TIROS-N (average of 18 passes)	
	Digital Counts	Uncertainty* of Temperature	Digital Counts	Uncertainty* of Temperature
200	233.4+0.6	2.1	237.6+0.7	2.6
210	227.4+0.6	1.7	233.0+0.8	2.2
220	219.7+0.6	1.3	227.3+0.9	1.8
230	210.2+0.7	0.9	220.3+1.0	1.4
240	198.5+0.8	0.9	211.7+1.1	1.2
250	184.3+0.9	0.7	201.3+1.2	1.0
260	167.8+1.1	0.6	188.6+1.3	0.8
270	149.6+1.0	0.6	174.0+1.3	0.7
280	129.8+0.5	0.5	157.8+1.3	0.6
290	107.8+0.5	0.5	139.8+1.2	0.6
300	82.7+0.9	0.4	119.9+0.5	0.5

*   assuming ± 1 digital count

2.2 Gridding of Images

2.2.1 Resolution of Image

As mentioned previously, the resolution between and within scan lines is 3.3km by 5.2km respectively. The smallest area of information, or pixel, represents an area of approximately 17 km^2. By comparison, resolution at the satellite subpoint before processing for APT transmission is 1.1km by 0.8km. The area of a small cumulonibus cell may be less than 50 km^2 or only 3 pixels on the APT image. Clouds of this size are too small for the temperature and brightness structure to be properly resolved on the APT images. For such cases, where possible, images with full resolution from the High Resolution Picture Transmissions (HRPT) of satellite have been obtained from AES. These pictures contain a grey scale enhancement curve so that the temperature of any pixel can be determined within a certain temperature range. While this does not allow accurate interpretation of the temperature, comparison to the APT derived value will give some indication if the resolution is deficient. This is discussed in greater detail in chapter 3.

2.2.2 Gridding Accuracy

In order to relate satellite measurements to rainfall observed on the ground, it is necessary to locate the position of the rain gauge on the satellite image. This requires transforming from a coordinate system described by latitude and longtitude to one defined by a scan line number and position along that scan, a procedure which will be called "gridding" here. The equations to perform this task are given in great detail by Reinelt et al (1975). A summary of the essential equations can be found in Greaves (1981) or Wieler (1981) and are repeated here in appendix B. The input required for the equations are the orbital parameters given in Figure 2.1 plus the time and longtitude at which the satellite last crossed the equator. Basically, the gridding procedure is as follows. The time of acquisition of the satellite's signal is recorded and subtracted from the time the satellite last crossed the equator. Using the satellite's orbital period and regression rate, it is then possible to determine the satellite's position at the time of signal acquisition. The same orbital parameters, along with the scan rate (120 scans/min) can then be used to calculate the position of any pixel or, as done here, to transform from a

latitude-longtitude position to one described by the number of the scan lines after acquisition of signal, and the position along that line.

For each satellite pass, "grid marks" are applied directly onto the satellite image at calculated latitude-longtitude intersections. The positional accuracy of these marks is determined by comparing the satellite image to an overlay of prominent landmarks (e.g. large lakes) and the known position of latitude-longtitude intersections. The overlay is superimposed on the satellite picture and adjusted so that landmarks visible on the satellite picture are aligned with those on the overlay. The gridding is accurate if the grid marks are co-located with the latitude/longtitude intersections. If not, the gridding is in error and can be corrected, based on the magnitude and direction of mis-alignment of the grid marks. After correcting for any error, the position of the rain gauge on the satellite image can be calculated. When the gridding is poor, the usual reason is uncertainty in the time of equator crossing which has been in error as much as 10 seconds (20 scan lines). The error normally varies slowly from day-to-day, so rather than applying a large correction each day, an approximate correction is applied to the equator crossing time before gridding is preformed, and updated as necessary. The amount and need for updating is determined from a daily check of the gridding accuracy as described above. It is fortunate that timing errors vary only slowly, for when no land marks are visible it is impossible to check the accuracy of the grid marks.

The time of satellite equator crossing is, at best, accurate to only the nearest second so that the corresponding uncertainty in distance is:

$$\frac{(\pm 0.5 \text{ sec})(2\pi)(6368 \text{ Km})}{(102 \text{ min})(60 \text{ sec/min})} = 3.3 \text{ Km}$$

This is, of course, the distance between scan lines. However, an informal survey of lab technicians who perform the gridding operation on a regular basis revealed that the smallest discernable shift between grid marks and the overlay latitude-longtitude intersections is two scan lines, corresponding to a distance of 1.4mm on the satellite images produced at the University of Alberta. A shift of one scan-line is undetectable, while a three-line shift is quite noticable. Even so, it is difficult to maintain an accuracy of two scan lines across the entire picture. A good match in one area might be made at the

expense of a poor match elsewhere. An uncertainty of ±3 scan lines (10km) in gridding has therefore been adopted. Strictly, this uncertainty should prevail only in a direction perpendicular to the scan line. Errors in equator crossing time do not affect the position along a scan line. While uncertainties in this direction can be incurred due to errors in the longtitude of satellite equator crossing, they are generally quite small and result in an error less than the distance between pixels. However, for the sake of simplicity, the uncertainty in the position of the rain gauge is assumed to be described by a circle of radius 10km.

Finally, in order to deduce cloud motion, two sequential images must be overlaid This can be done using landmarks or the grid marks as a guide. However, due to the rotation of the Earth beneath the satellite and the Earth s curvature. the latitude-longtitude intersections do not form right angles. This produces a distortion across the image so that it is not possible to overlay two images with complete accuracy. If the area of interest is small, then the error is usually less than 10km. However, if the area is large. uncertainties of 30km are possible. This is of crucial concern when trying to map possible rain areas along the path of a convective cell, as will be seen in Chapter 6.

3. Selection and Analyses of Data

3.1 Introduction

As was stated at the outset, the objective of this study is to correlate precipitation, as measured on the ground, with satellite-observed cloud-top temperature and brightness of a convective storm. In this chapter the criteria by which case studies were selected, sources of data and their limitations, as well as the method used to analyze the data are discussed.

3.2 Selection of Sample

3.2.1 Required Rain Amounts

Case-studies were selected on the basis of observed point rainfall, the only discriminator being a lower limit on the hourly amount that must be exceeded. A rather high limit was chosen for a variety of reasons. A small amount of rain could be due to either a weak convective cell passing directly overhead or the result of a more intense storm that just grazes the observing site. As large rainfalls are relatively uncommon, when they are observed it is more likely that the cell passed directly overhead and the observed rain amounts are representative of the storm's maximum output. Also, storms which produce large rainfalls are of great general interest as they can, in extreme cases, cause local flooding or crop damage. Often, a single storm can contribute over 25% of the total monthly rainfall at a given location. Finally, if too low a limit is placed on the rain amount, the sample size becomes unreasonably large. AES, for the purposes of weather reporting, defines heavy rain as a rain rate of > 7.5mm/hr. This, of course, refers to rain intensity. There are no guidelines as to what accumulation constitues a "large" amount so, somewhat arbitrarily, 10mm has been adopted here. There is no objective basis for this choice. However, amounts of 5mm or less are fairly common and may pass without notice, while 20mm within an hour is a rare event and generally receives considerable attention.

The requirement for a storm to be included in the sample, then, was a report of > 10mm of rain in one hour or less. A further requirement was that the rain must have

occurred within one hour of the satellite pass.

3.2.2 Area of Study

It is desirable to confine the study area to regions which fall under the same weather regime and climatic controls. Precipitation amounts may be dependent on geographical location without being reflected in the cloud-top temperature or brightness. An example is the lower rainfall over the Plain States as compared to the eastern United States due to the lower water vapour content of the air. Relatively uncomplicated topography is also required. Mountains and valleys contribute to mechanisms which can result in great variations of local weather and precipitation patterns over small distances.

The above conditions refer to the need for the study area to be homogeneous. As the area becomes large, there is a greater risk that some unknown variable will affect precipitation amounts. Homogeneity is of great importance, but, from a practical viewpoint, if the area is made too small then the sample becomes too small to be of any value. This is especially true here, as there are only a few observation sites distributed over a very large area. Consequently, the study area is of considerable size, namely Alberta and Saskatchewan. These two provinces are characterized by flatland or rolling hills in the south, a mixture of forests and lakes in the north and the Rocky Mountains to the west. However, even within a relatively homogeneous region the climate may vary considerably. Southern Saskatchewan, for example, is much drier than most of Alberta, and the area near Red Deer, in central Alberta, is well known for its frequency of hail-storms.

British Columbia was excluded because of its complex terrain. Manitoba was not included as it can come under the influence of warm, moist air from the south, a condition which is uncommon in Saskatchewan and very rare for Alberta (Hare and Thomas 1974).

3.3 Sources of Rain Data

3.3.1 Tipping Bucket Rain Gauge

Ideally, a running total of rain accumulations over a very short time period (i.e. of order one minute) is best suited for comparison to satellite pictures. This would allow calculations of rain intensities while the satellite was overhead, as well as accumulations over the time period between passes. At selected observing sites this information is recorded using a device known as a tipping bucket rain gauge (TBRG). The gauge is connected to a rotating drum (one revolution in 24 hours) on which a tick is placed for each 0.2mm of rain that falls into the bucket. Unfortunately, these records are not easily accessible. Instead, hourly amounts and maximum accumulations for time periods ranging from 5 minutes to 12 hours are calculated from the TBRG chart, and monthly summaries are made available to the public on a form known as TAB31, an example of which is given in figure 3.1. The right hand side of the chart gives the hourly accumulations in tenths of millimeters. The left hand side gives maximum accumulation over various time periods which can then be converted to rain intensities in mm/hr. However, at best, the time that these values occurred is known to only the nearest one-half hour, and then only if there was no more than one period of heavy rain that day and it lasted less than one hour. This would be the case, for example, if just one convective storm passed over the rain gauge on any given day. Fortunately, this is a relatively common occurrence so that the left hand side of the TAB31 chart can be used to estimate both amount and duration of precipitation.

Column 3 of the TAB31 chart is the ratio of the 24-hour rain accumulation as measured by a standard gauge and the TBRG. This is used to correct the TBRG amounts so that there is only one estimate of 24-hour rainfall. When the factor is outside the range 0.5 - 1.5, the amounts are left uncorrected and flagged as such. Normally, this occurs only when rainfall totals are very light.

There is no guarantee, though, that the rain accumulation has been accurately measured by the standard gauge. Under windy conditions, when rain is blown away from the vertical, the gauge amount can be a gross under-estimate of the true rainfall. Even when it is not windy, large errors may be incurred. Barrett and Martin (1981) give results

Recording Precipitation Gauge – Monthly Report										
Station Name		Province		Station No.	Chart Change Hour (L.S.T.)		Tab 31	Month		Year
Precipitation Day				D A T E	Corrected Hourly Precipitation Amounts					24 Hour Total
(A)	(B)	(A) (B)	Corr. Amt. For Duration of Minutes Hours		Hour of day in Local Standard Time					
Standard rain gauge total for Precipitation Day	Recording rain gauge chart total for Precipitation Day	Applied correction factor (A divided by B)	Corrected daily maximum intensities for the Precipitation Day for durations of 5 minutes to 12 hours	Day of the Month	Hourly precipitation amounts for calendar day of the month, starting with hour ending at 1 AM through to hour ending at midnight.					24 Hour total Rainfall for each calendar day
Maximum Monthly Intensities					Frequency of Hourly Precipitation		Hours of Record		Monthly Total	
The maximum intensities and date of occurrence for durations of 5 minutes to 12 hours					Lists the total number of times hourly precipitation amounts occur within the classes from .01 to 2.00 or more inches/hour		Total number of hours of recorder operation		Sum of all hourly totals	
									Date of computer run	
Note: Special comments are listed here.										

Figure 3.1 Recording Precipitation Gauge
Monthly Report (TAB31) form.

from various investigators which indicates that the difference of measured rain amounts from co-located gauges is in the range 5 - 20% but can be as large as 30%. When hail accompanies the rain, errors are probably larger. Hail cannot enter the TBRG but can easily fall into the standard gauge. The following procedure is used to determine the amount of liquid precipitation. Hail is collected from an undisturbed area on the ground (equal in size to the opening of the gauge) and its water equivalent measured. This is then subtracted from the total amount of precipitation (hail plus rain) in the standard gauge. Under these conditions, uncertainties in rain amounts of 20-30% are expected.

While such large uncertainties are disquieting, they do not present a major drawback. Rather, they represent a limit on the accuracy of any satellite-inferred rain amounts. The ultimate goal to strive for then is for predicted and measured rain amounts to agree within 20%.

The geographical distribution of stations equipped with TBRGs is given in figure 3.2. Not all stations are operational at the same time as they open and close as economic, industrial and social needs dictate. The total of stations given in figure 3.2 is 63, with 31 in Alberta and 32 in Saskatchewan. Normally, approximately 59 of these are operational at any given time. The majority of stations are south of latitude 55 with only two stations in the mountains. As a result, most case-studies are from the southern half of Alberta and Saskatchewan.

3.3.2 Climate Stations

Daily rain accumulations are available from the AES climate station network shown in figure 3.2. The 24 hour period is normally 08:00 to 08:00 local standard time. These can be used as an aid in verifying satellite-inferred rain amounts in that they represent an upper limit to the predicted amounts. This will be discussed in more detail in chapter 6.

3.3.3 Surface Weather Reports

There are a number of observing stations (see figure 3.2) which report weather conditions every hour and more often if there is a "significant" change. The significant changes of concern here are: begining or end of precipitation, beginning or end of a thunderstorm and certain changes of visibility or cloud ceilings. Changes in rain intensity

Figure 3.2a   Precipitation network over Alberta
- • – climate / forestry stations
- ■ – stations equipped with tipping bucket rain gauge
- ▲ – stations reporting surface weather

Figure 3.2b   Precipitation network over Saskatchewan
  • - climate/forestry stations
  ■ - stations equipped with tipping bucket rain gauge
  ▲ - stations reporting surface weather

need not be reported, but they are often accompanied by significant changes in ceilings or visibility. From these reports it is possible to obtain the duration of precipitation and, more importantly, the time it occurred accurate to within a few minutes. This is much better than the one-half hour provided by the TAB31 chart. Important information can also be obtained from the remarks section of the reports, such as movement of thunderstorms or location of heavy showers. Finally, cloud amounts may reveal whether or not a storm passed directly overhead. For example, a report that showed only a few tenths of the sky covered by cloud would indicate that the cell only grazed the station.

3.4 Selection Effects

Attention is now turned to some implications induced by the method of selecting the sample.

A typical thunderstorm cell goes through three stages of development: growing, mature and dissipating. Most of the rainfall occurs in the mature stage, and very little is associated with the dissipating stage. Often, three cells are present in a single convective storm, each in a different stage. The lifetime of a single cell may be less than one hour, but because new cells are being generated as old ones dissipate, the storm may endure for several hours.

By choosing the sample based on rain amounts > 10mm, the sample assuredly consists mainly of mature storms. However, when a rain-estimation technique is applied to randomly selected satellite images, storms in all stages of development might be represented. A correct prediction of rain for a storm in its mature stage would be a vast overestimate should the cell be in the dissipating stage. For any rain-estimation scheme to have a chance to succeed it must be able to distinguish between the different stages of development.

Normally, the stage of development can be determined from a sequence of satellite images. Scofield and Oliver (1977), for example, characterize a dissipating storm by the cloud area shrinking or stationary with time. Unfortunately, with a time resolution of 100 minutes, this procedure is not feasible here.

By necessity, a different approach is used. A growing storm will not be as "cold" as a mature storm as the cloud top is still rising upwards. Similarly, due to the large thin

anvil, a dying storm will be less bright than a mature storm. It may be, then, that some broad limits of temperature and brightness can be used to delineate a cell in the mature stage. This is an imperfect solution at best, but without more frequent satellite pictures, it is the only alternative.

Another difficulty imposed by the selection method is that to infer rain amounts successfully requires not only that mature storms are cold, bright clouds but also that all cold, bright clouds produce rain. The sample selection procedure excludes the possibilty of finding cold bright non-raining cells. To detect these would require selecting cases strictly from the satellite images. However, the useable cases would still be restricted to those in which the storm passed directly over a tipping bucket rain gauge. Considering the small number of gauges, a large number of storms would have to be considered just to find these few fortunate events. As a compromise, a small number of days have been chosen using only the satellite imagery (the independent sample) to test against any results found from cases selected using rain data (the dependent sample).

3.5 Analyses of Satellite Data

Convective storms suitable for study are determined from the hourly amounts given in the TAB31 charts. For these storms, contour maps of satellite viewed temperature and brightness are produced. The next step is to determine whether or not the convective core passed directly over the station. Moreover, when the time of the satellite image and observation of rain are considerably different, it is necessary to adjust the position of the cloud, in order to estimate the temperature and brightness over the station at the time rain was observed.

3.5.1 Position of Raingauge Under Cell

The relative position of the rain gauge beneath the convective cloud is of great importance in determining the expected amount of rain. The most copious rain falls beneath or very close to the deep convective core, with lesser amounts associated with the anvil. On a satellite image it is often difficult to separate the core from the cirrus debris in which it is embedded. There are some clues which make this task easier, as outlined by Scofield and Oliver (1977). In most cases the core is usually found near the

direction of upper level winds
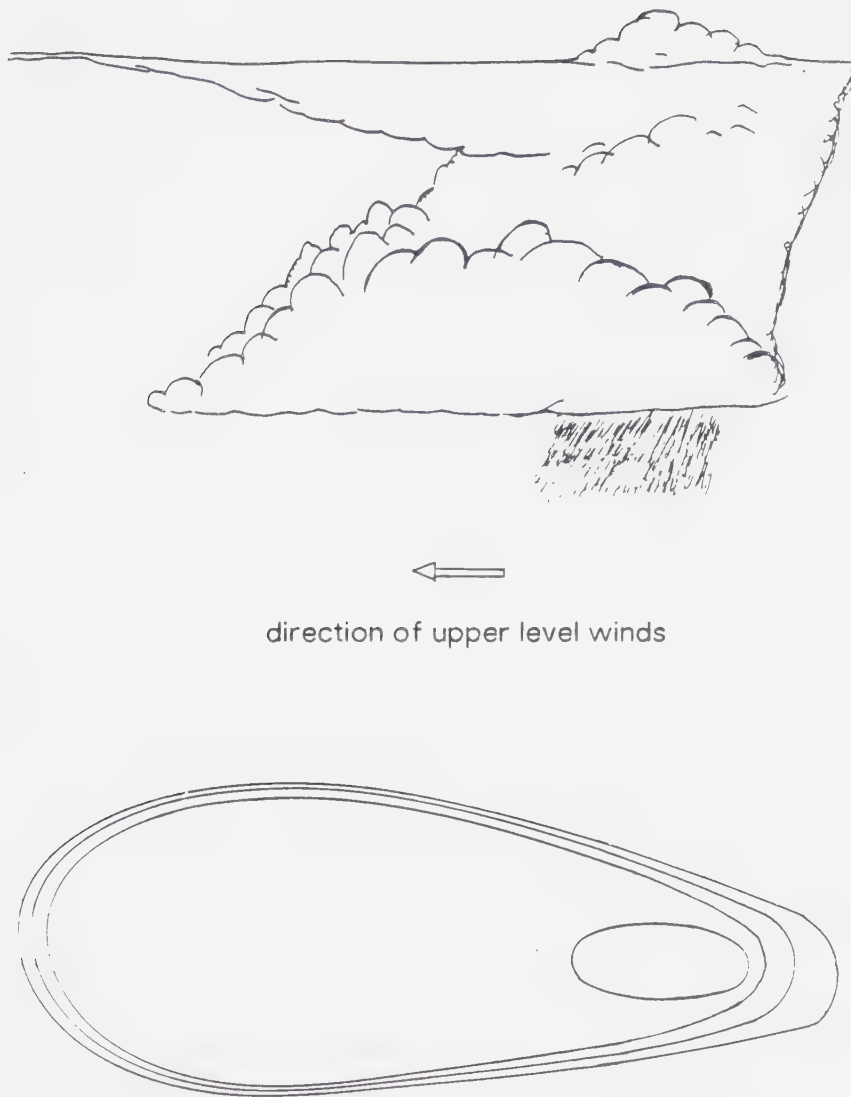
Figure 3.3   Relation of a typical thunderstorm's rainfall pattern
to the cloud-top temperature contours.

tightest temperature gradient on the upwind side of the cloud. This is shown schematically in figure 3.4. However, if the cell is small or growing so that the anvil has not yet spread downwind, then the core is in the middle of the cloud. Another difficulty is determining the size of the rain area. When inferring rain from satellite images over Montana, Griffith et al. (1981) found that apportioning most of the rain to only 1 - 10% of the cloud area best fit the radar-derived rain areas. In the same region, Wiley and Laitsch (1983) assigned rain to 25 - 50% of the cloud area. These studies were estimating rain amounts, but the situation here is somewhat different. All that is required is some means of dividing the cloud area in order to separate the most likely area which contains the convective core from the rest of the cloud. Using the two studies noted above as guidance, this has been done by dividing the convective cloud into three zones. Zone 1 comprises 20% of the cloud's area nearest the upwind temperature gradient, or the central area if there is no large elongated anvil. This is presumed to contain the convective core, though it is possible for the core to be much smaller than this area. Zone 2 represents a transition between the core and the anvil under which rain is expected, even if the storm only grazed the station, and consists of 30% of the cloud area. Zone 3 encompasses the remaining 50% which represents the thin, non-precipitating anvil.

Case studies are classified according to which cloud zone passed over the station in order to remove the dependence of rain amounts on distance from the convective core. When two or more cells have merged the brightness can often be used to separate the storms before attempting to construct the zones.

3.5.2 Adjustment of Cloud Position

When the time of the satellite pass and observation of rain are nearly coincident, it is immediately apparent which cloud zone passed over the rain gauge. However, when they differ, the motion of the storm needs to be known. Given two sequential satellite images this is a simple task, assuming straight-line motion, a reasonable assumption over the short intervals considered here. However, when cells are merging or evolving rapidly, then it may not be possible to identify which zone passed over the station. For these cases, two zones may be quoted with the most likely given first. When only one image is available, storms are assumed to move with the 700mb flow. As this is only an

approximation, two possible zones will be given for the majority of these cases.

The adjustment of the cloud position is also necessary for determining the temperature and brightness over the rain gauge at the time rain was observed. If the time of rainfall is not accurately known, then it is assumed that the rain is associated with the lowest temperatures that passed over the gauge, as determined from the track of the storm. In all cases, after adjusting for cloud position, the temperature associated with the rain is assumed to be the lowest within 10km of the gauge, to account for position uncertainty. This is especially important near areas of tight temperature gradients. The positional accuracy here is insufficient to determine if the rain is associated with the gradient or merely an artifact of the uncertainty in the gauge's position.

3.5.3 Evolution of Cloud

While the above procedures can be used to correct for the position of the cloud, it cannot account for any evolution that may have taken place in the interval between observation of rain and the satellite pass.

Adler and Fenn (1979) showed that, for severe storms, the cloud-top temperatures can decrease faster than $1^{\circ}K/min$. through the range $240^{\circ}K$ to $235^{\circ}K$ ($-33^{\circ}C$ to $-38^{\circ}C$). However, the associated severe weather occurs 15 to 30 minutes after the period of maximum growth, when the minimum temperature is reached. From their published curves, below approximately $-45^{\circ}C$ to $-50^{\circ}C$ temperatures decrease at a much slower rate (as low as $0.1^{\circ}C/min$). Accordingly, reasonable temperature estimates ($\pm5^{\circ}C$) are possible if the satellite pass is within 30 minutes of rain observation. Furthermore, both the Scofield and Oliver, and Griffith and Woodley techniques use 30-minute GOES data to infer rain successfully. This would also indicate that, except for a rapidly growing cell, the temperature at a given instant is representative of conditions over one-half hour. Unfortunately, no parallel study exists for brightness, and its rate of change is unknown.

Generally, the longer the time between satellite pass and observation of rain, the larger the uncertainty of the quoted temperature and brightness values. However, as the rate of evolution for any particular storm studied is unknown, the maximum time difference for which results become unreliable is also unknown.

3.5.4 Additional Sources of Satellite Data

As was noted earlier, the APT images consist of only every third scan from the AVHRR and that the data along each scan are averaged. HRPT images employing all scan lines with full resolutions are available from AES.

A "grey scale" is applied to the HRPT images so that each pixel is represented by a certain shade of grey, dependent on its temperature or brightness. The calibration of the temperature grey scale is made using a curve similar to that given in Table 2.1. An enhancement curve can be constructed so that certain temperature ranges are highlighted, but for most of the infrared pictures and all of of the brightness images used here, the 0-255 range of digital values is divided evenly into 17 shades of grey. This leads to increasingly larger ranges of temperature at high digital counts. For example, the -40°C to -56°C range is represented by only one shade of grey.

While such large ranges might appear to make the HRPT images useless, this is far from true, due to their superior resolution. The resolution at the satellite subpoint is approximately $1.2km^2$ compared to $17km^2$ for APT pictures. Small cloud areas that may be poorly resolved on the APT images, especially those with tight temperature gradients, may be better represented on the HRPT photographs. If the HRPT and APT temperature estimates differ by more than one shade of grey, the APT estimate is disregarded because of its lower resolution. As will be seen, this occurred on two occasions.

3.5.5 Brightness

As mentioned earlier, brightness values are left as digital counts, and have not been corrected for sun angle. As the specific cases examined here are all confined to a one-month period only (though not of the same year) at approximately the same time of day, the sun angle is approximately constant. However, because brightness values have not been "normalized", comparisons to most other studies cannot be made.

3.6 Application of Sample Selection and Analyses

The previous sections have explained the procedure used to obtain and analyze the dependent sample. Given below are the steps taken in the application of these procedures.

The time period for selection of the sample was restricted to May through September, as convective activity is rare outside this period. Satellite data were availabe for June -Sept. I979 and May-Sept. 1982. Locations for which > 10mm of precipitation in less than one hour were reported were found using the TAB31 charts (charts for Saskatchewan had to be ordered specially and those for May 1979, 1982 and June 1982 were not received). Only those storms for which the precipitation was within one hour of the satellite pass were considered. Next, satellite pictures were then inspected to determine if the precipitation was the the result of convective activity. This was generally not a problem; isolated cells or obvious cells embedded in other clouds were evident in all but two cases.

Temperature and brightness contour maps were then produced and the location of the rain gauges placed on the maps. Finally, the cloud position was adjusted as explained in section 3.4.2 and the temperature and brightness over the gauge estimated. Where other convective clouds, not selected by the procedure given above, were found to lie near a rain gauge, the temperature, brightness and precipitation amount were also recorded. These additional storms serve two purposes. They may aid in determining the temperature and brightness cut-off for which < 10mm is expected or reveal the existence of cold, bright, non-precipitating storms.

Each case is discussed in some detail in the next chapter. Even cases which eventually proved not to be useable are included, as they illustrate some of the difficulties encountered.

4. Case-Studies

4.1 introduction

For each case, temperature and brightness contour maps are given. Unless otherwise indicated, the scale of all maps is approximately 1 cm = 45 Km. An arrow is drawn in the upper-right hand corner of each map pointing northwards. Generally, only the 0°C and 80 digital count contour, for temperature and brightness respectively, are labelled. Shading is used to indicate areas enclosed by temperatures below and brightness above some "critical" value. The value changes from one case to the next and is given in each figure. The contour intervals are given in Table 4.1. When available, weather observations were obtained and these are listed in appendix C. At the end of the chapter. a summary table of all pertinent information is given.

4.2 Case Studies

4.2.1 July 07 1979

Edson received 11.1mm from 20-21 GMT, with the heaviest precipitation occurring from 20:05 GMT to 20:40 GMT. as seen from the weather observations given in Table C.1. Edson was scanned at 20:30 GMT on the first of two satellite passes over Alberta on this afternoon. The temperature and brightness maps are given in Figure 4.1.

A large storm is seen to lie over western Alberta. As Edson was scanned while the heavy rain fell. the temperature and brightness associated with the rain are those values directly over the station, namely -53°C and 170 respectively. Lower temperatures of -57°C lie just 20km to the northwest. Even though the cloud extends far south of Edson, it is very narrow and the area encompassed is quite small. Consequently. Edson is determined to have been passed by Zone 1 of the cloud.

The second satellite image is at 22:10 GMT. Temperature and brightness maps are given in Figures 4.2. It is seen that the storm decayed while moving northeast at approximately 50km/hr. Minimum cloud-top temperatures decreased 5°C. No heavy rain was being reported at this time.

Table 4.1 Contour Intervals for Temperature and Brightness Maps

Temperature (°C)	Contour Interval (°C)	Brightness (counts)	Contour Interval (counts)
$T \leq -50$	5	$B \geq 140$	10
$0 \geq T > -50$	10	$80 \leq B < 140$	20
$0 < T$	not contoured	$80 < B$	not contoured
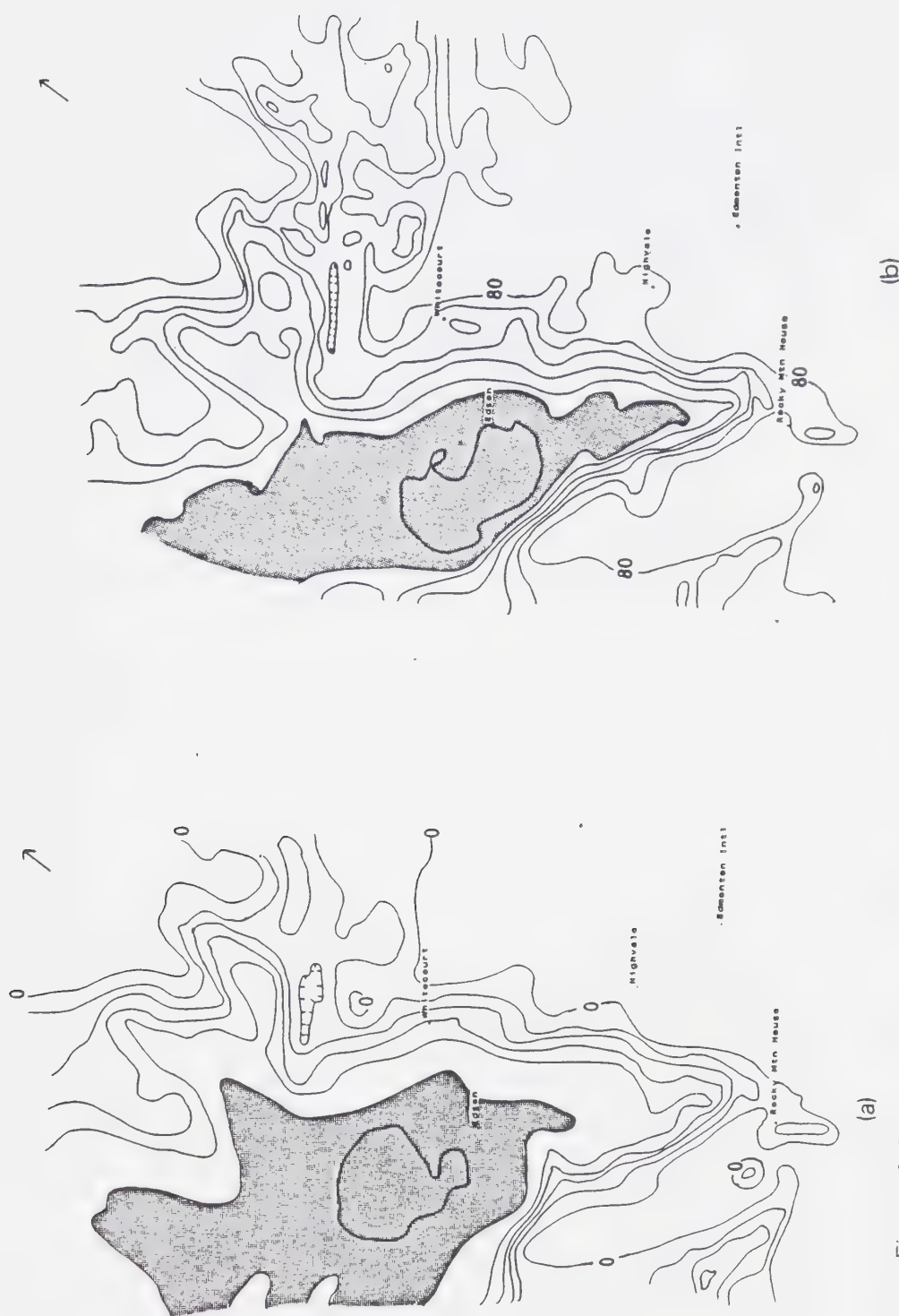
Figure 4.1   Cloud-top temperature and brightness contours for July 07, 1979 at 2030 GMT.
(a)temperature (T) in °C, shading indicates areas of T < −50°C
(b) brightness (B) in counts, shading indicates areas of B > 160.
For an explanation of the contours intervals, see Table 4.1.
The arrow in the upper-right hand corner points northward.

(b)

(a)
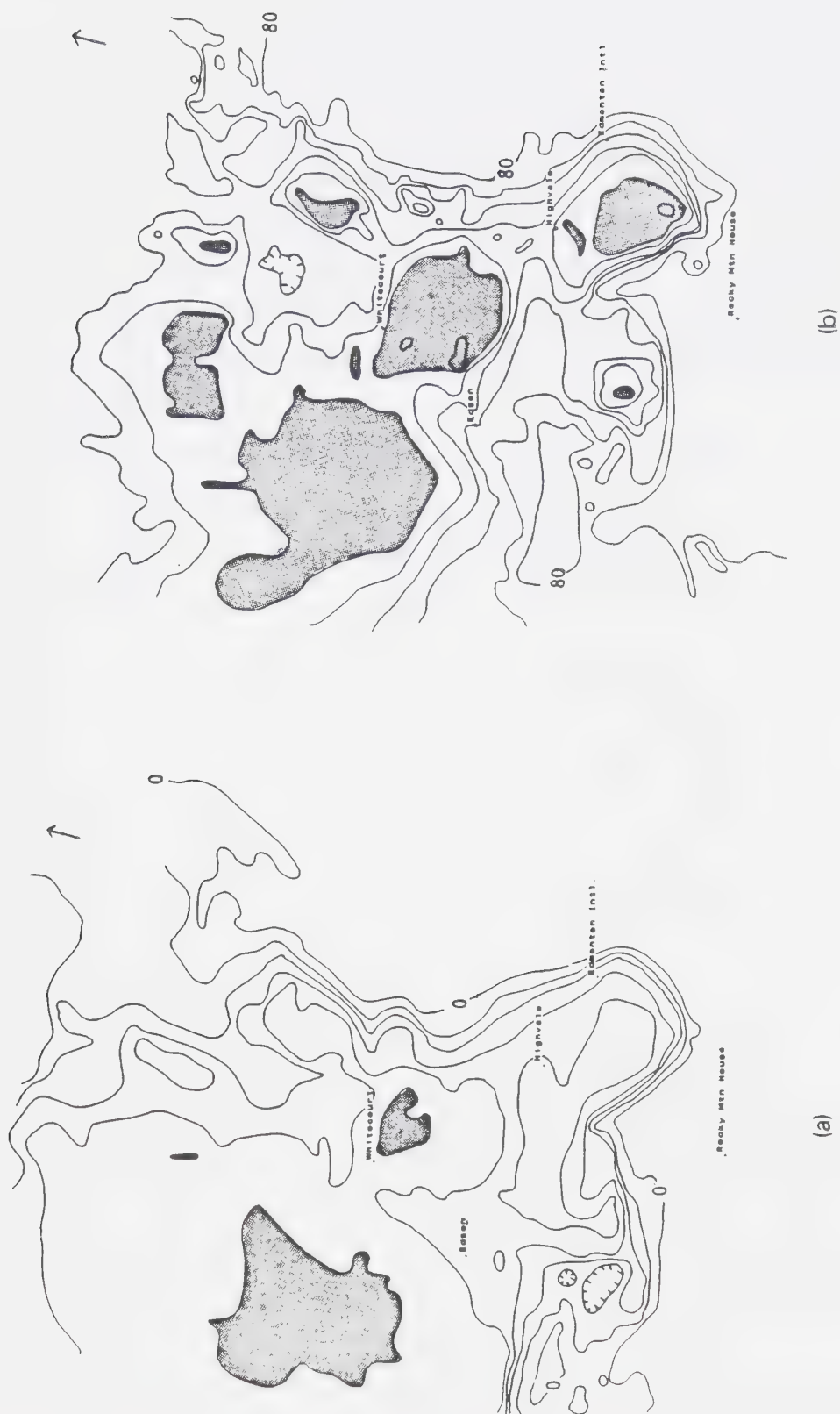
Figure 4.2   As in Figure 4.1 except at 2210GMT.

4.2.2 July 10 1979

The temperature and brightness maps for the 21:40 GMT satellite pass are given in Figure 4.3 and 4.4 A number of stations recorded precipitation near this time with both Edson and Saskatoon receiving at least 10.0mm. Only one image is available for this day. The upper air flow (not shown) was predominantly from the southwest, except over central and northern Alberta where it was light and variable.

Figure 4.4 shows a cloud band with embedded cells running through central Alberta before curving southward over Saskatchewan. A number of isolated cells are also evident over Saskatchewan as seen in Figure 4.3 Each area of interest is discussed separately below.

In Alberta, Edson is under Zone 1 at the southern end of a bright cell. The temperature and brightness over the raingauge are -49°C and 156, respectively. Brightness values in excess of 170 are only 10-20km to the west.

Edson received 11.3mm of rain from 21-22 GMT. The weather observations, given in Table C.2, show that only light rainshowers were present at 21:00 GMT, but moderate showers were occurring at 22:00 GMT. While no heavy rain was reported, it is assumed to have occurred closer to 22:00 GMT. This is consistent with Edson under Zone 1 at the time of the satellite pass. Accordingly, the temperature and brightness over Edson from the contour maps have been adopted as being associated with the heavy rainfall. It is also noted, from the 2200 GMT report, that the storm was moving to the northeast.

Another large cell lies over central Alberta. At the time of the satellite pass, Calgary was just south of this cell with Penhold and Rocky Mountain House east of the cloud. Assuming a northeasterly motion, both Penhold and Rocky Mountain House would have been passed by Zone 3 of this cloud. It is possible that the storm missed Calgary completely.

As expected, very little rain was observed at these three stations. Calgary did not receive any rain from 21-22 GMT, while Rocky Mountain House and Penhold had only 0.8mm and 2.6mm, respectively from 22-23 GMT.

In southern Saskatchewan, a complex of three cells lie near Swift Current. The high resolution AVHRR visual image shows that there are distinctive breaks between the

cells. This is also detectable on the APT images, but is not as obvious. There are two TBRGs in Swift Current, one at the airport and another operated by the Canadian Dept. of Agriculture. Both lie very close to the breaks between the cells, with the temperature and brightness overhead equal to -49°C and 143 for Swift Current A, and -49°C and 153 for Swift Current CDA.

Swift Current CDA received 4.4mm from 20-21 GMT and 3.9mm fell at the airport during the following hour. A northeasterly cloud motion would result in the storms just grazing the gauges, so that they would have been passed by Zone 2 or 3 of the cloud, although Zone 2 seems more likely. Considering the proximity of the cloud over the airport, the temperature and brightness values overhead are accepted as representative of the conditions prevalent when the rain was observed. As the rain at the agricultural station occurred at least 40 minutes before the satellite pass, it will not be considered here.

The final cloud of interest is the large cell lying over central Saskatchewan. Outlook, at the southern end, would have been crossed by Zone 2 or 1, while Saskatoon is under Zone 1 and North Battleford is beneath the anvil. The temperature and brightness over Saskatoon are -52°C and 165, respectively. The speed and movement of the cell are unknown; however, assuming that the storm moved northeast, then the temperature and brightness values that would have passed over Outlook are -45°C ±5 and approximately 160.

Saskatoon received 10mm in just 15 minutes. The weather observations, given in Table C.2 show that heavy showers occurred from 21:03 to 21:26 GMT, which is close to the time of the satellite image. As the gradients are quite flat, the temperature and brightness values over Saskatoon are representative of those associated with the heavy showers.

Outlook received 6.1mm from 20-21 GMT with 5.7mm in only 5 minutes. North Battleford recorded 3.7mm from 19-20 GMT. Weather reports for North Battleford, given in Table C.2, show that heavy rain was observed, but 50 minutes before the satellite pass which is to long to be of use here.

Figure 4.3   As in Figure 4.1 except for July 10, 1979 at 2140 GMT over Saskatchewan. Shading indicates areas of T < -40°C or B > 150.
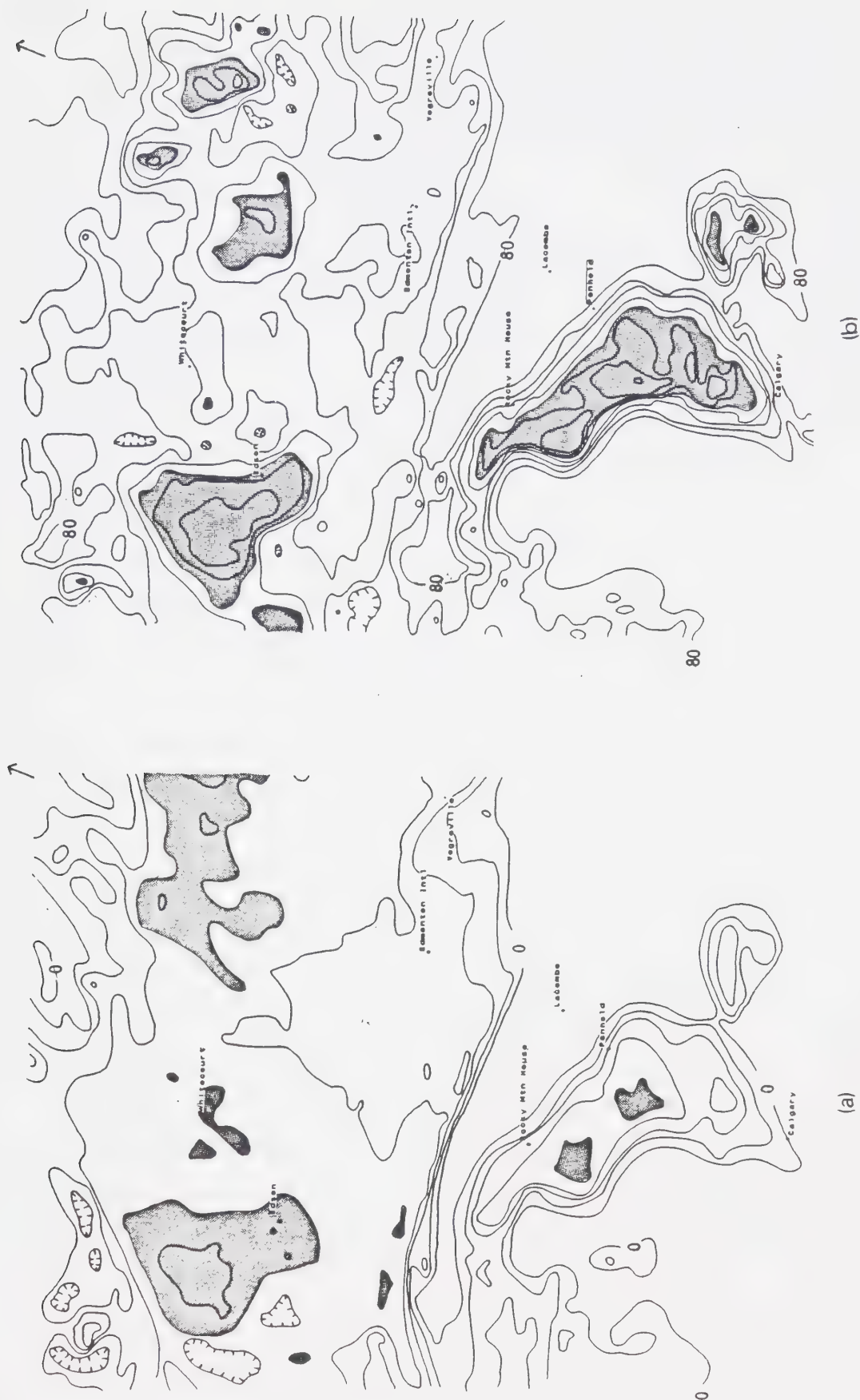
Figure 4.4   As in Figure 4.3 except over Alberta.

4.2.3 July 11 1979

This is one of two cases where the resolution of the APT data was insufficient to measure the cloud-top temperature accurately. (see also July 15, 1979). The rain-gauge data from around Edmonton confirm that the disturbance treated here is of a very small scale. Edmonton Municipal Airport received 39.5mm of rain between 19-22 GMT. During the same time period Edmonton Namao, Ellerslie and Edmonton International Airport received 8.0mm, 2.1mm and 0.6mm, respectively. From 20-21 GMT, the Municipal Airport recorded 17.7mm, while the other three stations received barely more than a trace of precipitation. In the next hour (21-22 GMT) a further 10.3mm fell at the Municipal Airport. The weather observations, given in Table C.3, show that the Municipal Airport reported heavy thundershowers from 21:26 GMT to 21:32 GMT. The movement of the shower was toward the east or southeast. Namao reported heavy showers to the south at 21:00 GMT and thunder at 21:37 GMT but no precipitation until 22:00 GMT. During this time the International Airport reported heavy showers to the north. At Ellerslie, the University of Alberta climatological station, only 1.3mm fell from 21-22 GMT

Attention is now turned to the temperature and brightness maps for the 20:35 GMT satellite pass, shown in Figure 4.5 and 4.6. No large convective clouds are seen over Edmonton although considerable activity is evident to the north. Both Namao and the Municipal Airport are under an area of relatively high temperatures, whereas it is known that heavy rain was occurring at this time. The nearest clouds to the Municipal Airport lie less than 10km to the west, with a cloud top temperature of -27°C. However, close inspection of the HRPT infrared image for this day (not shown) reveals a small bright spot in the centre of the cloud which is definitely a whiter shade of grey than the surrounding cloud. Comparison to the grey scale gives a temperature in the range -40°C to -56°C.

It is assumed that this is the storm which dumped heavy rain on the Municipal Airport and that positioning errors account for its apparent location west of, rather than over Edmonton on the satellite image. Comparing the APT and HRPT data, the derived temperature differs by > 13°C, indicating that the cloud is below the limit of resolution of the APT image.

While this case is left in the sample (at least for the time being) it is of limited use as the temperature is known only to within ±8°C. The maximum brightness of the cloud,

from Figure 4.5b, is 165. A visible range HRPT image was not available for this day, and so due to lack of any other information the above brightness value is accepted as found. Considering the large amount of rain, it would seem safe to assume that the Municipal Airport was crossed by Zone 1 of the storm.

Figure 4.5   As in Figure 4.1 except for July 11, 1979 at 2030 GMT.
              Shading indicates areas of T < -30°C or B > 150.
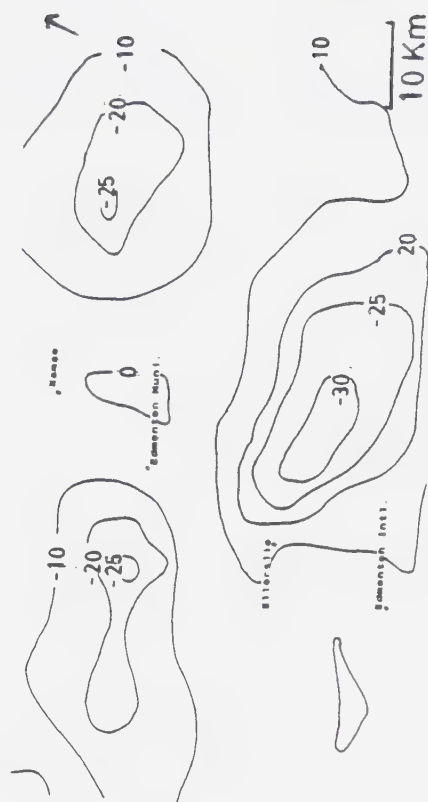
Figure 4.6   Expanded view of temperature contours near Edmonton
              on July 11, 1979 at 2030 GMT

4.2.4 July 14 1979

On this day, Kindersley received 8.6mm of rain from 21-22 GMT. Temperature and brightness contour maps for the satellite passes at 21:50 GMT and 22:30 GMT are given in Figures 4.7 and 4.8, respectively.

Based on the surface weather reports, given in Table C.4, most of the rain occurred near 21:30 GMT. This is 40 minutes after the first pass and 60 minutes before the second. Due to this large time lag, it is difficult to discern which cloud passed over Kindersley and produced the precipitation. By overlaying the two maps, a general southerly motion of clouds in western Saskatchewan is evident, but it is very difficult to follow any particular cloud area. The direction of flow at 500mb and at the surface (not shown) also supports this movement.

The disorganized nature of both the temperature and brightness fields belie the convective nature of the precipitation (as reported in the surface observations). Even though it is known that Cb's are present, this is far from obvious from Figures 4.7 or 4.8. It is possible that they are hidden by a layer of higher cloud. However, if Cb's are present, then their tops must be quite warm, as no particulary cold cells are evident near Kindersley on either image; temperatures being in the $-30^{\circ}C$ to $-35^{\circ}C$ range.

The lack of any well defined cells and the large time lag between the satellite images and the observation of rain over Kindersley make it impossible to identify the rain-producing cloud. Consequently, this case it not used. However, it is important to note that cloud tops are quite warm. It is unknown if insufficient APT resolution played a role, as HRPT images were not available. The surface observations show that there were many brief showers, suggesting that the weather was dominated by many small cells. It is possible, but unsubstantiated here, that either some small cell beneath the resolution of the APT image or a cell with a short lifetime (or both) caused the heavy rain at Kindersley.
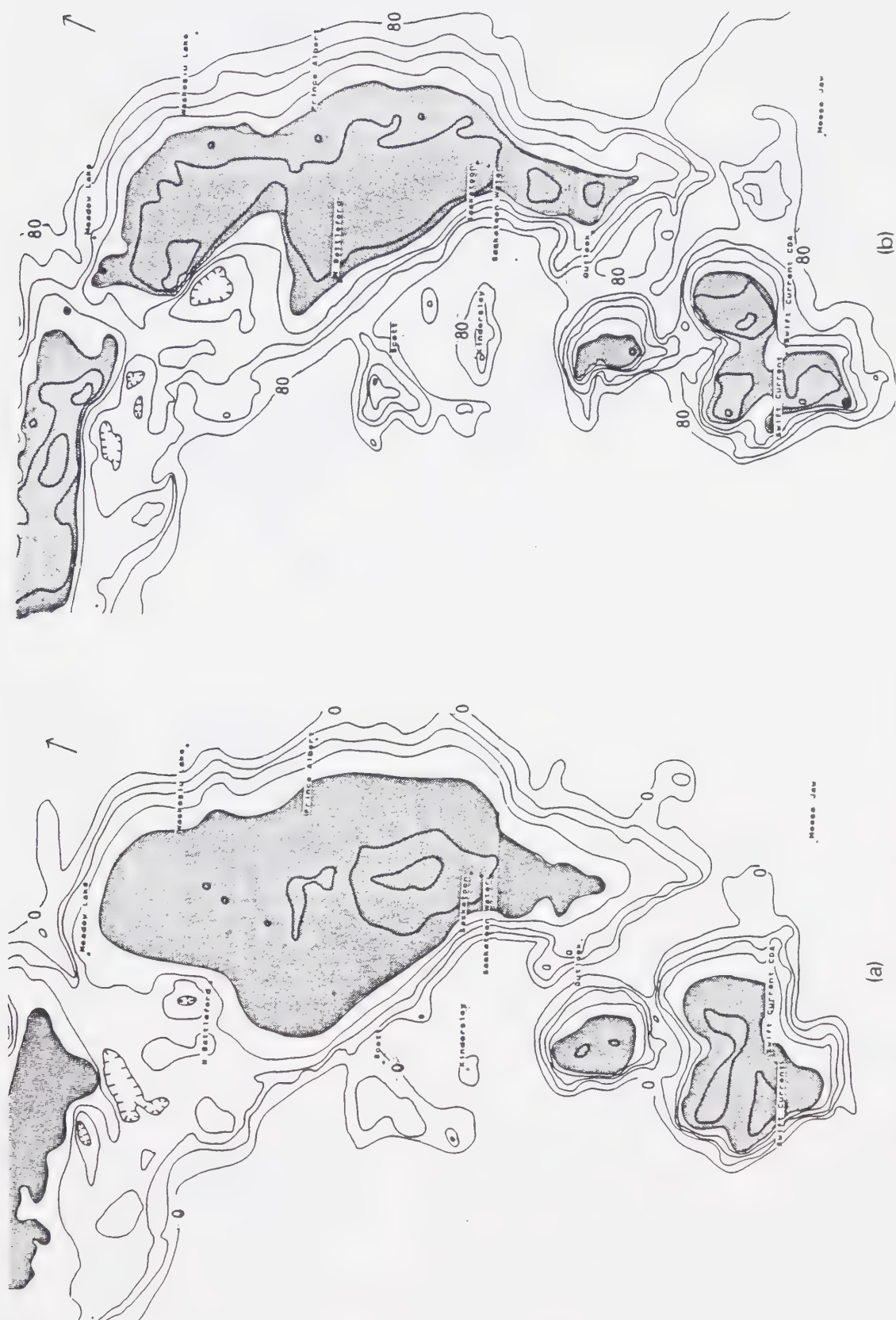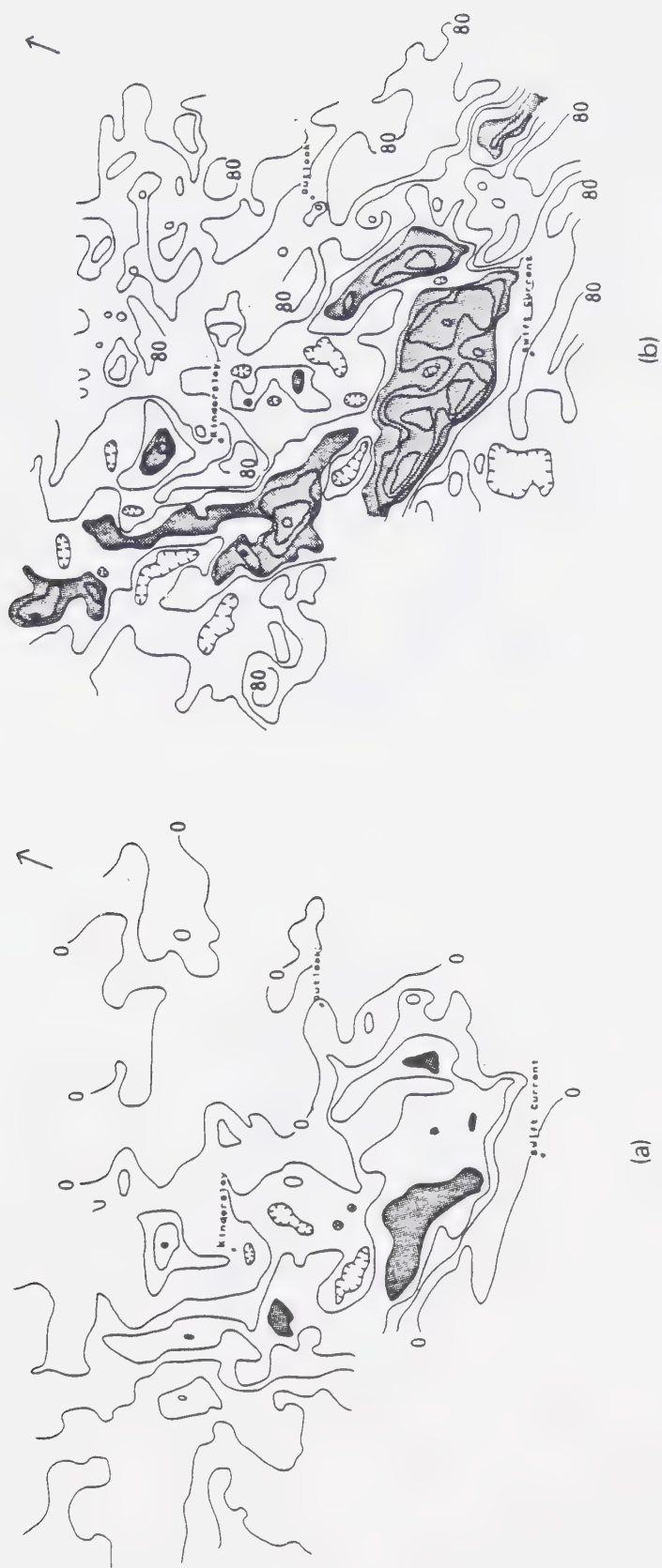
Figure 4.7   As in Figure 4.1 except for July 14, 1979 at 2150 GMT.
Shading indicates areas of T < -30°C or B > 140.

(a)

(b)
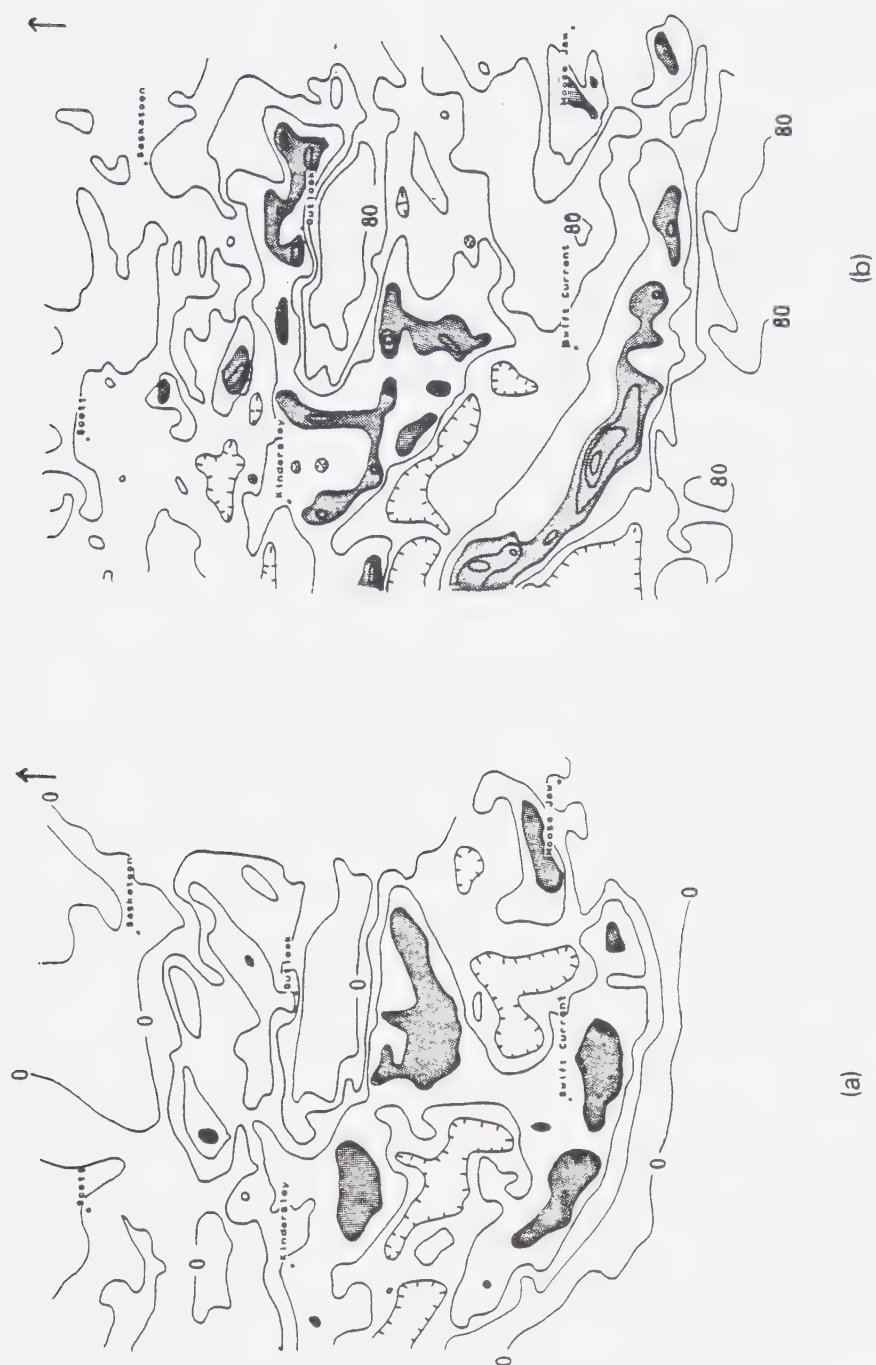
Figure 4.8   As in Figure 4.7 except at 2230 GMT.

4.2.5 July 15 1979

The satellite images at 20:45 GMT and 22:25 GMT show only scattered small cells, as seen on temperature and brightness maps given in Figures 4.9 and 4.10. However, when the satellite images are superimposed it is evident that one of the small clouds did indeed pass over the rain gauge. Outlook received 11.7mm in only 15 minutes, sometime between 22 GMT to 23 GMT.

From Figure 4.11, the minimum cloud top temperature is only -35°C, quite warm for a suspected Cb, and the small cloud size raises suspicions regarding possible problems with resolution. From the HRPT infrared image for this day (not shown), comparison with the grey shade gives a cloud-top temperature in the range -40°C to -56°C. In fact, a few co-workers asked to determine the category for this cloud placed it in the next coldest range.

The temperature adopted is -48°±8°C with a brightness, from fig 4.10 of 155±5. However, similar to July 11,1979 while included in the sample, the large temperature uncertainty limits the usefulness of this case.

Figure 4.9   As in Figure 4.1 except for July 15, 1979 at 2045 GMT. Shading indicates areas of T < −10°C or B > 120.
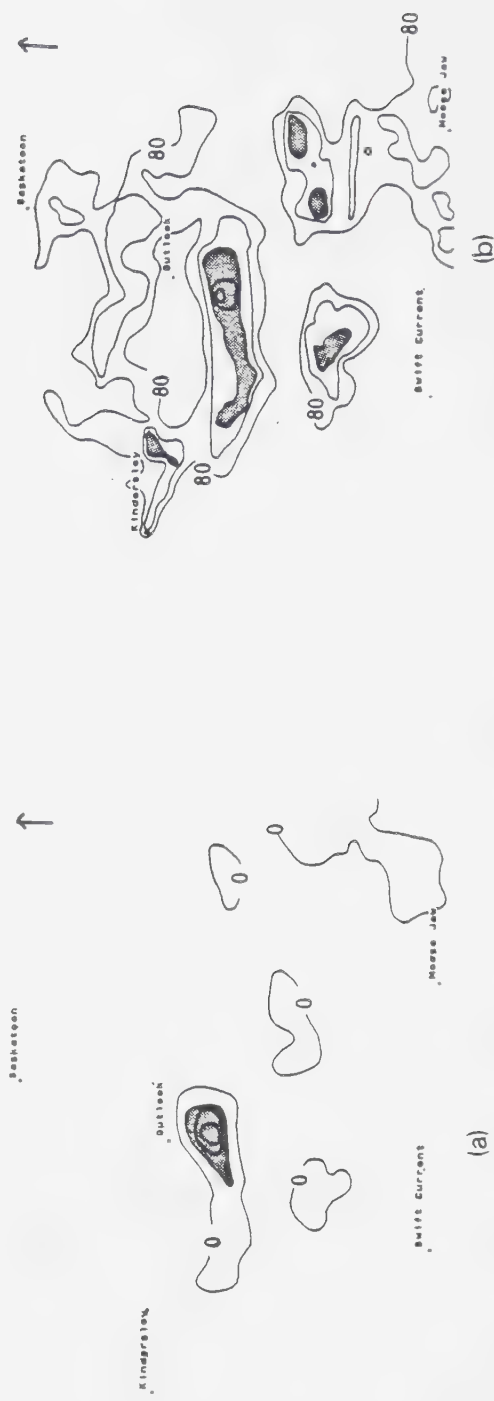
Figure 4.10   As in Figure 4.9 except at 2225 GMT.
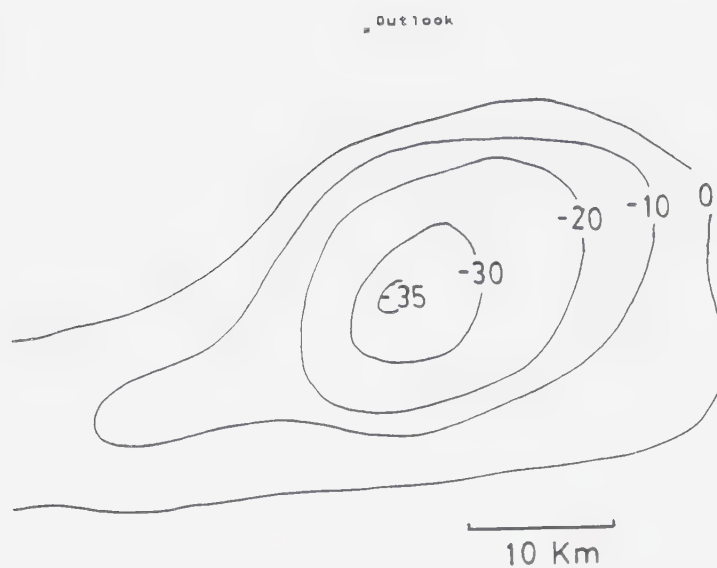
Figure 4.11   Expanded view of temperature contours near Outlook
on July 15, 1979 at 2225 GMT.

4.2.6 July 29 1979

The temperature and brightness maps for the 21:40 GMT pass are given in Figure 4.12 and show Calgary lying under Zone 1 of a large cloud. The temperature and brightness values over Calgary are -43°C and 168, respectively. However, the lowest temperatures of -48°C are only 10km to the southwest.

The second satellite pass at 23:00 GMT viewed only the western half of Alberta (not shown). A cloud mass with a temperature of -50°C is seen at the eastern edge of the image. If, as seems probable, this is the same cloud that was over Calgary, then cloud motion is easterly at approximately 45km/hr.

Calgary received 10.0mm of rain from 21-22 GMT with 8.1mm in 30 minutes. Weather reports for this day were not available, but there is little doubt that the cell over Calgary on Figure 4.12 produced the rain. In accordance with the discussion given in section 3.4.2, the lowest temperature within 10km of the gauge has been adopted as associated with the rainfall, namely -48°C. The brightness, however, remains unchanged at 168.
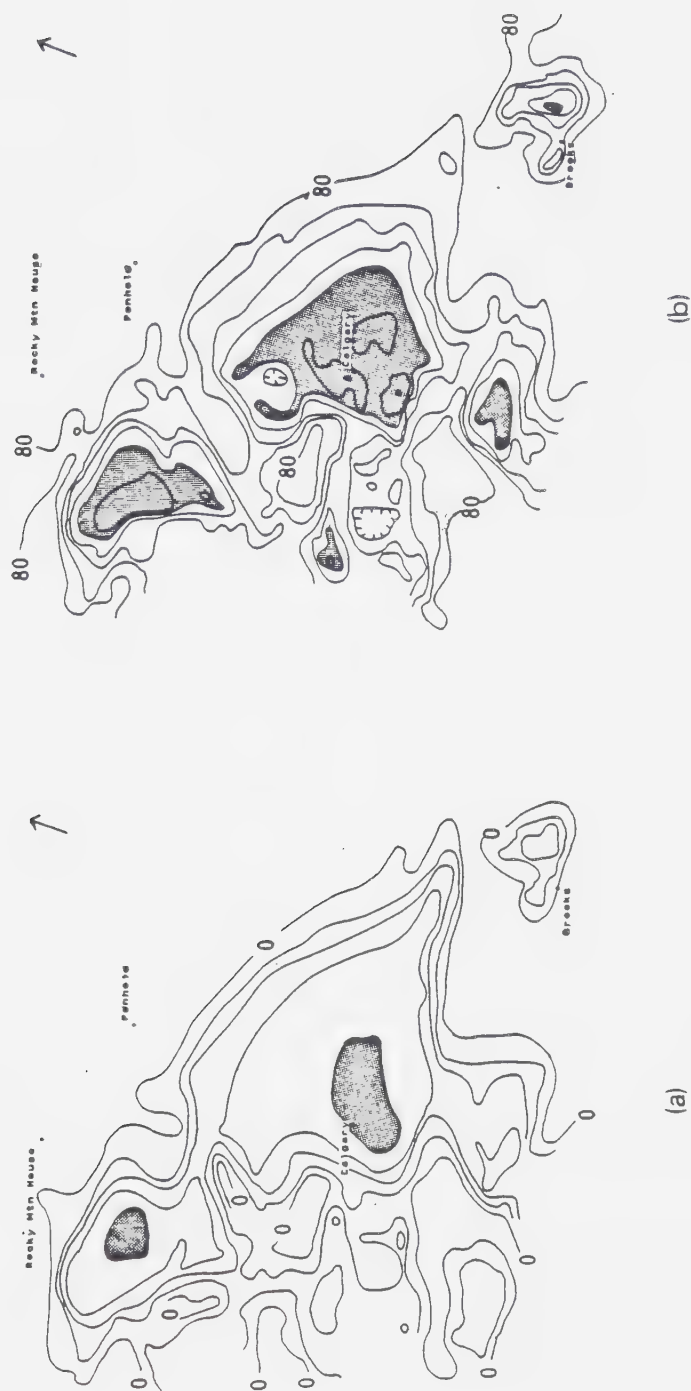
Figure 4.12   As in Figure 4.1 except for July 29, 1979 at 2140 GMT.
Shading indicates areas of T < -40°C or B > 150.

4.2.7 August 05 1979

The temperature and brightness maps for the 20:25 GMT pass are given in Figure 4.13. A large, organized band of cloud with embedded Cb's, lying along a TROWAL, is seen to curve northwest-southeast through Alberta and Saskatchewan. Other isolated cells cover western Alberta and southern Saskatchewan.

Cold Lake lies underneath a cold, bright area within the cloud band. The temperature and brightness overhead are -57°C and 153, respectively. Temperatures of -60°C and brightness values over 160 are only 20km to the west-southwest.

Cold Lake received 24.0mm from 20-21 GMT, all within 30 minutes. Weather reports for this day were not available, so a more accurate timing of the rainfall is not possible. For lack of any better information then, the values of temperature and brightness over Cold Lake have been adopted as associated with the rain.

From the temperature and brightness maps for the second pass, at 22:05 GMT, (see Figure 4.14) it is seen that the edge of the cloud band has moved approximately 80km eastward. The movement of the individual cells, however, appears to be to the northwest, but this is not certain. The cloud mass that was over Cold Lake has dissipated and merged with the background cloud. Consequently, its direction of motion is unknown and Cold Lake may have been passed over by Zone 1 or 2 of the storm.

Two cells are seen over western Alberta in figure 4.15. Edson lies directy under Zone 1 of one of these, with a cloud-top temperature of -50°C and brightness of 156. From 21-22 GMT, Edson received 14.1mm of precipitation.

Rocky Mountain House is under Zone 1 of the other cell, with a cloud-top temperature overhead of -35°C. The minimum cloud temperature is -40°C. The brightness over the station is 155 with values of 160 only 10km to the north. Rocky Mountain House recorded just 0.7mm from 21-22 GMT.

Based on the satellite maps, a cold, very bright storm passed directly over Outlook. In fact, the brightness value of 190, seen on Figure 4.14, was the highest value encountered for the entire study. Unfortunately, hourly rain amounts are missing for this day. For interest's sake only, the 24 hour accumulation was 14.1mm, though how much of this is due to this storm is unknown.

(a)

(b)

Figure 4.13   As in Figure 4.1 except for August 05, 1979 at 2025 GMT.
Shading indicates areas of T < -50°C or B > 150.

Figure 4.14   As in Figure 4.13 except at 2205 GMT.

(a)

(b)
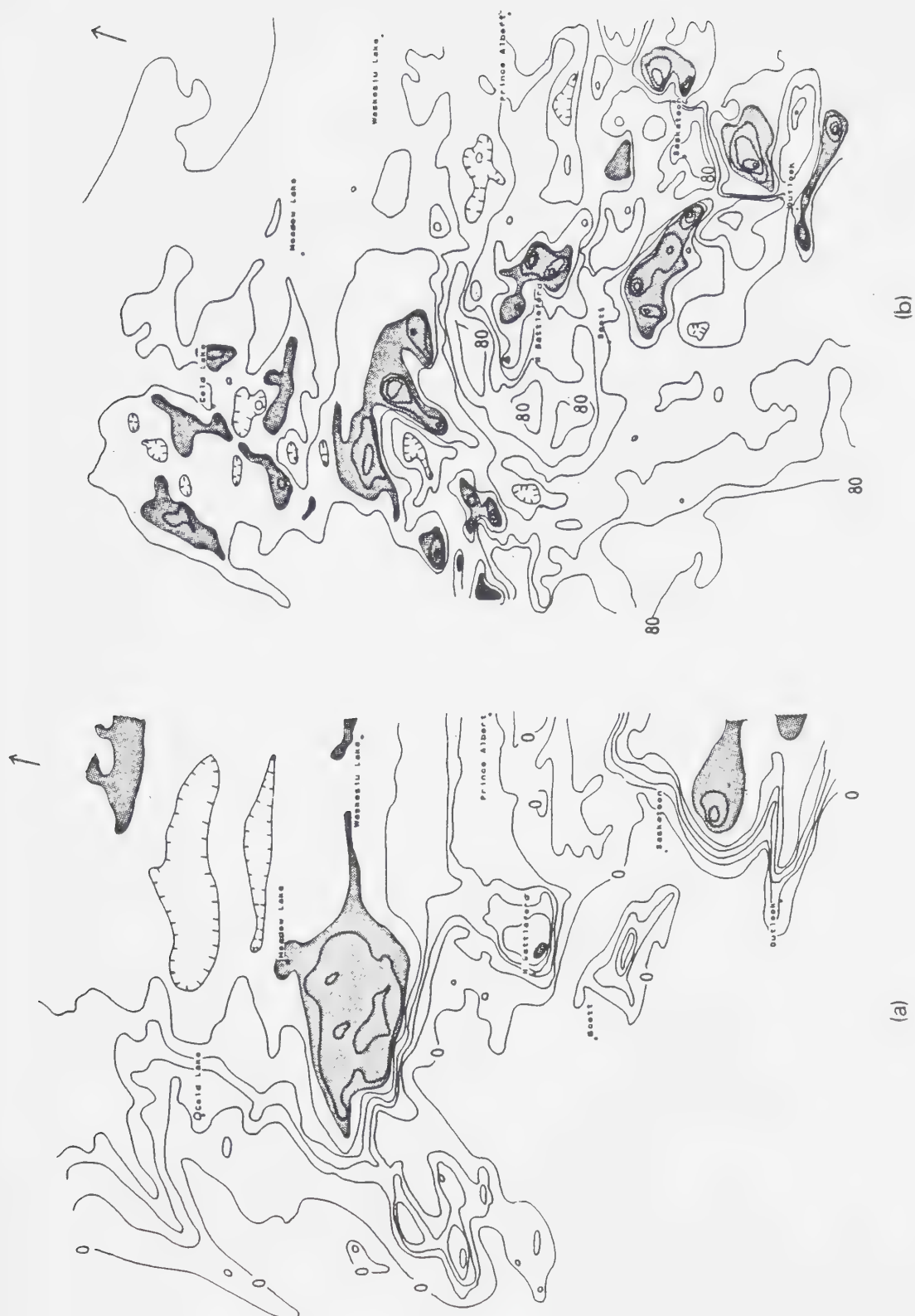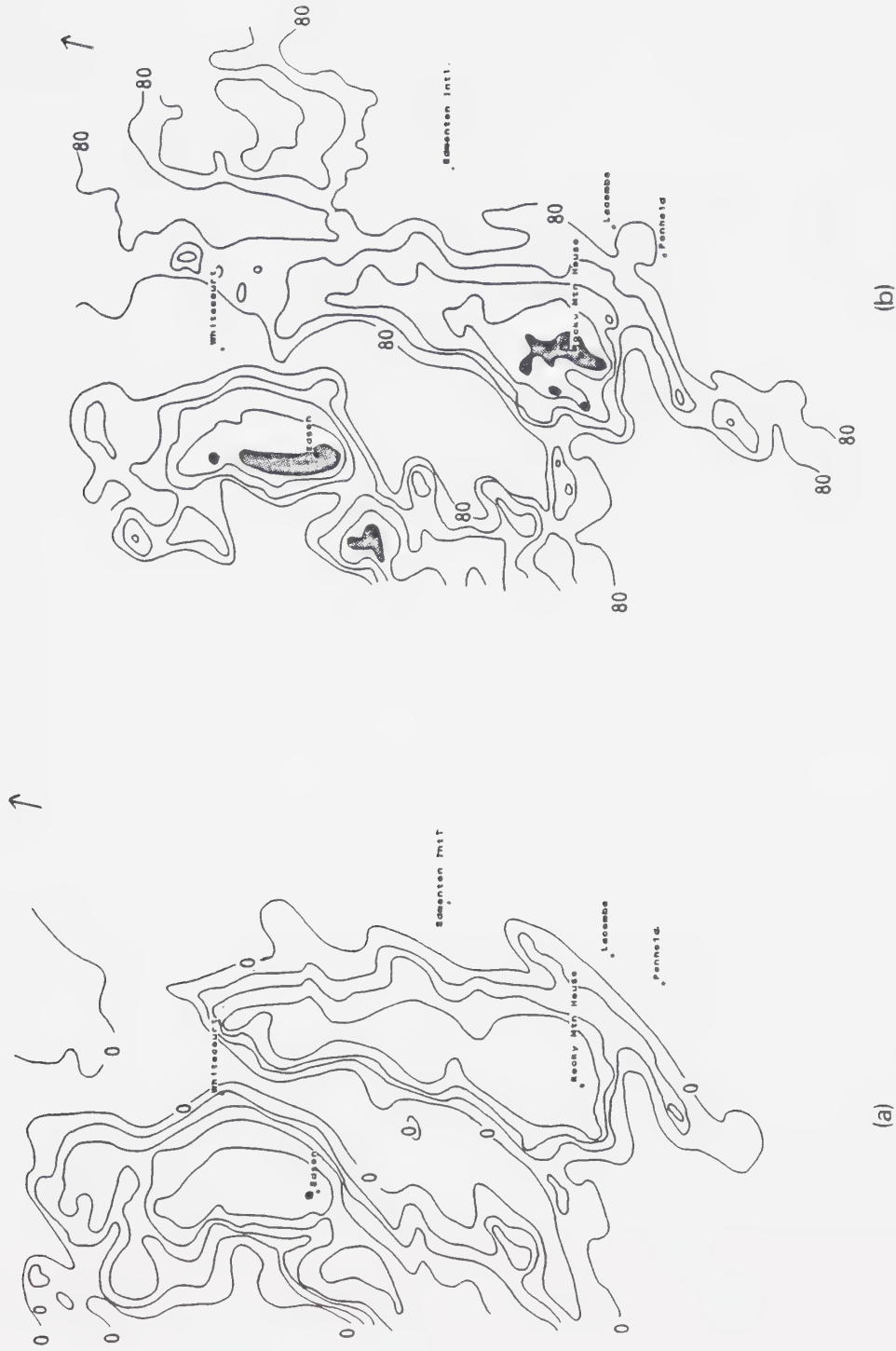
Figure 4.15   As in Figure 4.14 except over western Alberta

4.2.8 August 21 1979

The first satellite pass was at 21:00 GMT. From the temperature and brightness maps, given in Figure 4.16, a small Cb is evident 55km northwest of Lethbridge with a cloud-top minimum temperature of -54°C and maximum brightness of 161.

By the time of the second pass, at 22:40 GMT, considerable changes have occurred. The temperature and brightness maps in Figure 4.17 show a very cold cloud mass of low brightness covering southern Alberta. The coldest area lies close to the position of the Cb noted from the first pass, with a temperature of -64°C and brightness of 140. If this is the same cell as on the first image, then it has moved very little indeed. While the 500mb flow, as shown in Figure 4.18 is quite slack, it is unusual for a Prairie convective storm to remain stationary for over 100 minutes. More likely, the Cb noted from the first pass drifted southeast while a new cell developed in its place. The temperature and brightness over Lethbridge at 22:40 GMT are -55°C and 127, respectively while the highest brightness values in southern Alberta (155) are 15km south of Lethbridge. It is suggested that this is the remnant of the Cb seen at 22:00 GMT. The large increase in the area covered by cold clouds with decreasing brightness suggests that the storm is in its dissipating stage. Consequently, any rain received at Lethbridge should have fallen between passes. This is confirmed by the rain data.

Lethbridge received 10.4mm of rain from 21-22 GMT. The weather reports, given in Table C.5, show that a light shower was first reported at 21:14 GMT, and precipitation continued until 22:44 GMT. Although no heavy rain was reported, it must of occured between 21:14 and 22:00 GMT, probably towards the latter half of this period, as heavy showers surrounded the station at 22 GMT. Unfortunately, the Lethbridge observer did not indicate the shower's direction of movement.

Estimation of cloud-top temperature and brightness over Lethbridge requires interpolation between the two satellite passes, to correct for the storm's evolution. This cannot be done accurately, as the development is not a linear process, nor is it known exactly when the rain occured. However, some "educated guesses" can be made.

From Figure 4.16, the temperature gradient of the cell does not flatten out until the -40°C contour. On the temperature map for 22:40 GMT, this occurs in the range of -50°C to -55°C. Assuming that the precipitation is not associated with the tight

temperature gradient on the boundary of the cloud, then the cloud-top temperature was most likely in the range -40°C to -55°C when rain was observed. As noted previously, the rate of change of cloud-top temperature is more rapid in the early stages of the cell's development. As the heavy precipitation fell after the first pass, the associated temperature should be a good deal lower than -40°C, because the storm was still growing and the temperature decreasing. Similarly, as the rain ended before the second pass, the temperature over Lethbridge during the rain would be slightly higher than -55°C. Also, as the rain occurred closer to the time of the second pass, the temperature should be toward the colder half of the range given above. As a rough estimate, then, the temperature over Lethbridge while reporting precipitation is assumed to be in the range of -47°C to -52°C.

Brightness is even more difficult to estimate. The temperature field is relatively straight-forward. Cloud-top temperatures become progressively lower towards the centre of the cloud. The same can not be said of brightness (see Figure 4.17) as values fluctuate throughout the cloud area, with the highest values south of Lethbridge. Most likely, the brightness was in the 140-150 range (as the minimum and maximum values over two pictures are 130 and 160). However if the area of higher brightness south of Lethbridge passed over the station, then the range given above is an underestimate.

Even if all of the above is correct, it is still unknown if Zone 1 or 2 would have passed over Lethbridge. Obviously this case is of limited usefulness. Be that as it may, the final estimates of temperature and brightness over Lethbridge during the heavy rain are -47°C to -52°C and 140 to 150 respectively.

Figure 4.16   As in Figure 4.1 except for August 21, 1979 at 2100 GMT. Shading indicates areas of T < -40°C or B > 140.

Figure 4.17   As in Figure 4.16 except at 2240 GMT.

500MB ANALYSIS
HEIGHTS AND VORTICITY
2400Z 21 AUG 1979

21 AUGUST 1979

S/W TROUGH PASSAGE:

S/W RIDGE TIME:

CONVECTIVE DAY CATEGORY: 0

TOTAL HAIL REPORTS:

MEDIAN HAIL TIME: N/A

SURFACE ANALYSIS
2400Z AUG 21 1979
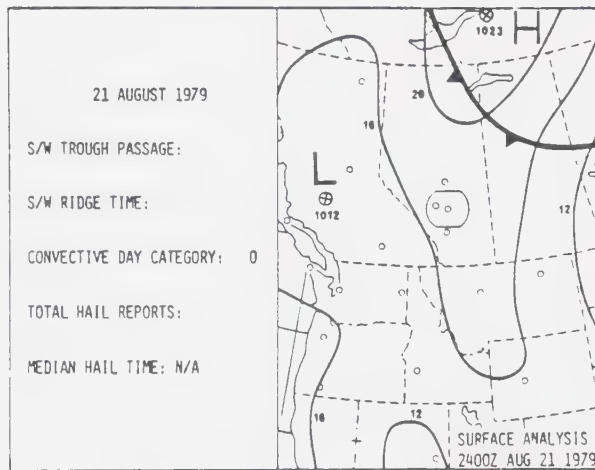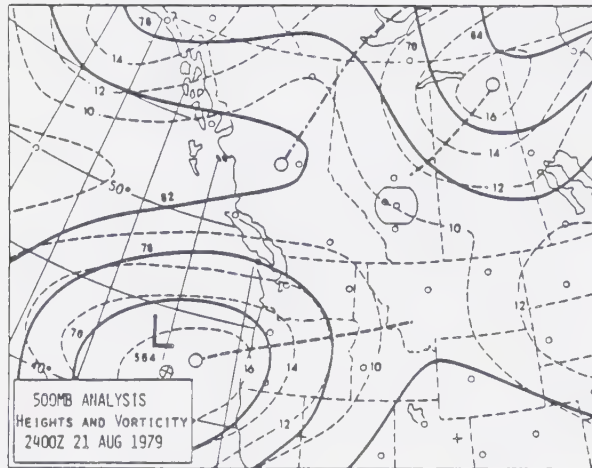
Figure 4.18   500mb and surface maps for August 21, 1979 at 2400 GMT.

4.2.9 July 01 1982

The two satellite passes for this day were at 20:30 GMT and 22:10 GMT; respective temperature and brightness maps are given in Figures 4.19 and 4.20.

A very large storm is seen to be moving east-northeast over southern Alberta. Between passes, minimum cloud-top temperatures drop from -59°C to -63°C. Brightness decreases dramatically from a large area with values > 160 (maximum of 170) to only a small area with values > 150 with a maximum of 153.

This storm dumped more than 66mm of rain on Lethbridge in less than one hour before moving eastward and giving Vauxhall 26.2mm from 20-21 GMT and Brooks 21.5mm in the next hour. As seen on Figure 4.19, the temperature and brightness over Vauxhall are -49°C and 157, but, less than 30km away, along the storm's track, the temperature and brightness are -58°C and 168, respectively. It is assumed that Zone 1 of the cell passed over Vauxhall and that the latter quoted temperature and brightness values are associated with the rain. From Figure 4.20 Brooks is seen to be directly below the storm. The temperature and brightness are -58°C and 147, though brightness values of 150 are just to the east.

This is a straight-forward example of a large well-defined storm. Its velocity is approximately 55km/hr toward the east-northeast. Considering the large rainfall at Lethbridge and the fact that point accumulations of over 20mm were produced for at least 2½ hours, this must be judged as a severe storm.

It is also of interest to note that Calgary, on the 20:30 GMT satellite image, is under the storm's anvil in an area that is both cold (-56°C) and bright (162), but no rain was observed. This illustrates that temperature and brightness alone are insufficient predictors of rainfall.
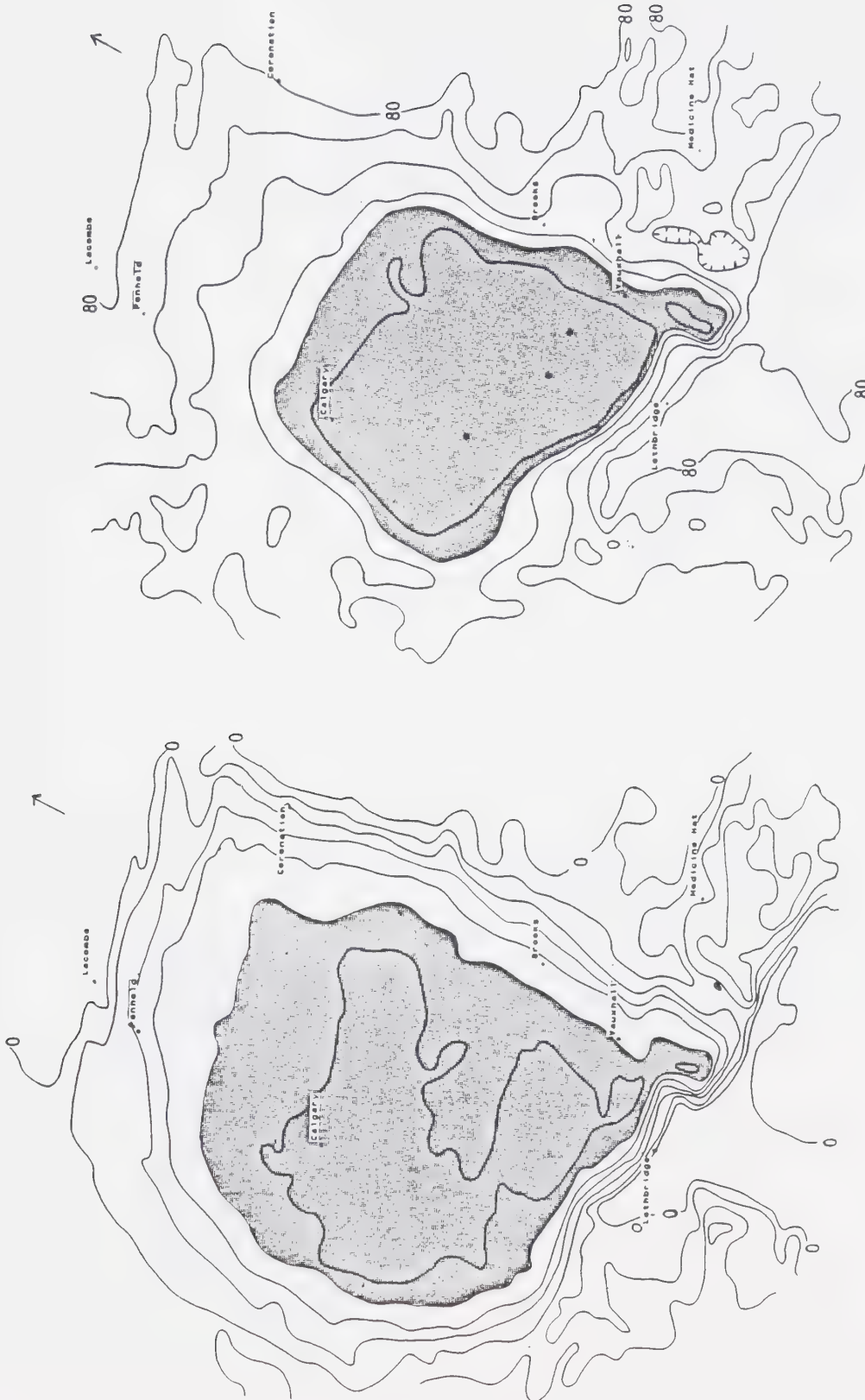
(a)

(b)

Figure 4.19   As in Figure 4.1 except for July 01, 1982 at 2030 GMT.
Shading indicates areas of T < -50°C or B > .150.

(a)

(b)

Figure 4.20   As in Figure 4.19 except at 2210 GMT.

4.2.10 July 10 1982

The satellite passes were at 20:30 GMT and 22:10 GMT. Coronation received 11.0mm of precipitation from 22-23 GMT. The surface weather observations, given in Table C.6, show that heavy rain began at 22:40 GMT and subsided by 23:00 GMT. Figure 4.21, the temperature contour map at 22:10 GMT, shows that there are two cells west of Coronation, with minimum temperatures of -55°C and -41°C. As it is not possible to determine which of these cells gave Coronation its rain, no further consideration is given to this case.

Figure 4.21   Temperature contour map for July 10, 1982 at 2210 GMT.
Shading indicates areas of T < -40°C

4.2.11 July 14 1982

At 21:20 GMT, many Cb's covered Alberta and Saskatchewan as shown on the temperature and brightness maps given in Figures 4.22 and 4.23. Those in Alberta are embedded in a large cloud mass. The second pass, at 22:55 GMT, viewed only western Alberta, as can be seen from temperature and brightness maps given in Figure 4.24. There is little continuity in cloud pattern between passes, in that individual cloud areas cannot be followed from one image to the next. However, it is known that cloud continued to move into northwest Alberta from British Columbia, resulting in 75-100mm of rain over the Smoky River Basin, north-west of Grande Prairie.

Underneath this cloud mass, heavy rain fell at both Grande Prairie and Edson. Weather reports for the two stations are given in Table C.7. At Edson, continuous rain and stratiform clouds dominated the weather, indicating a synoptic-scale disturbance. Grande Prairie, on the other hand, experienced lightning and thunder with moderate or heavy rain reported for almost 7 hours, beginning at 15:30 GMT. Most probably, the rain was due to a combination of a synoptic disturbance with embedded Cb's, resulting in continuous rain of varying intensity.

Since the rain at Grande Prairie and Edson is not the result of convective activity alone, these two cases are not suitable for inclusion in this study. From Figure 4.23, the cloud over Edson was neither very cold nor very bright. This indicates that the temperature and brightness threshold values used to infer heavy rain will be quite different for convective and synoptic-scale situations.

There were 3 other locations which recorded > 10mm of precipitation on this day. Vegreville received 12.5mm from 20-21 GMT. Figure 4.23 shows a small bright cloud slightly north-northeast of Vegreville. The cloud-top temperature and brightness are -59°C and 164 respectively, although over Vegreville the values are only -47°C and 160. The temperature gradient is very tight. After shifting the cloud by 10km (the uncertainty in position) the cloud tops over Vegreville could be as cold as -55°C, with brightness essentially unchanged. The movement of the cloud is unknown. However, a general easterly motion would place Vegreville under Zone 1 or 2 of the cloud, with the latter more likely.

In Saskatchewan, Outlook is seen to be under Zone 1 of a large cell with a temperature and brightness of -60°C and 154, respectively. Brightness values over 160 are only slightly to the west. Unfortunately, the hourly rain data are missing. The 24 hour rainfall total was 24.0mm. Slightly to the southwest, the same storm gave Elbow 23.8mm from 22-23 GMT and 24.2mm over 24 hours. Given this situation, it seems reasonable to assume that the 24 hour accumulation of 24.0mm recorded at Outlook was also due solely to the passage of this one storm. Elbow would have passed under Zone 1 of the storm and, if no drastic evolution took place, the temperature during rainfall would have been -55°C to -58°C with brightness in the range 155-170.

Saskatoon Airport, crossed by Zone 2 of the storm, received 5.4mm of rain between 22-23 GMT. The temperature and brightness associated with this rain would be -55°C to -57°C and 155-160 respectively. Nearby Saskatoon Water received 4.8mm in the same time period, and with the same temperature and brightness values.

Further south, a small cell is seen to lie over Moose Jaw. The temperature and brightness overhead are -54°C and 145, respectively. However, the extreme temperature and brightness values are only 10km to the south-west, at -58°C and 165. The cloud is very small and were it shifted northwards by 10km, it would miss Moose Jaw entirely.

Only 0.7mm of rain was observed from 21-22 GMT. The weather observations, given in Table C.7, report light rain-showers from 20:12 GMT to 23:00 GMT with a thundershower at 21:17 GMT. Since there is no special report noting the end of the thunderstorm, it is assumed that this is an oversight on the observer's part and not simply a missing report. Mammatus, a sign of intense convective activity, was observed with this storm as well.

There is no doubt that the cloud over Moose Jaw was a Cb. As little rain was reported, this is an example of a cold, bright cloud that did not produce any significant rain, at least not at the time it was in the satellite's field of view. While it is possible that heavy rain associated with the storm just missed the station, this does not seem to be the case as the observations give no indication of heavy showers nearby. It is noted, however, that only 20km to the west, Caron received 6.0mm on this day. No other nearby station reported more than 2.0mm, consistent with the small size of the storm.

Figure 4.22   As in Figure 4.1 except for July 14, 1982 at 2120 GMT.
Shading indicates areas of T < -50°C or B > 150.
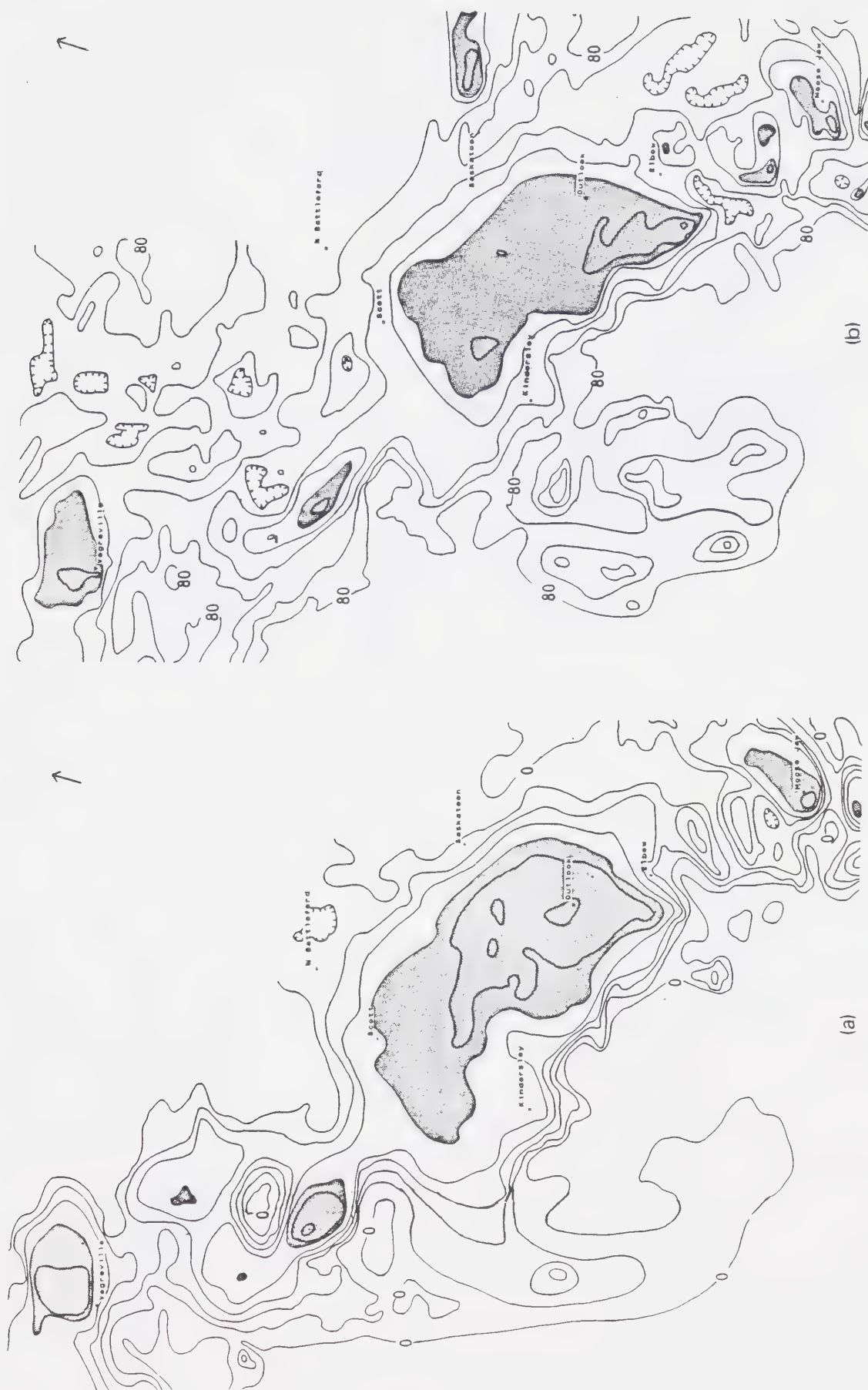
Figure 4.23   As in Figure 4.22 except over western Alberta.

Figure 4.24   As in Figure 4.23 except at 2250 GMT.

4.2.12 July 16 1982

Figure 4.25 gives the temperature and brightness maps for the 20:55 GMT satellite pass. A large, cold, bright cloud consisting of two cells is seen to cover much of southeastern Saskatchewan. This cloud moved northeast and gave 75-100mm of rain near Duck Mountain, in eastern Manitoba.

TBRG data are available for Regina and Indian Head PFRA, both of which would be under Zone 2 of the storm.

Regina received 2.6mm from 20-21 GMT. The weather observations, given in Table C.8, show that a moderate shower occurred at 20:37 GMT. At 21:00 GMT, heavy showers were observed north to southeast of the station. Indian Head received 6.9mm from 20-21 GMT and another 10.4mm from 21-22 GMT. However, no accurate timing of the precipitation is possible and it is not known if the 17.3mm total is the result of one or two periods of rain Consequently, Indian Head is not included in the sample. The temperature and brightness over Regina are -55°C and 162, respectively. It should be noted also that a northeasterly cloud motion would have taken Zone 1 of the western cell over Indian Head and could have produced the heavy rain from 21-22 GMT.

(a)

(b)
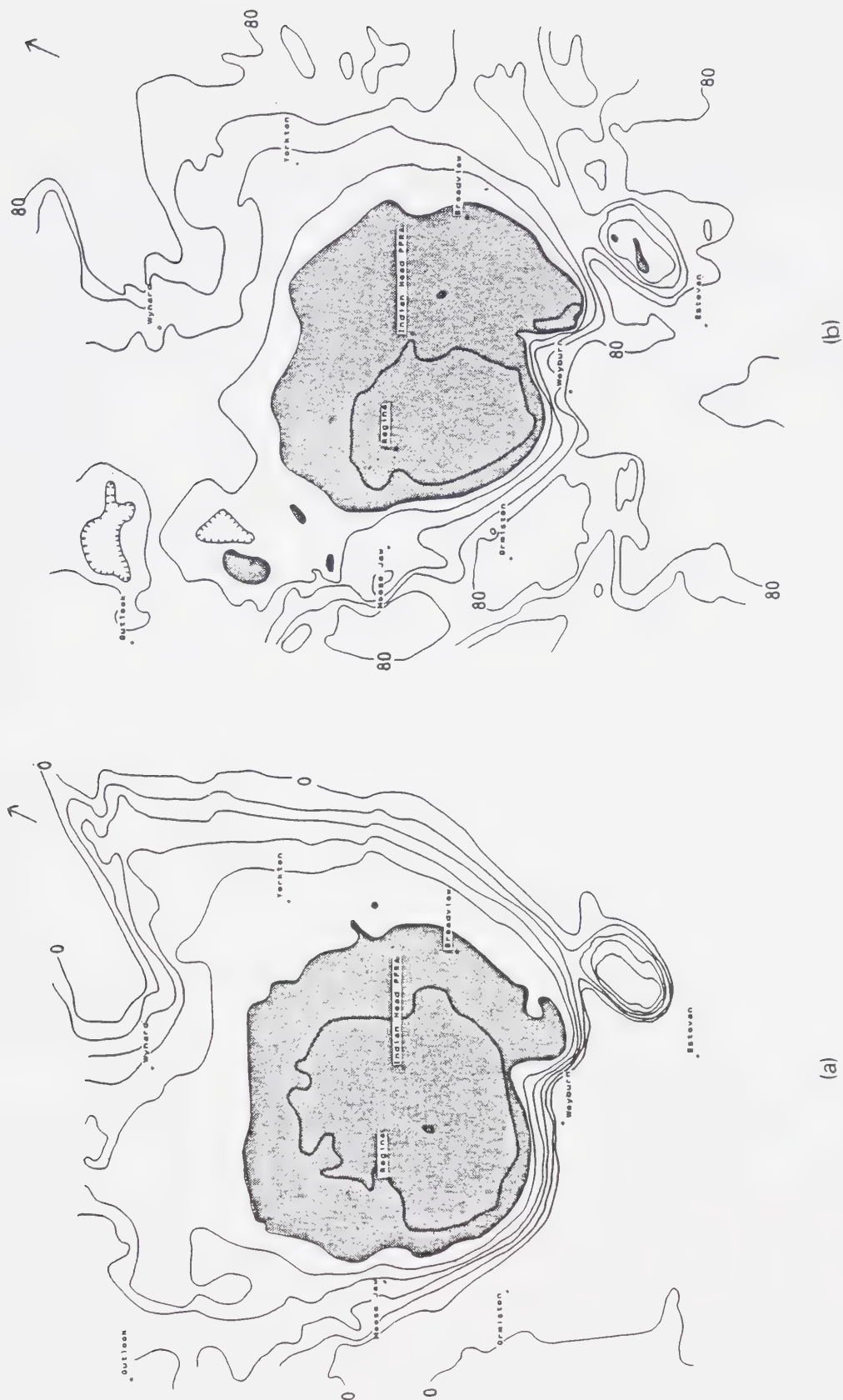
Figure 4.25   As in Figure 4.1 except for July 16, 1982 at 2055 GMT.
Shading indicates areas of T < -50°C or B > 140.

4.2.13 July 18 1982

Temperature and brighness contour maps for the first pass, at 20:35 GMT, are given in Figure 4.26 and 4.27. A bright cell lies just northeast of Cluff Lake, in northwestern Saskatchewan. The temperature and brightness figures over Cluff Lake are only -29°C and 141, but 10km to the north-east the respective values are -49°C and 152. The centre of the cloud is 35km northeast of the station.

Temperature and brightness maps for the 22:15 GMT pass are shown in Figure 4.28 and 4.29 The cell near Cluff Lake has moved northeast at approximately 60km/hr to lie south of Uranium City. Its temperature and brightness have both decreased. Another cell now lies just to the northwest of Cluff Lake with a temperature and brightness of -54°C and 148, respectively.

Cluff Lake received 10.0mm of rain between 19-20 GMT. This is consistent with precipitation falling from the cell shown on the 20:35 contour maps. It is also noted that 2.6mm were received from 21-22 GMT. This might be related to the cloud north of Cluff Lake shown in Figure 4.29. However, this second period has not been included in the sample.

Other stations in the area reported less than 10mm. However, North Battleford and Cold Lake were in the path of large cells. It is seen on Figure 4.26, that Cold Lake lies under Zone 1 of a large cloud mass. The temperature and brightness within 10km are -43°C and 154, respectively. Colder and brighter values (-47°C, 158) prevail 35km to the northwest. This cell moved northeast at 55km/hr and, as seen in Figure 4.28, temperatures are only slightly higher at the time of the second pass, while the brightness has decreased to 120.

The hourly rain amounts are missing for this day. The 24-hour total was 16.2mm, but how much of this amount came from this cell is unkown. The weather observations for 19-23 GMT are given in Table C.9. Outside of this period, only a few light rain showers were reported. It is seen that moderate or heavy rain occurred for almost the entire hour from 20-21 GMT. Using 5mm/hr as an average rate for the moderate rain, and 10mm/hr for the heavy rain leads to an estimate of 8mm during this hour. This is likely an underestimate as heavy rain during convective showers is often much greater than 10mm/hr. The only other period of moderate rain was 19:33-20:00 GMT. Assuming

2.5mm of rain in this period and 2.5mm during the rest of the day (excluding 20-21 GMT) implies 11mm may have fallen from 20-21 GMT. Accordingly, the rainfall total for the hour is estimated to be 8-11mm.

One of the coldest cells seen on the 22:15 GMT image lies east of North Battleford with cloud-top temperatures as low as -58°C. The cell is not very bright, however, with only a few pixel values greater than 140. One bright patch is only 20km east of North Battleford and may have passed over the station. It is not certain where this cell originated. From the 20:35 GMT contour maps it would appear to be due to the intensification of the small cell that is 35km west of North Battleford. Assuming this to be true, then the bright patch would have passed over North Battleford at 21:20 GMT with an estimated temperature and brightness of -51°C ±3°C and 145-150, respectively. This area is quite small, less than 10km in diameter, which is of the same order as positioning uncertainties. Consequently, either Zone 1 or 2 of the cloud could have passed over the rain gauge. North Battleford received 5.8mm from 21-22 GMT with 5.0mm in only 5 minutes. From the weather reports, given in Table C.9, the heaviest precipitation occurred at 21:32 GMT, very close to the estimated time that the bright area passed over the station.
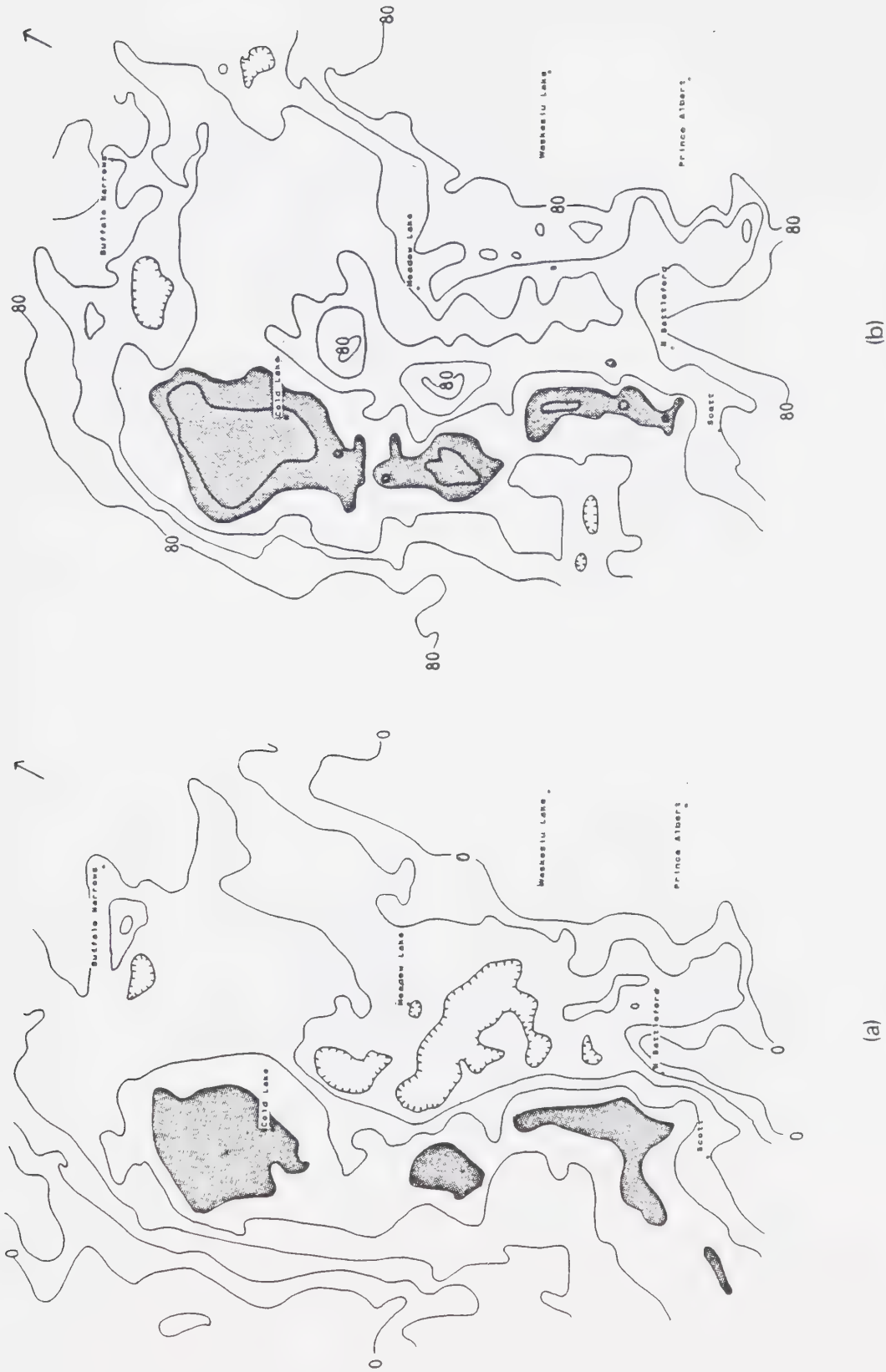
Figure 4.26　As in Figure 4.1 except for July 18, 1982 at 2035 GMT. Shading indicates areas of T < −40°C or B > 140.

Figure 4.27   As in Figure 4.26 except over northern Saskatchewan.
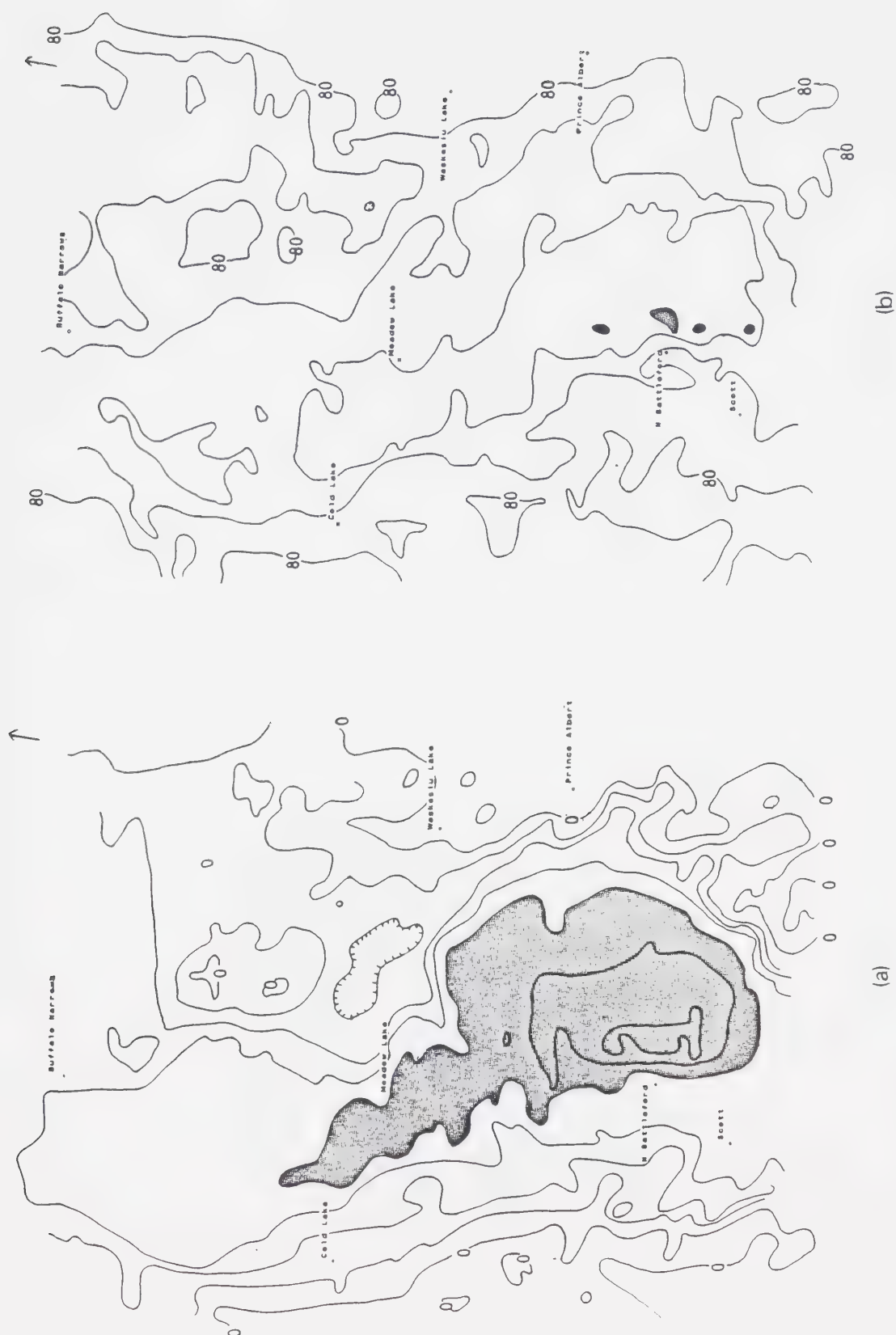
Figure 4.28   As in Figure 4.26 except at 2215 GMT.
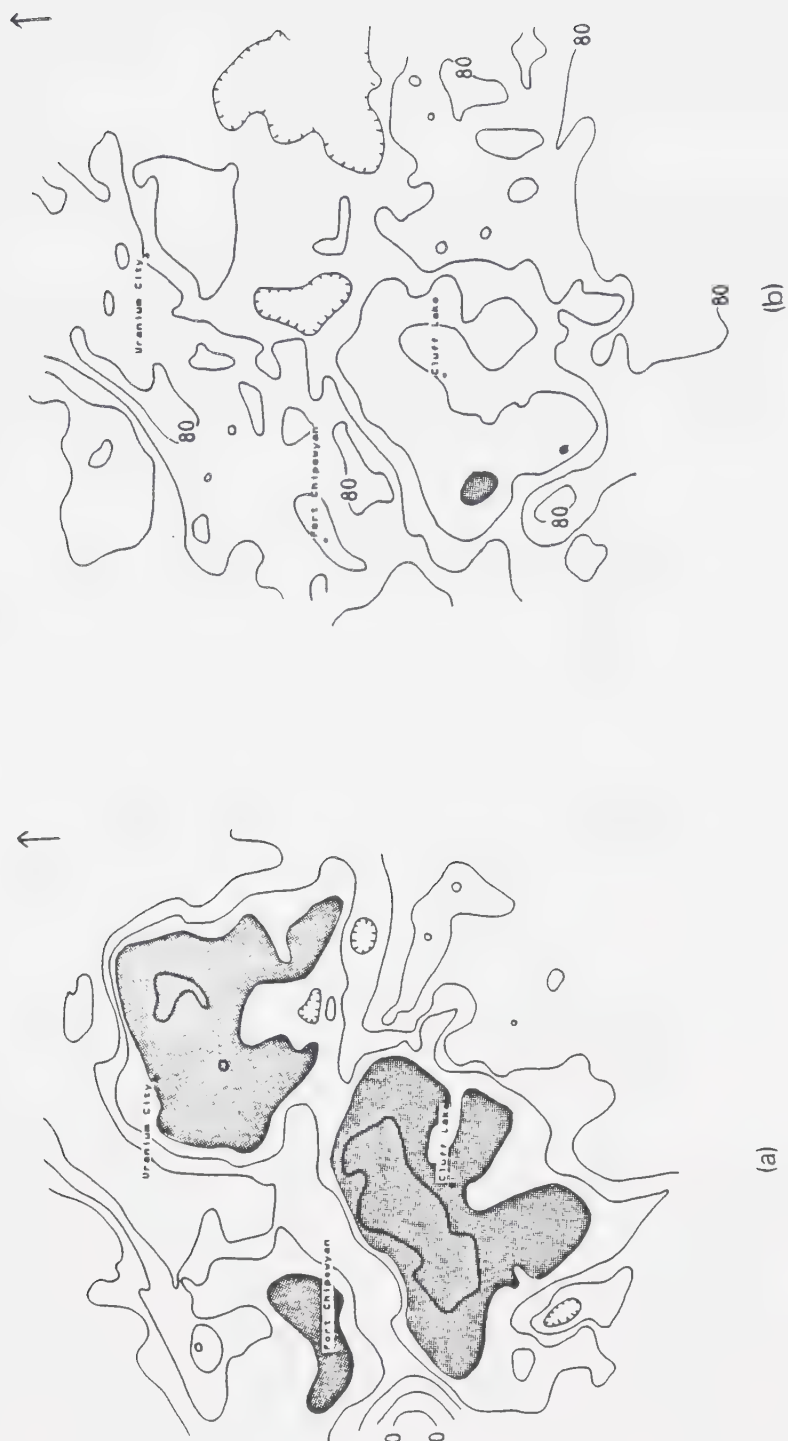
Figure 4.29   As in Figure 4.28 except over northern Saskatchewan.

4.2.14 August 11 1982

The temperature and brightness maps for the first satellite pass at 20:50 GMT are given in Figure 4.30. Numerous cells are evident over central Alberta. Rocky Mountain House lies under Zone 1 of one of these clouds, with overhead temperature and brightness values of -49°C and 147, respectively. Minimum temperatures of -53°C lie 15km to the north.

Considerable change has occured between the two satellite passes, as seen from the temperature and brightness maps for 22:30 GMT, displayed in Figure 4.31. The anvils of some cells have merged, while others have decayed and are no longer visible. Overall, brightness over central Alberta has decreased. The area of temperatures < -50°C that was near Rocky Mountain House earlier has moved east-southeast at 45km/hr to north of, and over Lacombe.

Rocky Mountain House received 9.7mm of rain from 20-21 GMT. The weather reports, given in Table C.10, show that the heaviest precipitation began at 20:20 GMT, which is 30 minutes before the satellite pass. After adjusting the cloud position for this time difference, the temperature and brightness over the station is -47°C and 145 respectively. These are the final values adopted as associated with the rainfall, without any correction for possible evolution of the cloud. The temperature and brightness over Lacombe, from Figure 4.31 are -50°C and 134 respectively. An area of higher brightness lies south of Lacombe, but there is no evidence it passed over the station. Because of the great amount of cirrus debris it is not possible to discern the location of the convective core. Based on extrapolation from the first satellite pass, either Zone 1 or 2 of the Cb may have passed over Lacombe.

The hourly rain data for Lacombe shows that 5.4mm fell from 22-23 GMT and a further 4.0mm from 23-24 GMT, with a total of 7.7mm in less than one hour. It would appear that the same cell that gave the heavy rain to Rocky Mountain House is also responsible, in part, for the rain at Lacombe. However, the area of temperatures less than -50°C has almost passed Lacombe at 22:30 GMT and yet 4.0mm was reported from 23-24 GMT. It may be that the small, cold, bright cloud near Rocky Mountain House at 22:30 GMT intensified while moving eastward and resutled in some of the 23-24 GMT precipitation at Lacombe. The amount ascribed to the 23-24 GMT period is, therefore,
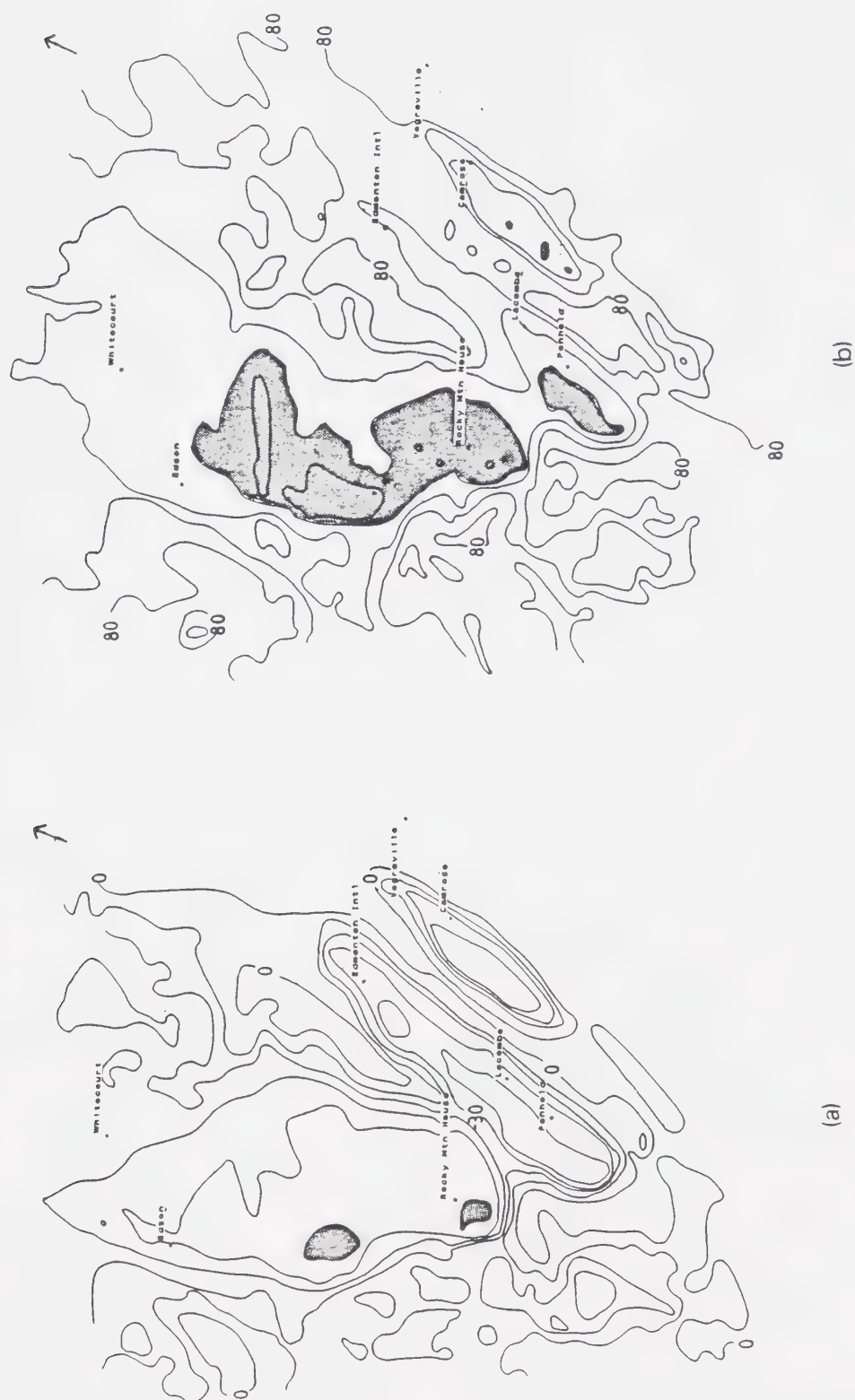
Figure 4.30   As in Figure 4.1 except for August 11, 1982 at 2050 GMT.
Shading indicates areas of T < -50°C or B > 140.

(a)

(b)

(a)

(b)

Figure 4.31   As in Figure 4.30 except for 2230 GMT.

5.4-7.7mm.

4.3 Summary

A summary table for all cases is given in Table 4.2. This includes cloud-top temperatures and brightness values, precipitation amounts and the cloud zones which passed over the station. Table 4.3. presents the duration and intensity of precipitation where this could be obtained from the TAB31 charts.

Table 4.2   Rain Accumulations,
Cloud Top Temperature (T) and Brightness (B)
For Case Studies Discussed in Chapter 4

Date	Station	Rain (mm)	T (°C)	B (counts)	Zone
07/07/79	Edson	11.1	-53	170	1
10/07/79	Edson	11.3	-49	156	1
	Penhold	2.6	-42	178	3
	Rocky Mtn House	0.8	-38	165	3
	Swift Current A	3.9	-49	153	2-3
	Saskatoon	10.0	-52	165	1
	Outlook	6.1	-45±5	160	1-2
11/07/79	Edmonton	10.3	-48±8	165	1
15/07/79	Outlook	11.7	-48±8	155±5	1
29/07/79	Calgary	10.0	-48	168	1
05/08/79	Cold Lake	24.0	-57	153	1-2
	Edson	14.1	-50	156	1
	Rocky Mtn House	0.7	-35	155	1
21/08/79	Lethbridge	10.4	-49±2.5	145±5	1-2
01/07/82	Vauxhall	26.2	-58	168	1
	Brooks	21.5	-58	150	1
	Calgary	0.0	-56	162	3
14/07/82	Vegreville	12.5	-55	164	2-1
	Outlook	24.0	-60	154	1
	Elbow	23.8	56.5±2.5	163	1
	Saskatoon A	5.4	-56±1	158	2
	Saskatoon W	4.8	-56±1	158	2
	Moose Jaw	0.7	-58	165	1
16/07/82	Regina	2.6	-55	162	2
18/07/82	Cluff Lake	10.0	-49	152	1
	Cold Lake	9.5+2.5	-43	154	1
	N Battleford	5.0	-51±3	148	1-2
11/08/82	Rocky Mtn House	9.7	-47	145	1
	Lacombe	6.5+1	-50	134	2-1

Table 4.3   Precipitation Amounts and Intensities
From the Monthly Rain Gauge Summaries   (TAB31)

Date	Station	Duration (min)	Amount (mmx10)	Intensity (mm/hr)
07/07/79	Edson	5	56	65
		10	58	35
		15	81	32
		30	113	23
10/07/79	Saskatoon	5	65	78
		10	86	52
		15	106	42
15/07/79	Outlook	5	82	98
		10	95	57
		15	117	47
29/07/79	Calgary	5	29	35
		10	44	26
		15	55	22
		30	81	16
		60	101	10
05/08/79	Cold Lake	5	96	115
		10	174	104
		15	204	82
		30	240	48
	Edson	5	118	142
		10	141	85
21/08/79	Lethbridge	5	32	38
		10	63	38
		15	95	38
		30	104	21

Table 4.3   (con't)

Date	Station	Duration (min)	Amount (mmx10)	Intensity (mm/hr)
01/07/82	Brooks	5	81	97
		10	110	66
		15	153	61
		30	212	42
	Vauxhall	5	66	79
		10	130	78
		15	192	77
		30	246	53
14/07/82	Elbow	5	101	121
		10	157	94
		15	220	88
		30	237	47
18/07/82	N Battleford	5	50	60
11/08/82	Rocky Mtn House	5	44	53
		10	55	33
		15	69	28
		30	87	17
		60	97	10
	Lacombe	5	27	32
		10	37	22
		15	48	19
		30	54	11
		60	77	8

5. Results

5.1 Introduction

An attempt will now be made to relate cloud-top temperature and brightness to precipitation, based on the case-studies given in the previous chapter. The interpretation of results presents its own difficulties and these too will be explained. Before proceeding, a warning with regard to the scope of this chapter is in order. The number of cases are few, the sample biased and many assumptions had to be made to estimate cloud-top temperatures and brightness. Consequently, it is unreasonable to expect the quality of data used here to reveal, in any great detail, the relationship between temperature or brightness to precipitation, should one exist. Instead, the goal is to develop some broad guidelines that can be used to distinguish heavy rain events.

The trend of precipitation amounts versus temperature and brightness can be seen from Figure 5.1. This gives the average precipitation amount (rounded up to the nearest ½mm) for various ranges of temperature and brightness for "Zone 1" cases only and "precipitation > 10mm" cases, as taken from Table 4.2. The number in brackets, below the amount, is the number of storms in that range. Three storms have been excluded because of their large temperature uncertainty: Outlook on July 14 and 15, 1979 and Edmonton on July 11 1979. Also, Vauxhall and Brooks on July 01, 1982 and Elbow and Outlook on July 14 1982 have been kept as seperate cases. It should be noted, though, that for the days given above, the precipitation at the two stations resulted from the same storm so that these are not independent cases. Figure 5.1a and b each contain 14 points with an overlap of 10 cases between the two.

The trend is very clear. Precipitation amounts increase with decreasing temperature. For all cases for which there was > 10mm (from the TBRG hourly amounts) the temperature is < -45°C. Changes in brightness do not seem to be correlated with precipitation except that a low cut-off is apparent. Heavy precipitation cases are all associated with brightness > 145.

These trends are now discussed in more detail, beginning with brightness.

	5.0	11.0	19.0	Average
≥165	—	10.5 (2)	17.0 (3)	14.5
155-164	1.0 (1)	12.0 (3)	—	7.5
145-154	9.5 (1)	10.0 (2)	23.0 (2)	15.0
≤144	—	—	—	

(a)

	11.0	22.0	
≥156	—	10.5 (2)	25.0 (2)	18.0
155-164	—	12.0 (3)	18.5 (2)	14.0
145-154	—	10.0 (3)	23.0 (2)	15.0
≤144	—	—	—	

| ≥-44 | -45 → -54 | ≤-55 |

BRIGHTNESS (counts)

TEMPERATURE (°C)

(b)

Figure 5.1   Precipitation amounts for ranges of cloud-top temperature and brightness for (a) Zone 1 cases and (b) heavy rain cases.

5.2 Precipitation and Brightness

A graph of precipitation amounts versus brightness for heavy rain cases is given in Figure 5.2 along with the least squares regression line. The correlation coefficient is only 0.08. Brightness values were not corrected for sun angle. Also, its rate of change is unknown so that the values adopted for those cases where the time of the satellite pass and observation of rain differed may be in error. That little correlation was found between precipitation and brightness may well be a result of these two deficiencies. All that can be said is to repeat what was noted earlier, namely that there may be a lower limit of 145 that must be exceeded for heavy rain to occur. It is also possible that this limit is not constant, but may depend on the time of year.

Attention is now turned to cloud-top temperature which, based on Figure 5.1, holds the best hope for success.

5.3 Precipitation and Temperature

5.3.1 Rain Amount and Temperature

Precipitation amounts versus temperature for Zone 1 cases and heavy rain cases are given in Figures 5.3 and 5.4, respectively. Data for the locations on July 11,14 and 15, given earlier, are excluded. Also, rain amounts and temperature for Vauxhall and Brooks (July 01, 1982) have been combined and averaged as have Elbow and Outlook (July 14, 1982).

Figure 5.3, for Zone 1 cases, exemplifies the difficulty in attempting to interpret results based on insufficient data. The regression line is given for this graph, and the correlation coefficent is 0.55, which is just significant at the 5% level. However, this value can be radically changed by the removal of only two points.

The point representing Rocky Mountain House on August 05, 1979 at (-35°C, 0.7mm) anchors the low end of the regression line. Without this point, the correlation coefficient drops to 0.37. On the other hand, Moose Jaw on July 14, 1982 represents the only example of a cold, bright cell with very little precipitation (-58°C, 0.7mm). Without this point, the correlation coefficient is 0.86, which is significant at the 1% level. It is interesting to note that none of the climate stations in the vicinity of Rocky Mountain

CLOUD-TOP BRIGHTNESS (counts)
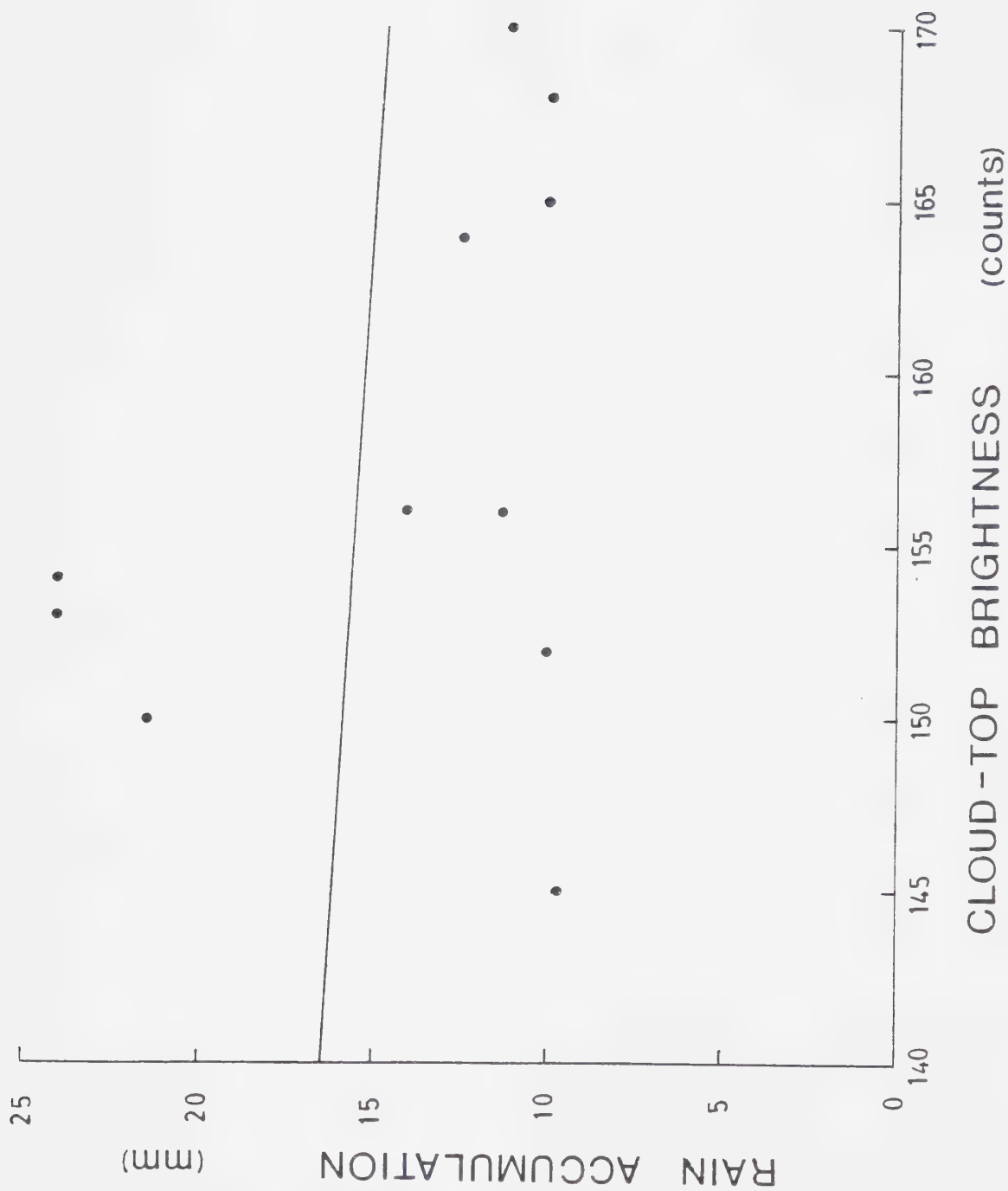
Figure 5.2   Precipitation amount versus brightness for heavy rain cases.

House reported more than 1.0mm, implying that the storm did not produce much rain. However, near Moose Jaw, 6.0mm was recorded at Caron. There is little evidence to indicate that a rain-producing cell just missed Rocky Mountain House, but this may have occurred at Moose Jaw.

Turning to Figure 5.4, the precipitation versus temperature curve for heavy rain cases (excluding Cold Lake on July 14, 1982 as the rain amount was not obtained from the TBRG records), it is seen that that there are two clusters of points. One is near (-50°C, 10mm) and the other is at (-58°C, 24mm). The correlation coefficient for this graph is 0.81, significant at the 1% level. This does not, however, take into account the uncertainties in either the temperature or precipitation measurements.

Based on Figure 5.4, then, given that > 10mm has occurred, it may be possible to infer the cloud-top temperature to within a few degrees. It is, of course, the reverse task that is of more interest, and for Figure 5.4 to prove useful in this regard, all cold, bright cells must produce rain. Stated another way, in order to have any hope of inferring heavy rain from cloud-top temperatures, it must be shown that the cloud top temperature distribution for convective storms producing heavy rain is significantly different than the population distribution for all mature Cbs. Unfortunately, the population distribution is unknown and it is not a trivial task to determine it.

Two options were considered here, neither of which proved feasible. First it was thought that the cloud-top temperature for all convective clouds viewed by the satellite on the days in the dependent sample could be used. However, there are two flaws that could lead to erroneous results:

1. some cells could be in the growing stage so that there might be a bias toward "warm" temperatures, and

2. the atmospheric conditions which produced the storms in the dependent sample might be widespread, so that cells would not be independent of each other.

An alternative is to assume that, on average, the cloud top of a mature Cb will reach the tropopause. If storms that produce heavy rain are colder than average, then the minimum cloud-top temperature should be lower than the average tropopause temperature.
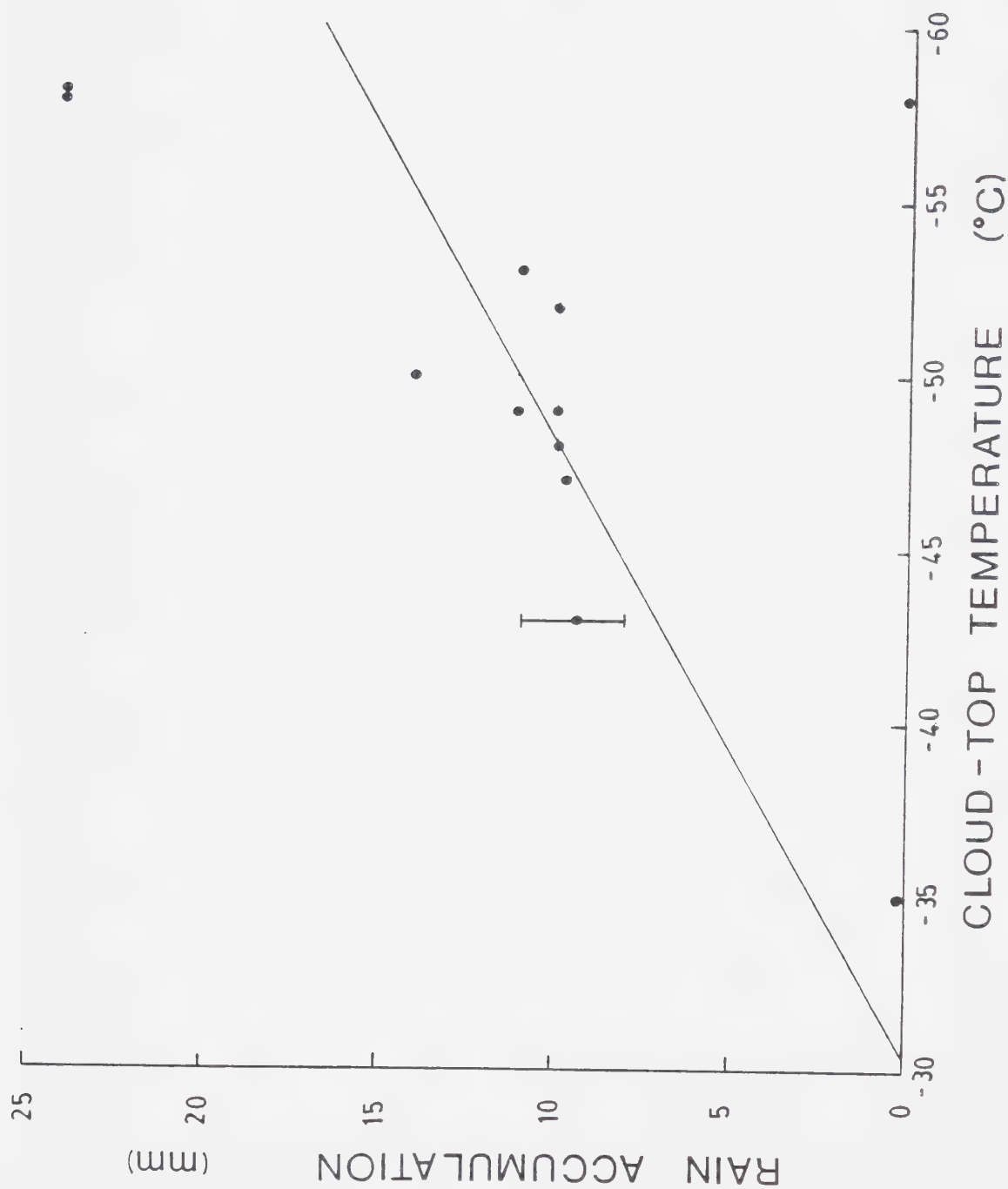
Figure 5.3   Precipitation amount versus temperature for Zone 1 cases.
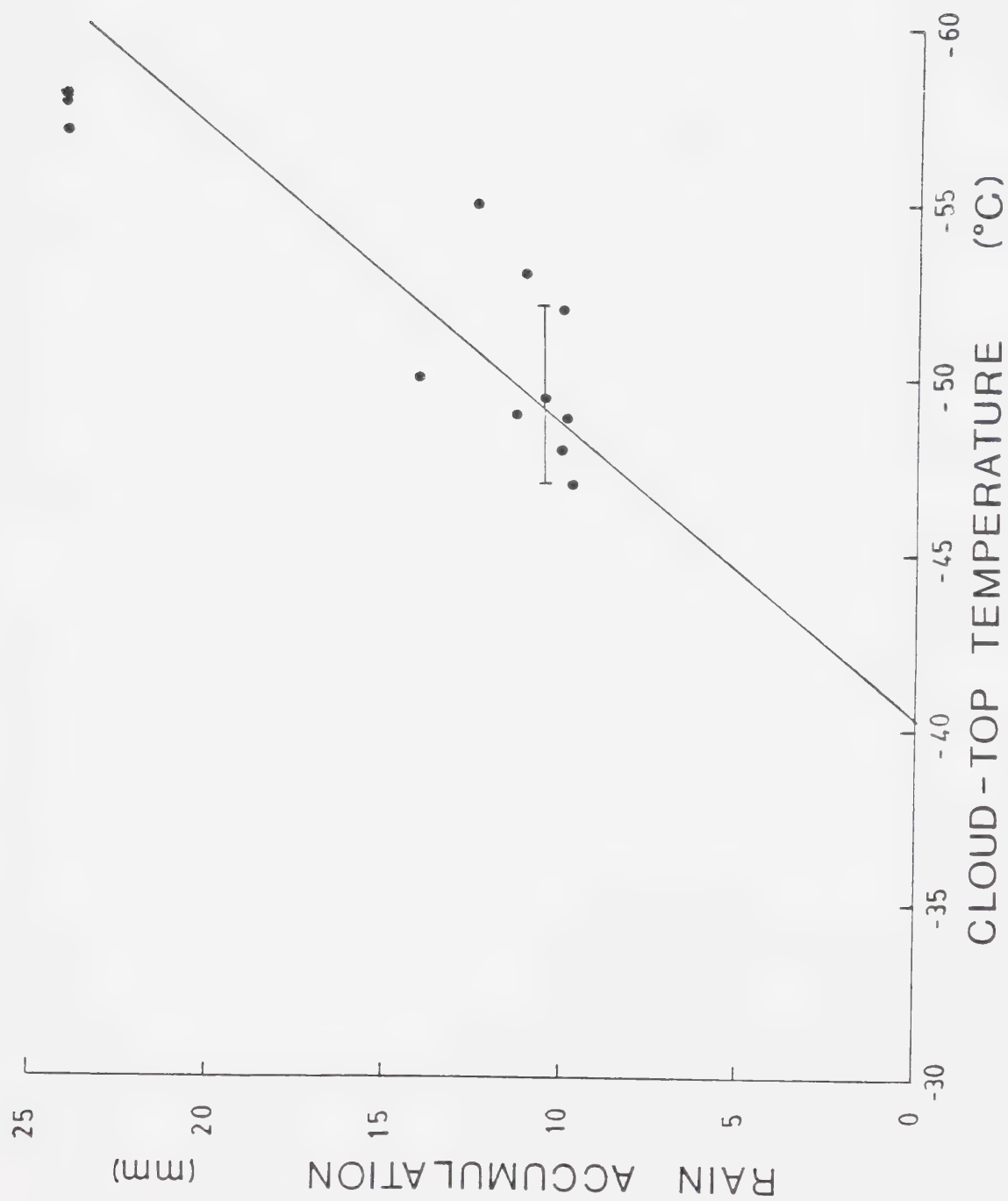
Figure 5.4   Precipitation amount versus temperature for heavy rain cases.

Tropopause temperatures are available only for Alberta at Calgary, Edmonton, Penhold and, for the summer of 1979, Rocky Mountain House. The test is, therefore, restricted only to Alberta storms which produced > 10mm of rain. Tropopause temperatures were kindly supplied by the Alberta Research Council for the summer of 1979 and 1982 (the same period as for the dependent sample). For 32 days on which Cb activity was evident on the satellite images, the mean tropopause temperature was -55°C±4°C. For only those days on which heavy rain was recorded it was -53°C±4°C, while the mean minimum cloud-top temperature of the rain-producing storms was -53°C±4°C. It cannot be said that the heavy rain-producing storms are any colder than the "average" tropopause temperature or, by extension, any colder than the average Cb. The obvious difficulty, though, is that it is unkown on how many of the 32 days selected there were heavy rainfalls. The average tropopause temperature may also be heavily biased.

The only alternative left to determine if useful estimates of rainfall can be deduced from satellite imagery is to simply test against an independent sample. This is done in Chapter 6, as will be discussed shortly.

Thus far, only rain accumulations have been considered. However, accumulation on the ground, due to the passage of a Cb, is a combination of:

1.   speed of the cloud
2.   size of the precipitating area within the cloud, and
3.   the storm's rainfall rate.

If cloud-top temperature is correlated to rain amount, it must also be related to one, or all of the above. Each possibility is now discussed in turn.

5.3.2 Temperature and Speed of Cell

For a given rain rate and rain area, the rain amount is inversely proportional to the speed of the cloud. Cell velocities could be measured directly from the satellite images for 8 of the storms investigated here. As shown in Table 5.1, the mean speed is 50±8km/hr. The uncertainty in a single measurement is given by the position error over two satellite images (20km) divided by the interval between images (100min.) or 12km/hr. The speed of the cells is, therefore, approximately constant. However, all of the storms in Table 5.1 are those that produced near 10mm of rain, so that very little useful

Table 5.1   Cell Speed as Determined From
                 Sequential Satellite Images

Date	Location	Speed (Km/hr)	Direction of Motion
07/07/79	Edson	50	towards NE
15/07/79	Outlook	50	towards SE
29/07/79	Calgary	45	towards E
18/07/82	Cluff Lake	60	towards NE
	Cold Lake	55	towards NE
	N Battleford	35	towards E
11/08/82	Rocky Mtn House	50	towards SE

Average Cell Speed   50±8 km/hr

information has been gained here. However, as there is no physical basis to expect rain amount to be related to the cloud's speed and there is no evidence here to suggest that it is, it is merely assumed that no intrinsic relationship exists.

5.3.3 Precipitation and Size of Rain Area

Recent work by Doneaud et al. (1983) and others have shown that the total rain volume (RV) is highy correlated to the area and duration over which rain occurred, as defined by the 25dbz radar echo. The latter quantity is known as the area time integral (ATI). The average rain rate over the storm's lifetime is given by RV/ATI and has been found to be approximately constant over many convective storms. The key point here is that only the area covered by the radar echo, and not the magnitude of the echo, is needed to determine the rain amount. This is consistent with the work of Lovejoy and Austin (1979b) who found that temperature and brightness could be used to determine the area over which rain was occurring, but not the instantaneous rain rate. Rain amounts could be estimated, though, using an average rain rate.

It is not possible to determine the area over which rain has occurred for the storms investigated here as the rain data are available only for a handful of sparsley distributed rain gauges. Also, the size of the heavy rain area (associated with the convective core) cannot be estimated directly from the satellite imagery, as it cannot easily be separated from the cirrus anvil in which it is embedded. However, the crucial question to be answered is: do larger rain areas result in greater rain amounts? With the appropriate assumptions this question can be addressed using the available rain data.

The duration of precipitation is given in Table 4.3. If the speed of the storm is known, and if it is assumed that a circular rain area passed directly over the rain gauge (ie. Zone 1 cases), then the diameter of the storm's precipitation area can be calculated. This also requires that the advection of the cell dominates over any changes in the intrinsic cell rain rate. According to Zawadski (1973), this is valid for time periods less than 40 minutes.

Precipitation amounts versus inferred diameter of the rain area for 10 Zone 1 cases are given in Figure 5.5. If the speed of the cell was unknown, 50 km/hr was assumed. The correlation coefficient is only 0.14. However, this includes the two points
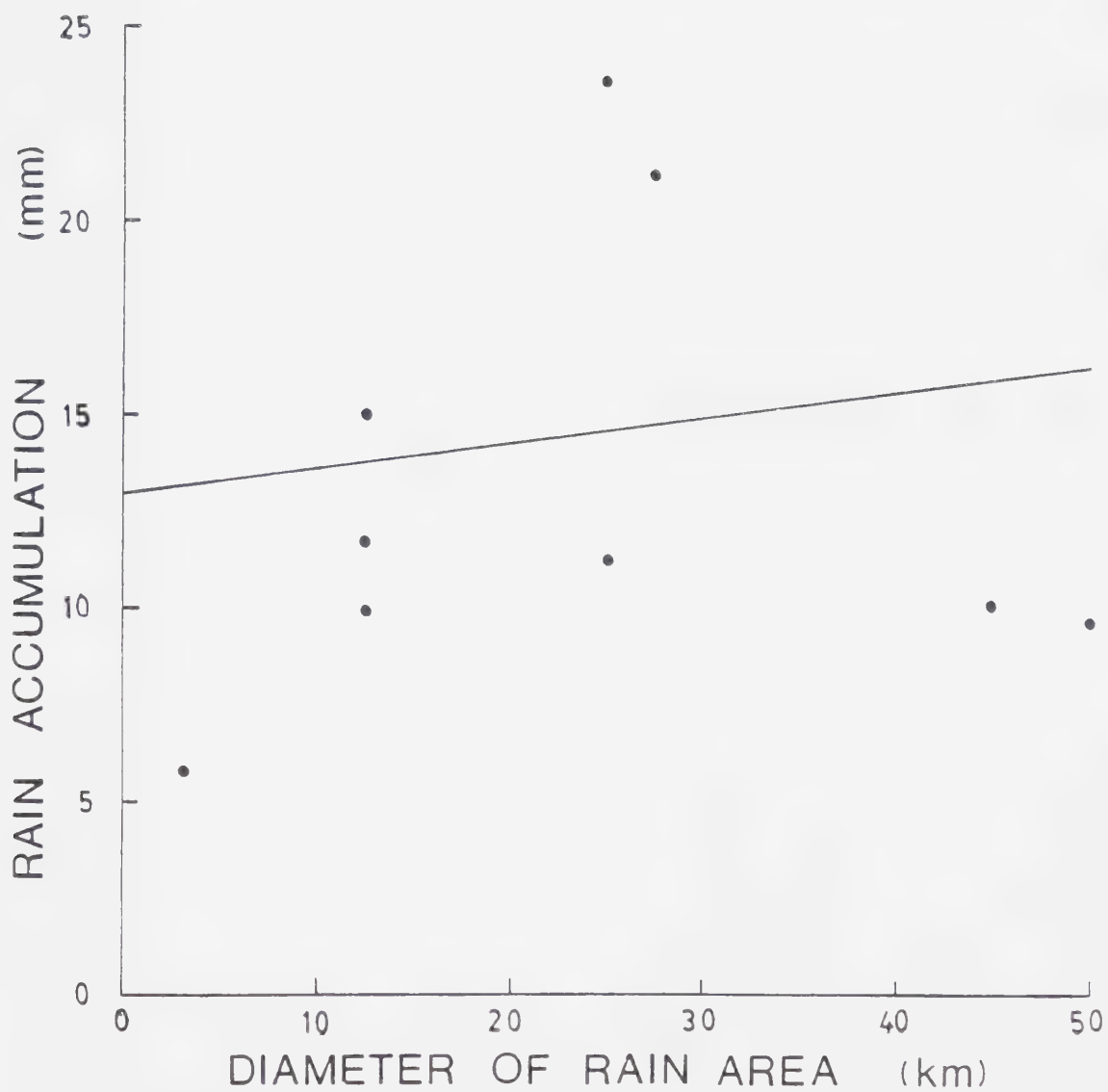
Figure 5.5   Precipitation amount versus diameter of the storm's
              rain area for Zone 1 cases.

with the largest diameter which are associated with a rain duration of 60 minutes. This is longer than the 40-minute limit given by Zawadski, and without these two points there would be evidence for increasing rain amount with increasing rain area. When these two points are included, the results are, once again, inconclusive.

Care must be taken not to attempt to extend the results given here to the radar work mentioned previously. Only a very small area and brief time span have been considered, whereas the radar estimates apply over the storm's entire lifetime.

5.3.4 Temperature and Rain Rate

Adler et al. (1981) related cloud top temperature to updraft velocity and hence also to rain rate. The coldest clouds are considered to be those that have penetrated the stratosphere. This requires a large amount of energy, reflected by higher updraft velocities. This, in turn, is related to a faster conversion of water vapour to liquid water, and hence to a geater rain rate.

The maximum rain rate versus temperature graph for storms producing heavy rain is given in Figure 5.6. A general increase of rain rate with temperature is seen, but the correlation coefficient is only 0.55, which is not significant at the 5% level. However, from the reasoning given above, the important parameter is not simply temperature, but the difference between cloud top and tropopause temperature. This gives a measure of the storm's penetration of the stratosphere. Figure 5.7 gives the graph of rain rate versus temperature difference (cloud top - tropopause) for Alberta, Zone 1, heavy rain cases. Tropopause temperatures over the rain gauge have been estimated from the nearest sounding. This requires some interpolation in time and space, but as tropopause temperature changes are slow, these should be accurate to within $2^{\circ}C$. The uncertainty in the temperature difference is, therefore, $\pm 7^{\circ}C$. Figure 5.7 shows that the rain rate does increase with increasing temperature difference. The correlation coefficient is 0.91, significant at the 1% level even with this few number of points. However, this does not take into account the temperature uncertainty, which is more than large enough to obscure any possible correlation. It is also noted that the temperature difference is negative for all but one case, indicating that most of the storms did not reach the tropopause. It is suggested that atmospheric stability begins to increase at some level below the
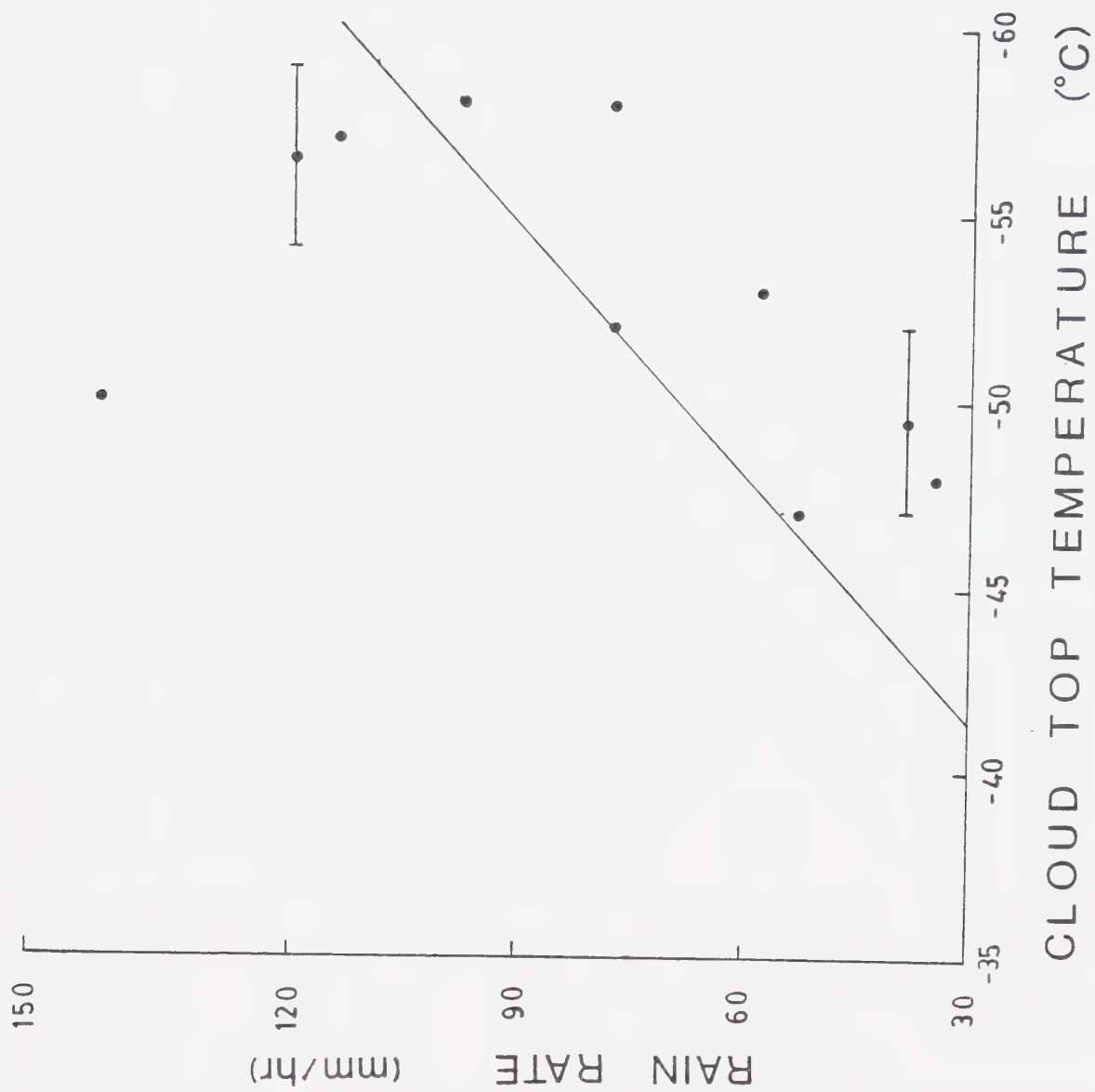
Figure 5.6   Maximum 5-minute rain rate versus temperature for heavy rain cases.
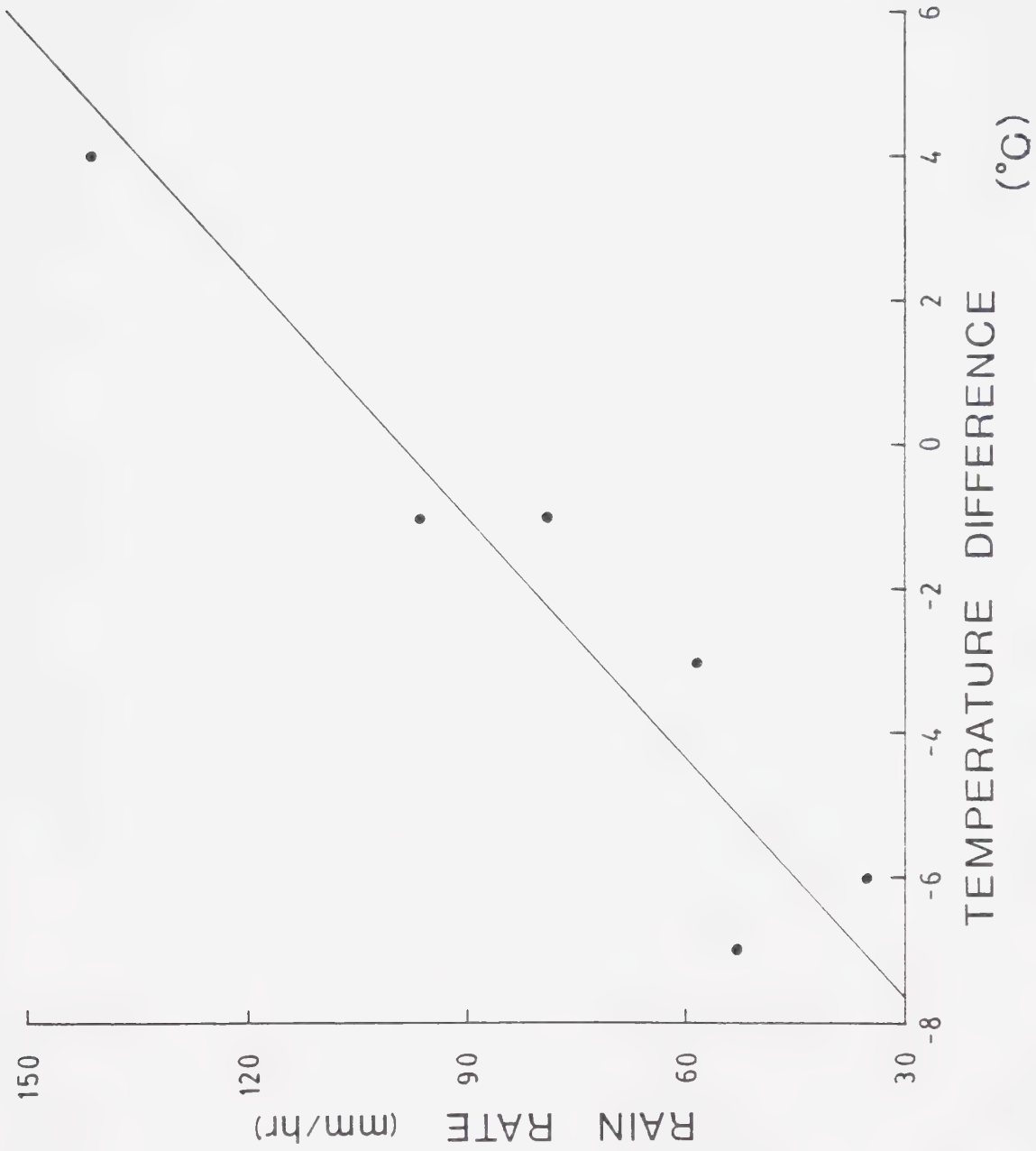
Figure 5.7   Maximum 5-minute rain rate versus temperature difference (tropopause - cloud top) for Alberta, Zone 1, heavy rain cases.

tropopause. The above difficulties not-withstanding, it appears that the relationship between cloud-top temperature and rain accumulation is due mainly to higher rain rates at lower temperatures, assuming some average tropopause temperature.

5.4 Prediction of Rain Amounts

Based on information presented in Figures 5.2 and 5.4, Table 5.2 presents suggested threshold values of temperature and brightness that can be used to infer heavy rain accumulations from satellite data. Large ranges of temperature and precipitation amount are used, as the uncertainty in each variable can be quite large. The threshold values are valid for a "typical" Cb which is raining over an area 15km to 25km in diameter and moving at approximately 50km/hr. It is interesting to note that the threshold values for heavy rain over central Alberta found by Wieler (1981) were -50°C and 145, essentially identical to those given in Table 5.2.

Before the guidelines, given in Table 5.2, are tested in the next chapter, a final note of caution: as the threshold values given here were obtained from measurements from the APT data of the TIROS satellites, they should be applied only to measurements from these satellites. It is quite possible that other data sources, with different resolution, would yield different threshold values. For example, the diameter of an overshooting Cb top can be < 10km, which is near the resolution limit of the APT images. The minimum temperature associated with this area would be underestimated by the APT data, due to averaging with the surrounding warmer anvil temperatures. It is unknown if such a bias is present here.

Table 5.2   Estimated Precipitation Amounts Based on
Cloud-top Temperature and Brightness

Temperature (°C)		Brightness (counts)	Precipitation (mm)
>-49	or	<145	<10
$-57<T\leq-49$	and	≥145	$10-20$
≤-57	and	≥145	>20

6. Satellite Rain Estimates

6.1 Introduction

The best test of any predictive scheme is its application to an independent data set. In this chapter, rain amounts will be inferred using only the the satellite-derived cloud-top temperature and brightness. It should be noted that Table 5.2 actually "predicts" cloud-top temperature and brightness, given some quantity of rain > 10mm. Here, Table 5.2 is being used in reverse, that is, to preform the more interesting task of inferring rainfall, which is not strictly valid. Consequently, some failures were both expected and encountered. Selection of the sample is discussed first, followed by the construction and interpretation of the satellite-derived rain maps.

6.2 Selection of Sample

HRPT images for the period May-Sept. 1982 were inspected for days exhibiting convective cells with cloud top temperatures < -40°C (as determined using the grey scale). High resolution, rather than APT images were used because of their more detailed and easily interpreted grey scale. Only four shades of grey are available for the APT products. However, temperature and brightness contour maps, on which the rain estimates are based, are from the APT data.

Clouds which were very small (ie. the size of the Edmonton and Outlook storms) were excluded as it was thought that the temperature and brightness fields would be poorly resolved on the APT images. Even though the data was restricted to only one year, there was no shortage of suitable cases, in fact, too many to be studied here. Those selected represent a cross section of situations, including small isolated cells, merging clouds and one very large, intense storm.

6.3 Rain Data

6.3.1 Climate Data

The main source of rain data is the network of climate stations shown in Figure 3.2. These give 24 hour rain accumulations based on a period from 08:00 to 08:00 local time. Hourly rain data are available only on those rare occasions when a cell passed over a station equipped with a TBRG. As there are no more than 2 satellite passes separated by 100 minutes, the climate data do not allow direct comparison of satellite-inferred to observed rain amounts. Instead, the satellite-derived amount represents only a lower limit to the observed 24 hour accumulation. Even when the estimated and observed amounts agree, it is still possible that the observed rain occurred outside the time period of satellite coverage. However, should there be a number of precipitation reports confined to the path of a storm (as viewed by the satellite) then it may be safely assumed that the rain is due to that storm.

Table 6.1 outlines the conditions under which a comparison of estimated to observed rainfall amounts is considered to be a correct, neutral, or incorrect prediction. Neutral, as used here, means that the prediction is not incorrect, but cannot be proven correct either. Of course, wherever possible, hourly rain amounts are used as a primary source of information in preference to climate data.

6.3.2 Radar Data

For a few cases, radar-derived rain accumulation were obtained from the Alberta Research Council radar at Penhold. Accumulations are calculated using an average rain rate over 5 to 7 minutes. Rain totals on the ground are inaccurate at the beginning and end of the accumulation period as the storm would not have moved entirely over a point on the ground. It is difficult, therefore, to know if a given rain amount is due to the cut-off of the accumulation period, or a weakening storm. To aid in resolving this problem, rain intensity maps for the beginning and end of the accumulation period are also included.

Table 6.1   Verification of Inferred Rain Amounts
Based on a Comparison to Observed 24-hour Accumulations

Prediction	Observation	Verification
no rain	no rain	correct
no rain	rain	neutral
rain amount=P	rain amount$\geq$P	neutral
rain amount=P	rain amount$<$P	incorrect

6.4 Construction of Rain Maps

The following describes the technique used to infer point rain amounts. Satellite derived rain maps were constructed before obtaining observed rain data in order to avoid biasing the inferred amounts.

6.4.1 Size and Placement of Rain Area

Not only must the amount of rain be inferred, but also the size and position of the precipitating area within the cloud. The size cannot be determined directly from the satellite images. Instead, it is merely assumed to be in the range 15-25km. These are the values obtained from the duration of precipitation for storms in the dependent sample, assuming a circular rain area moved directly over the station.

For the dependent sample, the cloud area defined as "Zone 1" was quite successful in isolating the portion of the cloud mass where most of the precipitation occurred. However, as Zone 1 constituted 20% of the cloud mass, it was usually much larger than the precipitating element. Consequently, while it is often not difficult to define Zone 1, the inferred position of the small rain area within the zone can be quite poor, especially if the cloud area is very large. As explained in Section 3.5.1, the convective core is generally near the upwind temperature gradient, and this was the main guideline used in determining the position of the precipitating area.

6.4.2 Speed of Cloud

As discussed in the previous chapter, point accumulations are dependent upon the cell's speed. Table 5.2 was constructed for clouds moving at approximately 50km/hr. Inferred rain amounts can easily be adjusted for different speeds. However, as the speed of the clouds in the independent sample used here (determined from satellite images or 700mb maps), were found to be in the range 40-60km/hr, no adjustments were necessary.

6.4.3 Construction of Rain Amounts

The construction of a rainfall map based on a single satellite image was a straight-forward procedure. For each cloud considered, temperature and brightness contour maps were produced. The cloud was then divided into the three zones. A 10 or 20mm rain contour was drawn near the upwind temperature gradient in Zone 1 if temperature and brightness values exceeded the threshold values given in Table 5.2. The diameter of the rain area drawn was in the range 15-25km with smaller areas corresponding to smaller warmer clouds. This is a subjective procedure used to indicate a growing or shrinking rain area when, over two sequential images, a storm appeared to be intensifying or dissipating. When a 20mm contour was drawn, a 10mm contour was sketched around it. No attempt was made to identify the position of the 0mm contour as this was not investigated in the dependent sample.

A more difficult task was interpolating rain areas between two sequential images. It may be that rain is implied on only one, or between images. In these cases, a linear interpolation of the extreme values of temperature and brightness was used to determine the position at which to start or end the rain contours. There are four conditions that can be encountered: rain indicated on both images, rain on first image only, rain on second image only, and rain between images.

When rain was inferred on both images, then the two precipitation maps were over-laid and the precipitation areas linked together. It is possible that rain actually occurred only at the time of the satellite passes and not in-between, although more likely the cloud produces rain continually, but in varying amounts during its lifetime.

For all other conditions given above, the procedure was to first plot the path of the storm. Extreme values of temperature and brightness from each image were used to interpolate linearly the temperature and brightness values along that path. Rain contours were drawn wherever the threshold values given in Table 5.2 were exceeded. This procedure is also used to infer changes of rain totals from 10mm to 20mm and vice-versa. The evolution of temperature and brightness is probably not linear over 100 minutes. However, considering the errors introduced by uncertainties in the temperature and brightness values, the uncertainty in the position of the convective core, and the fact that actual evolution rates are unknown, it would be pointless to attempt anything more

sophisticated than a simple linear interpolation.

The ends of the rain contours are left open when rain is inferred to be occuring at the time of the satellite pass. This indicates that the beginning or end location of the rain is unknown. Finally, if two storms pass over the same area, the rainfall from each is summed together. In this manner, 30mm or 40mm contours are possible.

6.5 Interpretation of Rain Maps

As the error in the position of the convective core can be quite large, (>30km for a large cloud) emphasis is placed on the correct prediction of rain amount. That is, if the inferred rain amounts and contour pattern are consistent with the observed amounts and pattern, then this is considered a "success", even if the position of the inferred and observed amounts are not coincident. There is no guaranteed sucess since, as previously mentioned, it is unknown when the rain given in the climate data occurred. However, should rain be predicted and none observed, then this is counted a definite failure.

If the only error is the placement of the convective core, it should be possible to shift the inferred contours so that they match the observed rain. This procedure is to be avoided unless there are observed amounts nearly equal to those predicted. When observed rain amounts are less than predicted, it is always possible to shift the contours so that they lie between, rather than over climate stations. In fact, as will be seen, more often than not storms pass between stations. This is expected, as the inferred diameter of the rain area is < 25km while the distance between neighbouring climate stations can be much larger. Consequently, all contours are left as originally drawn.

The following section presents satellite-derived precipitation maps for 9 days, with two or more storms investigated each day. Also given for each day are the cloud-top temperature maps. Contours are drawn only for those areas colder than -30°C. at 10°C intervals. The approximate scale for all temperature maps is 1 cm = 35 Km. The scale for the precipitation maps are given individually. For all maps (temperature and precipitation) an arrow is drawn pointing northwards. Each case is discussed individually with a subjective rating of how well the contours match the observed rain amounts. No objective measure is possible since the rain amounts over the time period covered by the satellite passes are unknown.

6.6 Case-Studies

6.6.1 June 02 1982

The cloud-top temperature contours at 21:10 GMT are given in Figure 6.1a. A band of cells are aligned along the mountains in northwestern Alberta. Figure 6.1b shows the temperature contours at 22:55 GMT. The band has moved eastward and rotated slightly so that it is aligned more east-west.

Three cells, marked A, B and C on Figure 6.1 have been identified, each with cloud-tops colder than -50°C. Brightness values greater than 145 are found only on the first image, implying that the rain ended before the second satellite pass. The corresponding rain contours and observed amounts are shown in Figure 6.2 There are no observations of amounts greater than 10mm, but three stations (Nose Mountain, Kakwa and Smoky) enclosed by the 10mm contour associated with Cell A are very close to this value. Also, as the stations are aligned along the contour it is strongly suggested thall all of the observed rain was due to the passage of this storm. The contours identified with cells B and C lie between stations so no verification of the inferred amounts is possible.

Based on the movement of the clouds and the orientation of the rain pattern, the area of precipitation east of the contours at Pass Creek, Eagle and Sweathouse is due to some cell other than those seen on the satellite photographs.

Figure 6.1   Cloud-top temperature contours at 10°C intervals
for June 02, 1982 at a) 2120 GMT and b) 2250 GMT.
The arrow in the upper right-hand corner points northward.
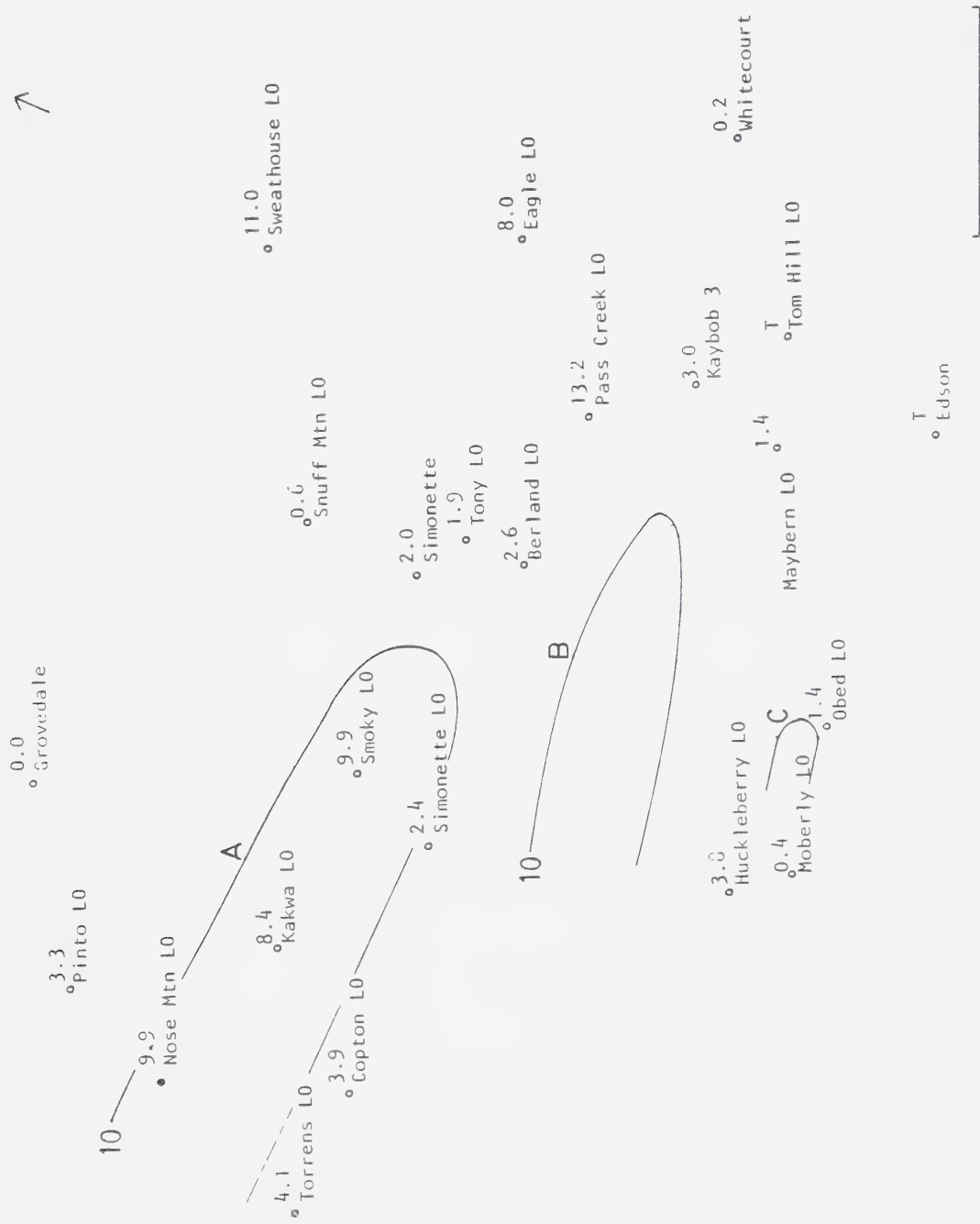
Figure 6.2   Satellite-inferred precipitation contours and observed   50 Km
24-hour accumulations, both in mm, for June 02, 1982.
The arrow in the upper right-hand corner points northward.

6.6.2 June 04 1982

Figure 6.3 gives the temperature maps at 20:50 GMT and 22:54 GMT respectively. A line of cells moved east-northeast from the mountains into central Alberta. Cloud-top temperatures were < -60°C with brightness > 150, although it decreased in both magnitude and area between satellite passes. The inferred rain contours are shown in Figure 6.4. A 20mm contour is drawn nearly east-west through central Alberta. Rain amounts greater than this are observed, but 35km north of the predicted area and only in central Alberta. From the TBRG records, the rain at Penhold and Lacombe occurred after the second satellite pass, which is consistent with a northeasterly cloud motion. Between 23-01 GMT Penhold received 11mm in less than an hour and 16.9mm fell at Lacombe (11.3mm from 00-01 GMT).

The fit between observed and derived rain amounts would be greatly improved if the contours were moved northwards. The area of maximum observed rain in central Alberta is 35km north of the predicted location. Generally, uncertainties of the contour position of this magnitude are possible due to the combination of errors in gridding, overlaying images and positioning the small convective core within the larger anvil. However, in this particular case, the errors do not appear to be larger than 20km. Furthermore, even after adjusting the contours, there is still too much rain inferred over western Alberta.

While not a complete success, the results are encouraging. Penhold and Lacombe both received > 10mm in less than one hour. It therefore is reasonable to assume that most of the rain recorded by the upstream stations also fell within a short time period. The rain-estimation technique was successful in that it correctly determined that heavy rain occurred.

(a)

(b)

Figure 6.3   As in Figure 6.1 except for June 04, 1982 at a) 2050 GMT and b) 2230 GMT.
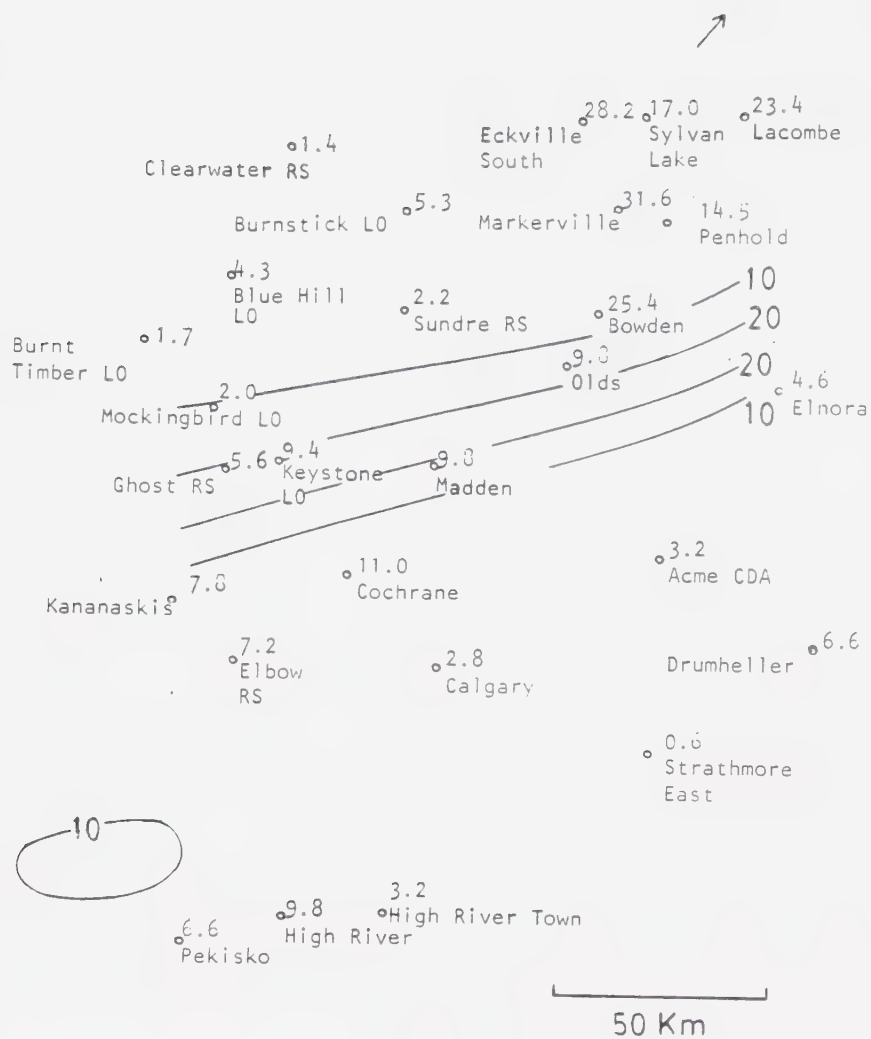
Figure 6.4   As in Figure 6.2 except for June 04, 1982.

6.6.3 June 05 1982

Two cells of interest are seen on the satellite passes at 20:35 GMT and 22:15 GMT. These are marked A and B on Figure 6.5. The storms moved eastward from the Saskatchewan-Alberta border at approximately 60km/hr. The interesting feature here is that the clouds are aligned along the direction of motion so that point rainfall accumulations are a combination of rain from each storm.

The temperature and brightness of Cell A is such that heavy rain is presumed to have ended before the time of the second satellite pass. The temperature of Cell A drops from -50°C to -57°C so that rain amounts increase from 10 to 20mm between passes. The resulting precipitation map is given in Figure 6.6. Moving from west to east, seen first is a 10mm contour associated with the rain from Cell A. Next is a 20mm contour which results from the overlap of two 10mm contours (one from each cell). This is followed by a 30 mm contours caused by the combination of 10mm amounts from the Cell B and 20mm from Cell A. The eastern edge of the 30mm contour marks the position where rain from Cell A ceased.

As with the previous case, rain amounts are reasonable but the position of the contours are, at first glance, poor. Kelfield received 20mm while 39.6mm fell at Biggar, but the centre of 30mm contour is 40km from Biggar. Considering that only a rough linear interpolation is used to determine the position at which to start and end the precipitation areas, this is actually fairly close. Only a small clockwise rotation of the contour pattern is needed to greatly improve the fit between observed and inferred amounts. As always, it must be noted that the observed rain is not necessarily due solely to the cells described above. However, the proximity of observed and predicted rain areas strongly suggests that this is the case.
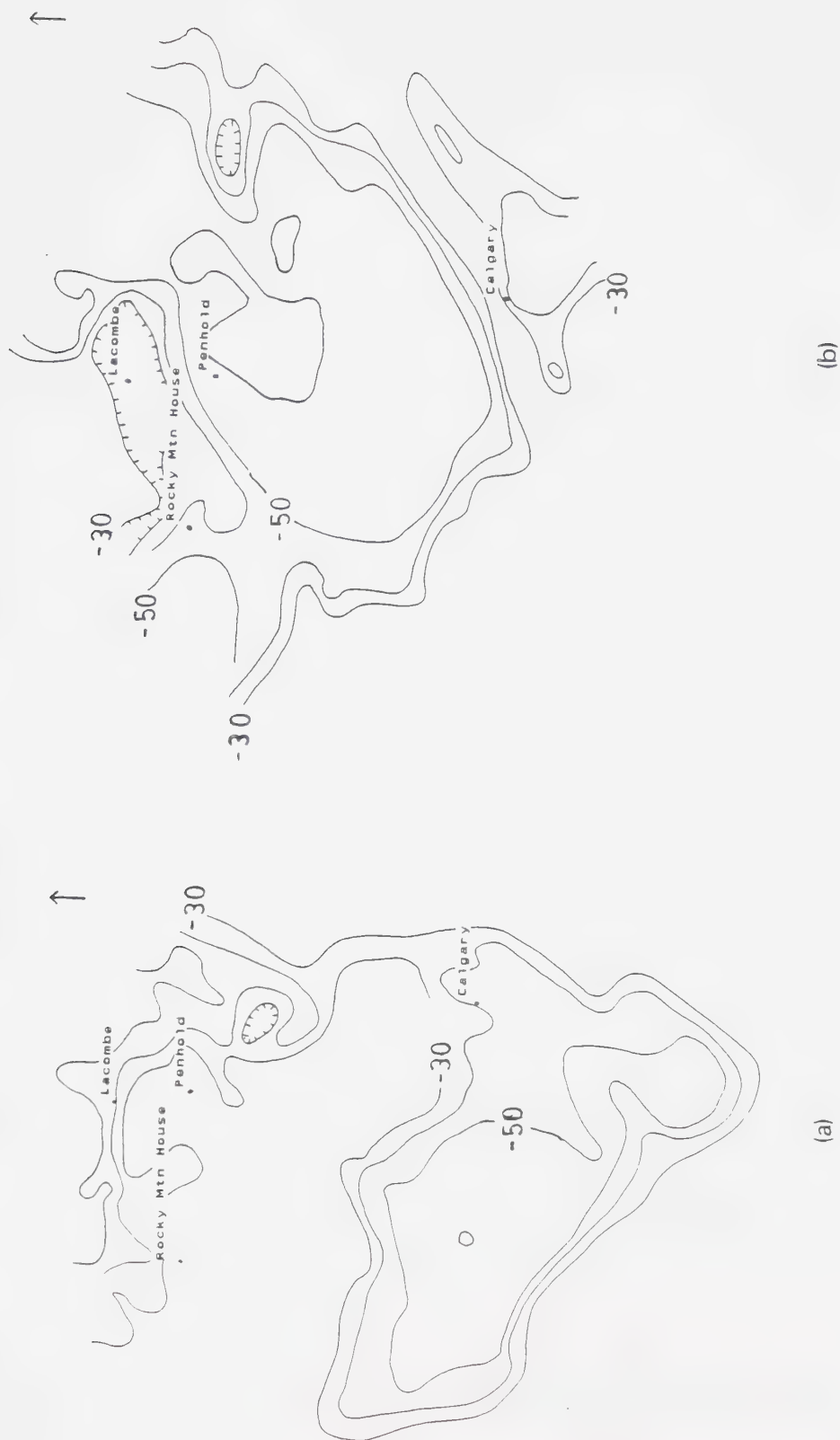
Figure 6.5   As in Figure 6.1 except for June 05, 1982 at a) 2035 GMT and b) 22 15 GMT.
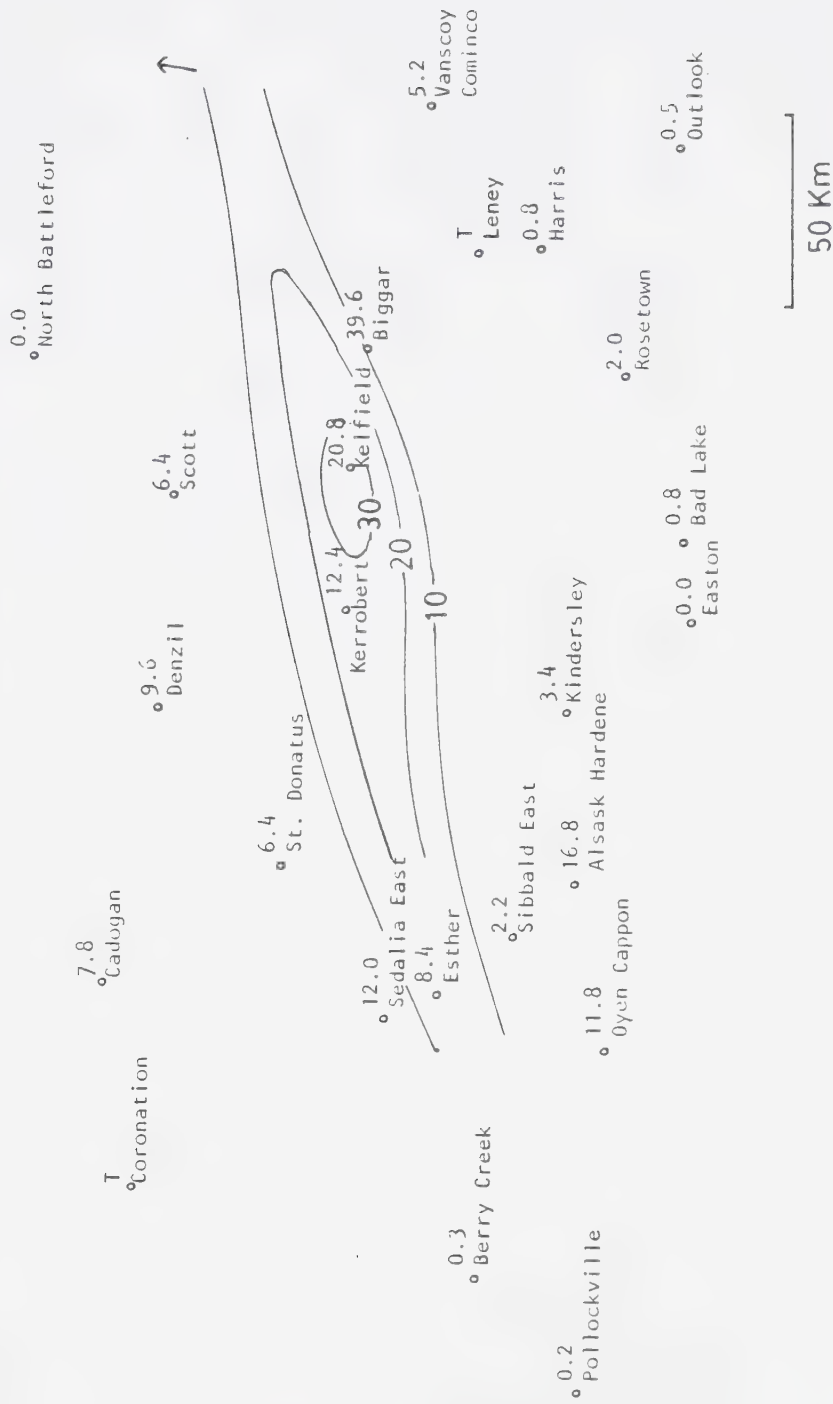
Figure 6.6   As in Figure 6.2 except for June 05, 1982.

6.6.4 June 14 1982

The cloud top temperature contours for the satellite passes at 20:30 GMT and 22:10 GMT are shown in Figure 6.7. Two cells, marked A and B have been investigated. Cell A is southwest of Edmonton and Cell B is near Coronation. Both are moving to the southeast. Cloud-top temperatures are in the range -58°C to -60°C, so that the rain contours, shown in Figure 6.8, exhibit a 20mm contour, albeit quite small. Unfortunately, both cells passed over an area devoid of climate stations. The largest reported rainfalls are 6.0mm and 7.0mm at Alliance and Brownfield, respectively. This rain could have been caused by either of the cells or a combination of both.

Cell A was just within range of the radar at Penhold. The radar accumulation map for 20:06 GMT to 21:46 GMT is given in Figure 6.9c. Rainfall amounts in the range 10-25mm are common. The rain rate maps, given in Figure 6.9a-b show that the rain intensity was also heavy at the above times.

Again, the satellite-inferred rain amounts are consistent with the observations so that this is scored as another success, at least for Cell A. It is noted, though, that the radar echoes place the track of the storm east of Camrose, rather than west, as shown on Figure 6.8.

Figure 6.7   As in Figure 6.1 except for June 14, 1982 at a) 2030 GMT and b) 2210 GMT.

1.0
° Hastings Lake

↗

°Vegreville

0.4
° Camrose

0.0
Gwynne °

0.4
Camrose 2

A

0.0
°Viking

0.0
°Manville South

0.0
° Kinsella
Ranch

0.6
° Fabyan

0.2
° Stettler
North

2.0
°Forestburg

10

20

6.0
° Alliance

0.0
° Wainwright
Heath

7.0
° Brownfield

0.0
° Hughenden

10

20

2.8
Coronation °

5.0
° Horshoe Lake

0.0
° Cadogan

2.2
° Hanna

B

0.0
° Scotfield

50 Km

1.0
° Sedalia East

0.0
° Esther
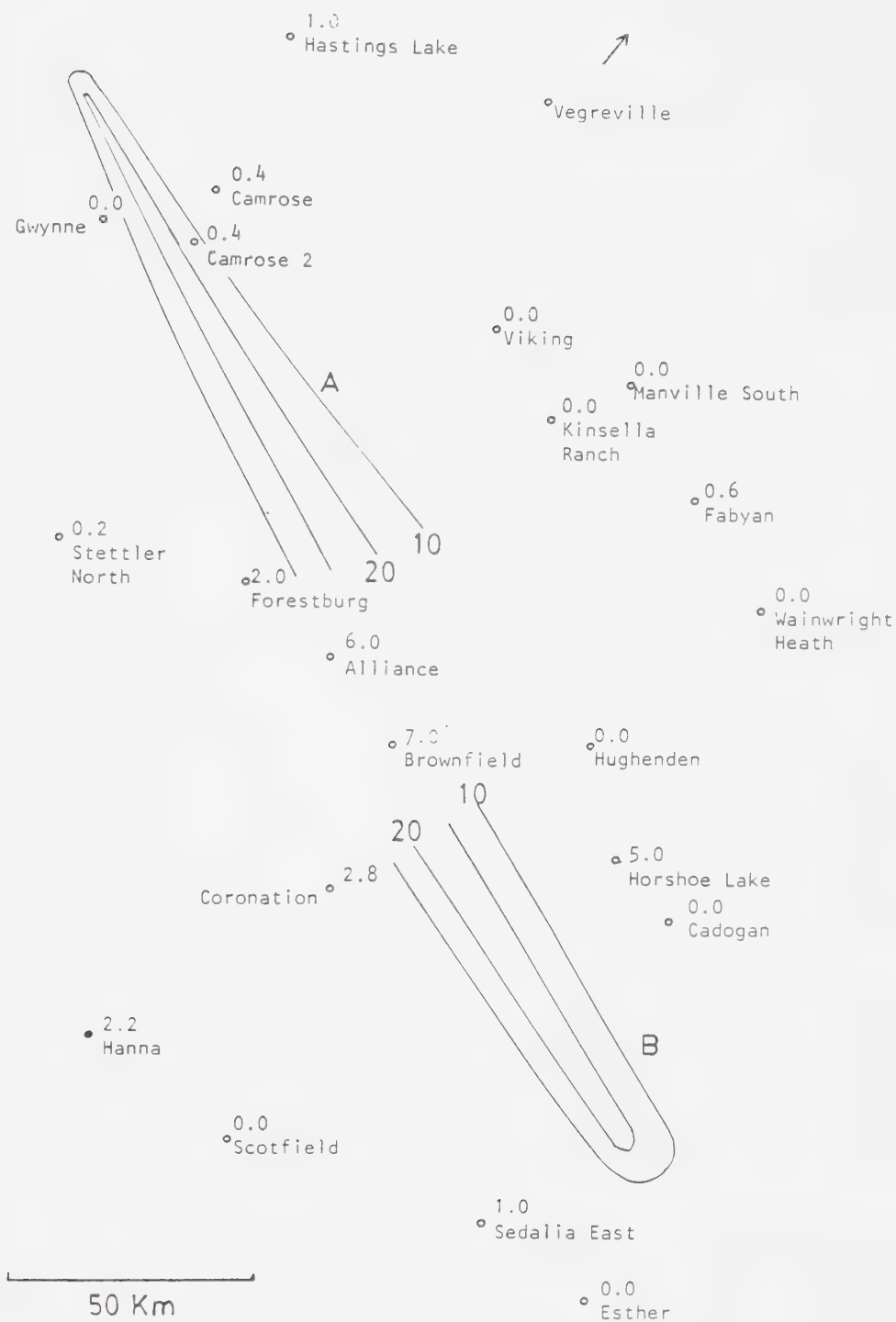
Figure 6.8   As in Figure 6.2 except for June 14, 1982.

(a)

(b)

(c)

Figure 6.9   Radar-derived rain intensities at a) 2003 GMT and b) 2146 GMT and c) the rain acumulation over
that time period. The numbers given on the maps indicate ranges of rain intensity (mm/hr) and
accumulation (mm) as follows:
4 = 1 to 2.5, 7 = 2.5 to 5, 3 = 5 to 10, 5 = 10 to 25 and 2 > 25.
A reading of 3, therefore, corresponds to 5 to 10 mm/hr on the intensity maps, and 5 to 10 mm
on the accumulation maps.

6.6.5 June 15 1982

On this day there were numerous cells in Saskatchewan as seen on the infrared images at 20:20 GMT and 22:00 GMT shown in Figure 6.10. The motion of the clouds was towards the southeast. Minimum cloud-top temperatures are in the range -60°C to -62°C, while brightness decreased from 165 to 150 between the satellite passes. On Figure 6.10a, the cells are quite small. By the time of the second pass, they have grown in size and the cirrus anvils have merged. Because of this merging, it is very difficult to follow any particular cell from one image to the next. Four cells, marked A-D are shown on Figure 6.10b, but the position of the convective cores within the cloud mass are very uncertain.

The satellite-derived rain contours are shown in Figure 6.11. Amounts over 20mm are predicted, but the majority of the observations indicate much less than this. Rain is also seen to lie between contours, but this is misleading. At Bad Lake, between cells A and B, for example, 4.2mm was observed, but the TBRG records show that this occurred after the satellite passes. More disturbing is the observation at Dana which reported less than 3mm, but is enclosed by the 10mm contour associated with Cell D. However, some points can be made in defence. Cells A, B and C appeared to have skirted around climate stations so that there is no firm evidence that the contours are incorrect. Near Cell D, Colonsay received 19mm. There are four climate stations in Saskatoon. The minimum reported was 2.0mm, and the maximum, at Saskatoon Central Avenue, was 11.0mm. If this observed rain is associated with Cell D, then the position of the rain contours are very poor, being displaced 30km to the east. However, as mentioned above, the position of convective cores are very uncertain and errors of this magnitude are quite possible. Note also that, the contours were shifted to the west, then Dana would be removed from the inferred heavy rain area. Overall, though, amounts appear to be greatly over-estimated so this case is considered to be a minor failure, at best.

It is noted that Outlook received 5.6mm while, only 13km to the southeast, Glenside reported 25.0mm. Such large variations over a small scale would not be easily detected by the method employed here except under very favourable circumstances. For example, the rain-producing cell would have to be exceedingly well-defined on the satellite image, without a large, obscuring cirrus anvil.
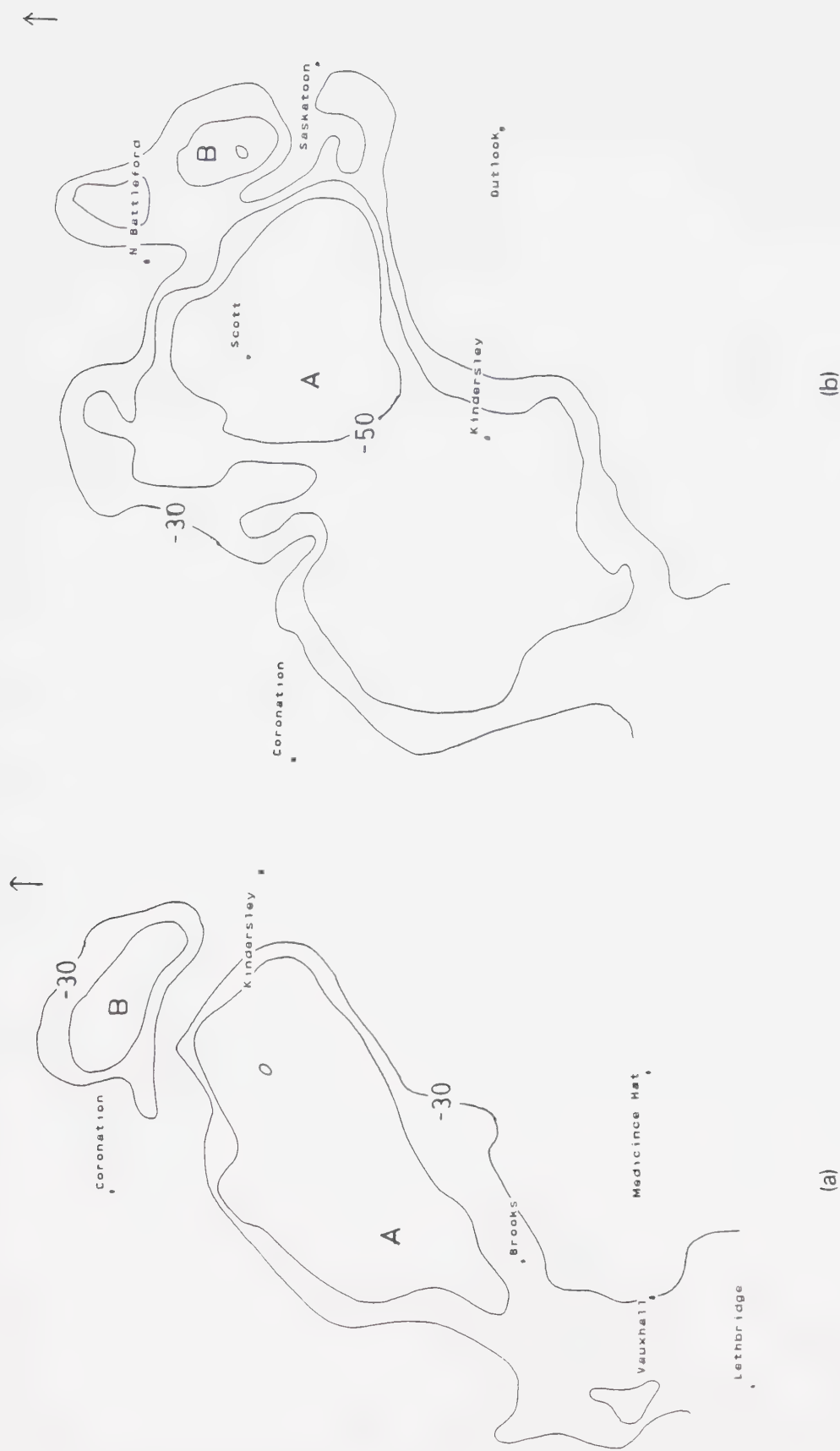
Figure 6.10   As in Figure 6.1 except for June 15, 1982 at a) 2020 GMT and b) 2200 GMT.

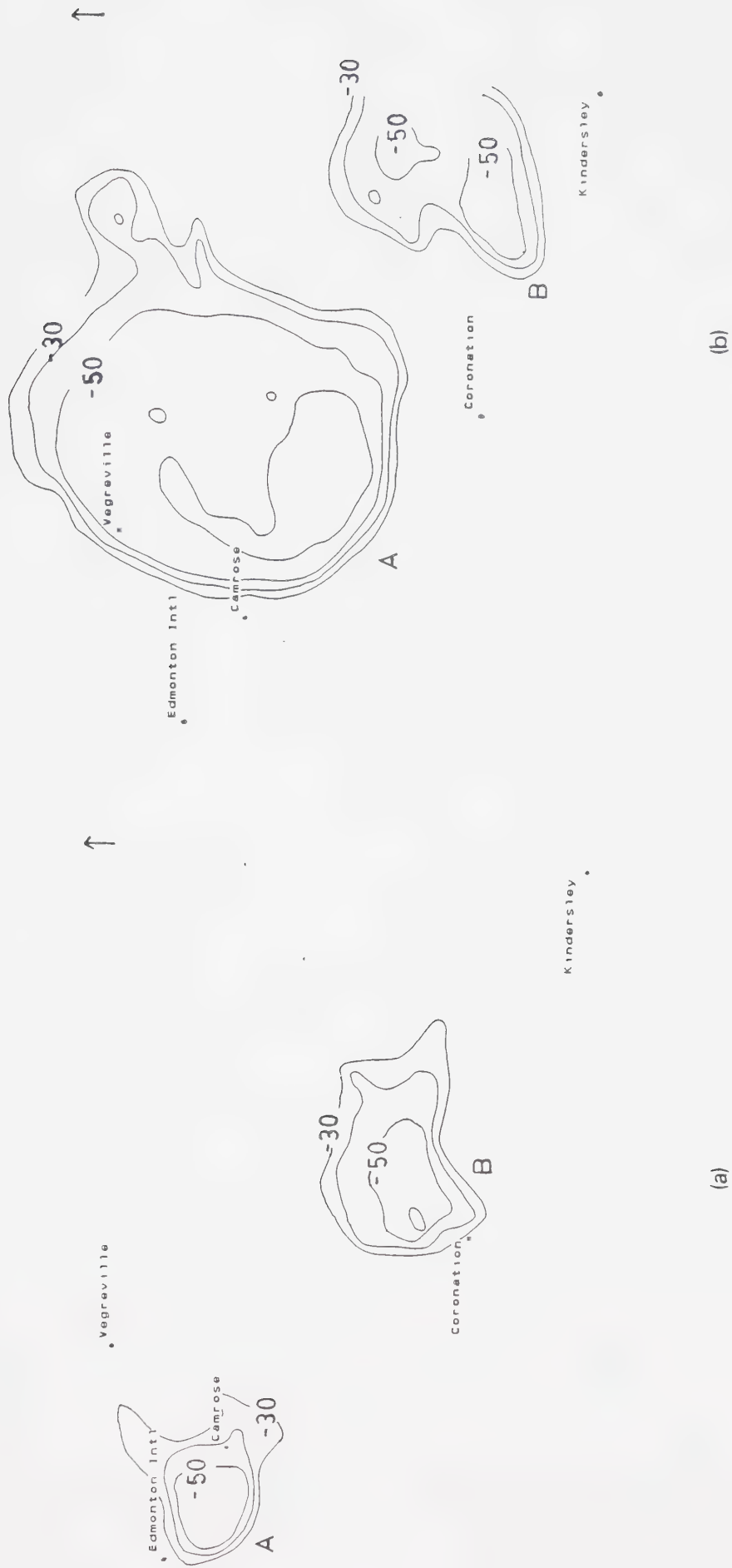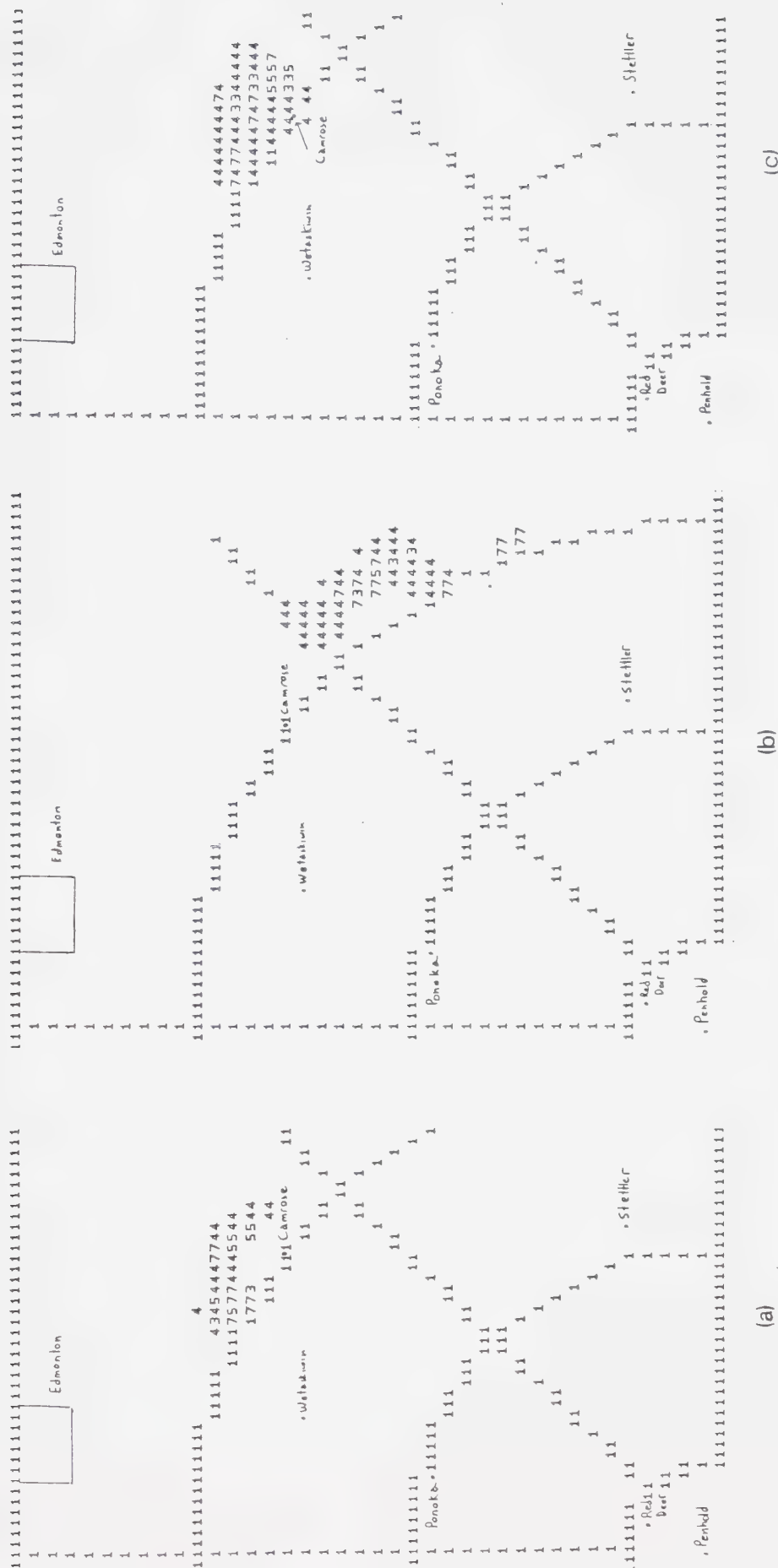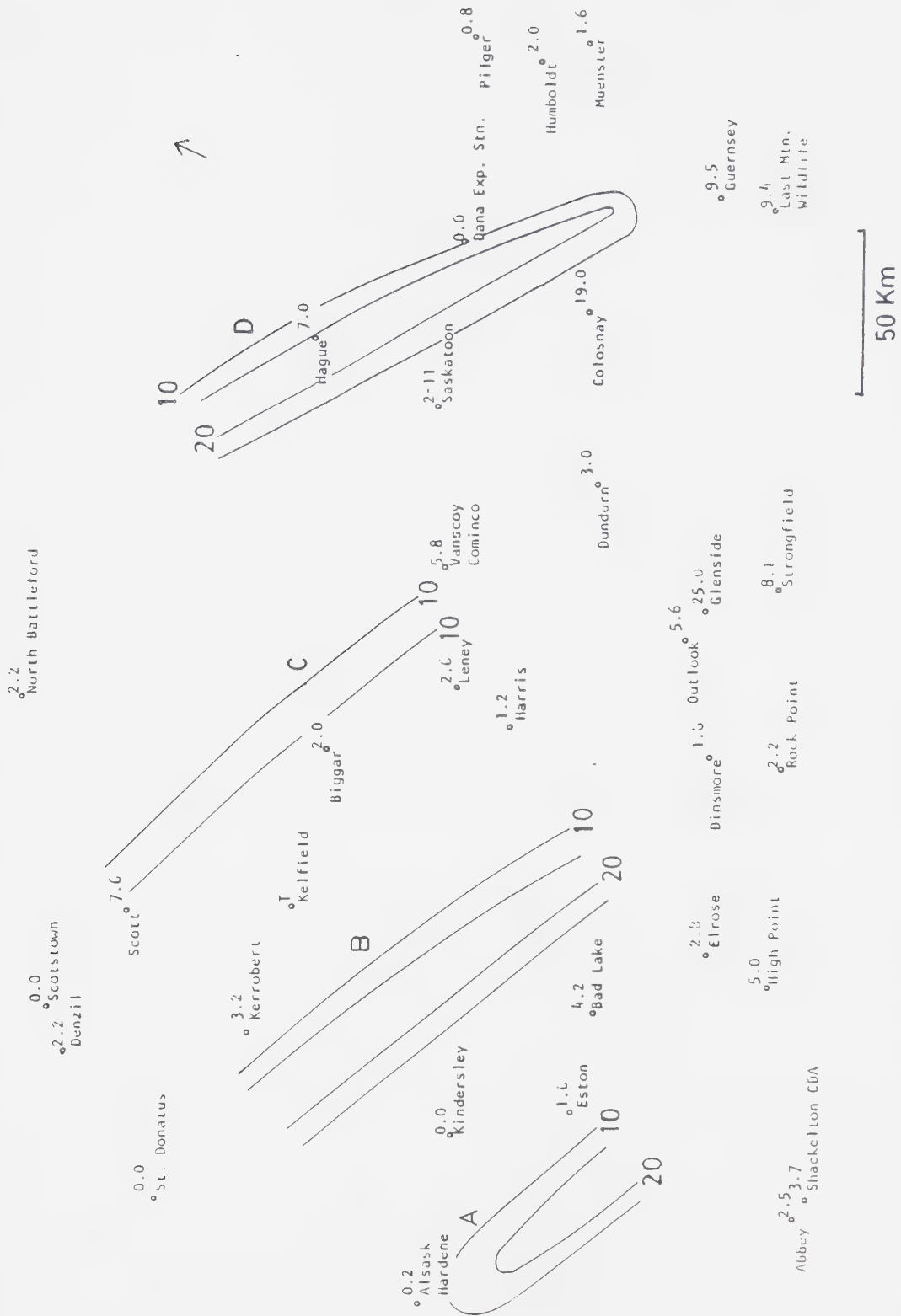Figure 6.11   As in Figure 6.2 except for June.15, 1982.

6.6.6 June 21 1982

Rainfall from three clouds has been mapped, based on the satellite imagery at 20:50 and 22:30 GMT. These are marked A,B, and C on Figure 6.12. In southern Alberta, Cell A moved north of Cochrane as its cloud-top temperature dropped from -51°C to -55°C and the maximum brightness decreased from 160 to 120. The resulting inferred rain contours are given in Figure 6.13a. This is yet another example of a cloud moving between, rather than over, climate stations, so there is little support for the predicted amounts. The largest observed amount is 5.5mm, just upstream of the contours. The radar-derived accumulation map for 20:41 GMT to 21:43 GMT is given in Figure 6.14c. Rain intensity maps for the same times are shown in Figure 6.14a-b. The accumulation period was stopped mid-way between the times covered by the satellite passes, as the cell was clearly dying. Amounts > 10mm were detected by the radar, but only upstream of the satellite rain contours. Over the area covered by the contours, satellite estimates are greater the those of the radar. On the positive side, even though the cell moved over the area near Acme, no rain was predicted, because of the low brightness values, and none was observed.

Two cells, marked B and C, in the vicinity of Whitecourt were also investigated. Precipitation was inferred to have started after the first satellite pass for both storms and, for Cell B, to have ended before the second pass. The resulting rain contours are given in Figure 6.13b

The 10mm contour for the Cell B well represents the observed amounts. The 22:30 GMT weather report, given in Table 6.2, shows that the storm passed directly over Whitecourt, yet only light rain amounts were expected as the brightness was less than 145. This proved correct as Whitecourt received only 1.6mm from 22-23 GMT.

The contour associated with Cell C does not match the observed amounts as well, but the error in position is within estimated errors. Tony Hill, which received 12.5mm, is less than 15km north of the contours. Ansell, south of Edson, received 14.3mm, but as the temperature over Ansell was higher than -10°C, the rain probably occured at some other time. This is supported by the Edson weather reports given in Table 6.2. During the time period covered by the satellite images, the only storms observed were either over or north of the station. Also, Edson received only 2.6mm from 21-23 GMT.

Whitecourt

Edson

Edmonton Intl

Penhold

Calgary

−30

−30

B

C

−50

A

−30

−50

(a)

Whitecourt

Edson

Edmonton Intl

Penhold

Calgary

−30

−30

B

C

−30

−50
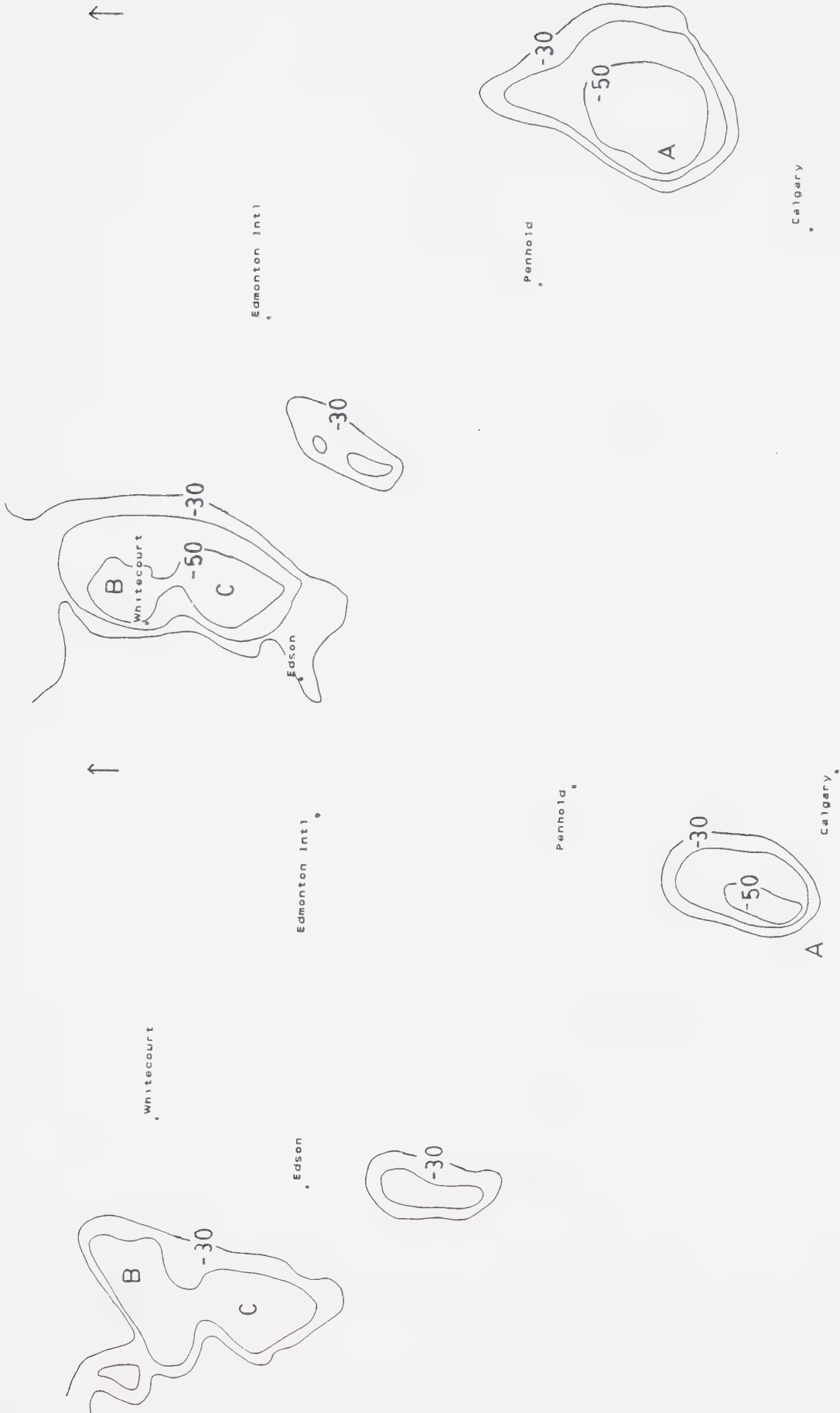
A

(b)

Figure 6.12   As in Figure 6.1 except for June 21, 1982 at a) 2050 GMT and b) 2230 GMT.

0.0
°Sundre RS

0.0
° Bowden

0.0
°Olds

5.j
°Mockingbird LO

A

T
°Madden

0.4
°Trochu Town

0.0
°Trochu Equity

°1.7
Ghost RS
Keystone LO ° °1.7

10

0.0
° Cochrane

Acme CDA °0.0

°0.0
Carbon

°T
Kananaskis
Boundary RS

50 Km
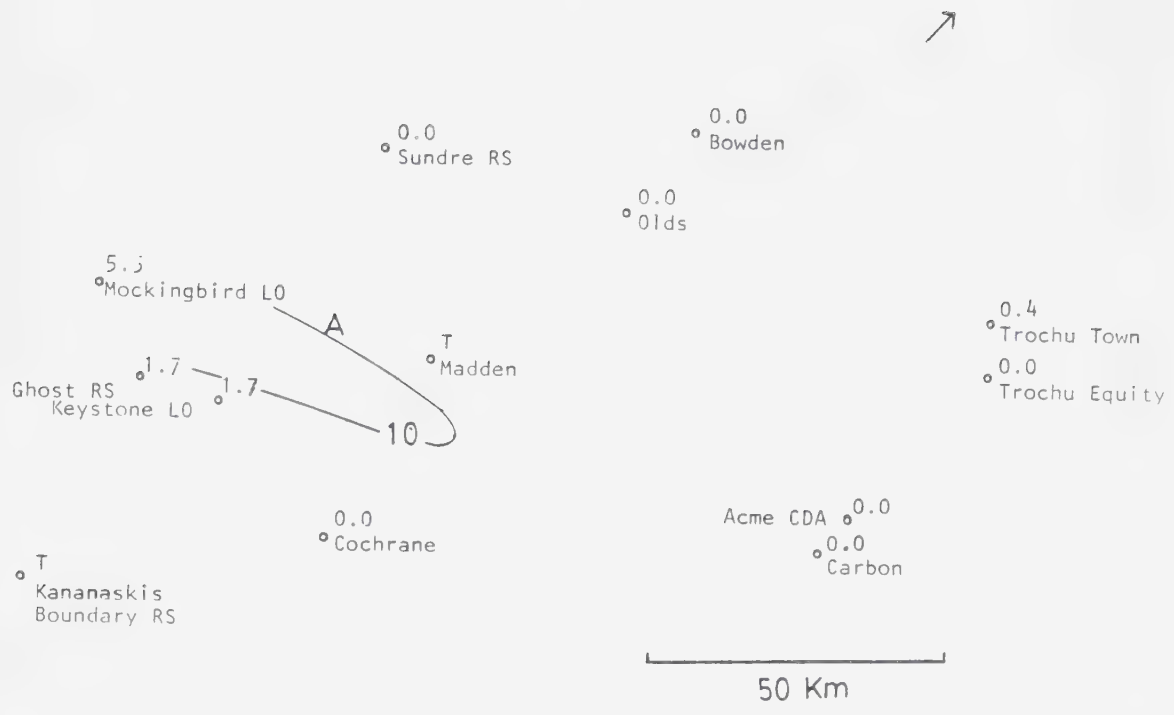
Figure 6.13a   As in Figure 6.2 except for June 21, 1982.
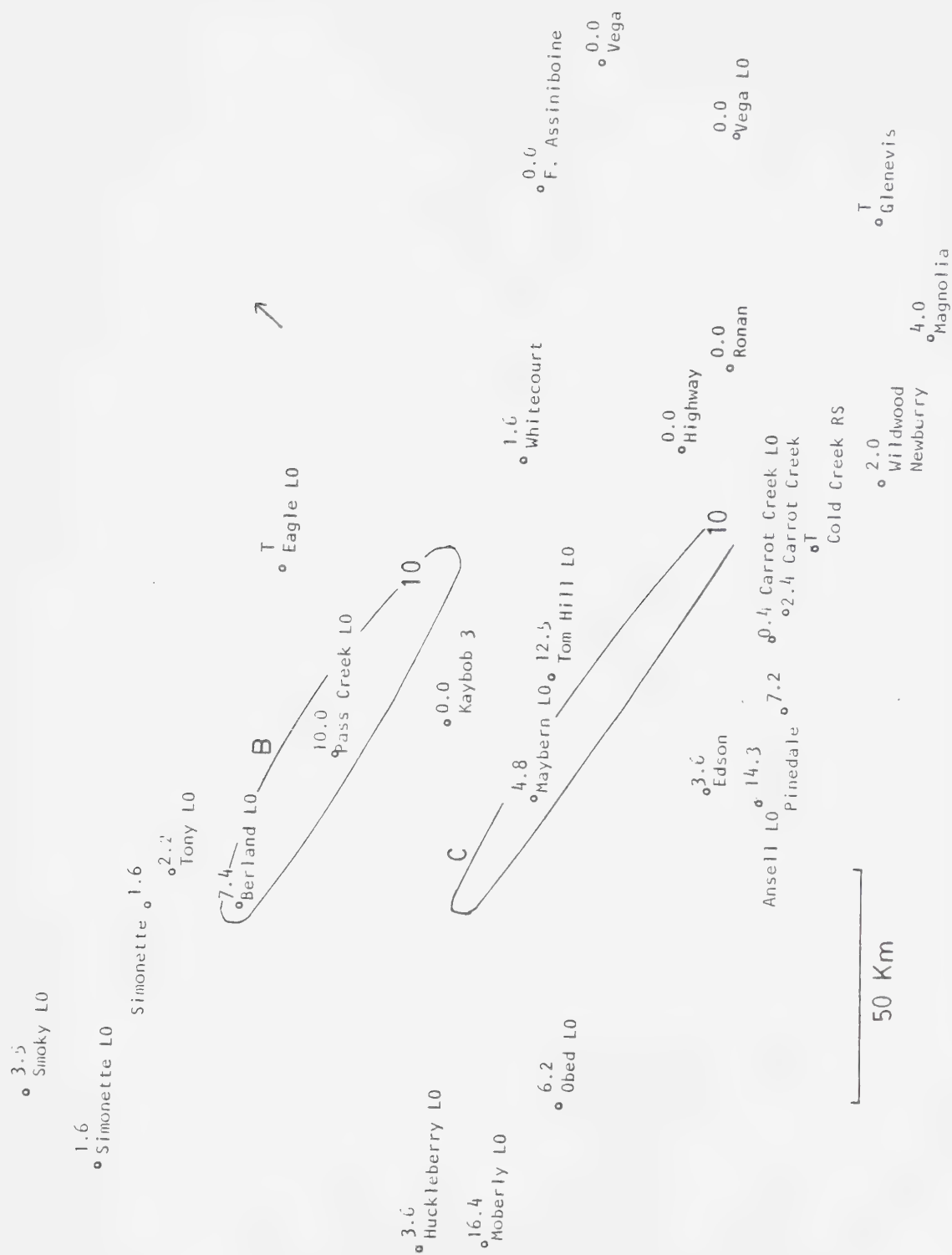
Figure 6.13b As in Figure 6.13a except over northern Alberta.

Figure 6.14   As in Figure 6.9 except for June 21, 1982 at a) 2035 GMT, b) 2143 GMT and c) 2035 - 2143 GMT.

Table 6.2   SURFACE WEATHER OBSERVATIONS FOR JUNE 21, 1982

WHITECOURT

YZU SP 2100 50SCT 65SCT 280-BKN 15+ CU2CB3CI1

YZU RS 2200 50SCT 65SCT E90BKN 15+T CU2CB3AC2CI1 LTGCG SW

YZU SP 2230 50SCT E60BKN 90BKN 280BKN 15TRW- CU2CB5AC1CI1
                                        TSTM OVRHD LTG ALQDS

YZU SA 2300 40SCT E60BKN 90BKN 15+ TRW- SC2CB6AC1
                                        TSTM MOVG E

YZU SP 2310 40SCT E60BKN 90BKN 15+T SC3 CB5 AC1 SHWRS E

EDSON

YET SA 2100 40SCT E60BKN 110BKN 40 CF1TCU6AC1 SHWR NW

YET SP 2109 40SCT E60VKN 40T CF1 TCU6AC1 SHWR NW

YET SP 2137 E60BKN 20TRW- TCU8 LTGCG W

YET SP 2150 E60BKN 10TRW-A- CB8 HAIL PEA SIZE

YET SP 2215 E50BKN 30T CB9 TSTM MOVG E

YET SP 2245 E50BKN 30 CB8

6.6.7 June 22 1982

Figure 6.15a-b gives the temperature contours at 20:35 GMT and 22:15 GMT respectively. The storms of interest are those in eastern Alberta that moved eastward over Saskatchewan, marked A,B,C, and the cells marked D and E in south-western Saskatchewan. Just north of Cell A is a large precipitating cloud band.

From the satellite images, it is clear that considerable changes have occurred between passes. Some cells have merged and new storms have formed. Similar to the situation outlined for June 15, the position and track of the convective cores is very uncertain. In fact, it appears that not all of the cells have moved in the same direction as reflected by the inferred rain contours given in Figure 6.16a and 6.16b.

This is by far the most complicated of all cases investigated. Generally, results are acceptable in central Saskatchewan, but poor in the south. Coronation and Sullivan Lake both received near 8mm over 24 hours, and are very close to the 10mm contour associated with Cell A. However, from the TBRG records, ony 5.5mm fell at Coronation during the period covered by the satellite images. The weather observations for Coronation are given in Table 6.3. Moderate rain occurred at 22:00 GMT, associated with gusty winds of over 30 knots. It is quite likely that the gauge-rain amounts are under-estimated because of these strong winds. The narrow 20mm contour associated with Cell B lies near three stations, two of which (Scotfield and Sibbald) received nearly 15mm. Further south, conditions are worse. Acadia Valley lies within the 10mm contour of Cell C, but did not receive any rain whatever. The nadir of all test results is found over southern Saskatchewan. There are a number of stations enclosed by a 10mm or 20mm contour for which only a trace of precipitation was recorded. There is no obvious explanation for the complete failure of the satellite rain estimates in this area.

Overall, the satellite rain estimates do not provide a good fit to the observations. However, this is by far the most complex case. It is possible that cloud areas identified as being the same cell over two images are, in fact, different cells. If true, then the area covered by the rain contours would be much smaller. A shorter interval between satellite images than the 100 minutes provided by TIROS is required to follow individual cells when they are merging and evolving at a rapid rate. It is not surprising that this example proved too complicated for the simple technique employed here.

Figure 6.15a   As in Figure 6.1 except for June 22, 1982 at 2035 GMT.

Figure 6.15b   As in Figure 6.15a except at 2215 GMT.
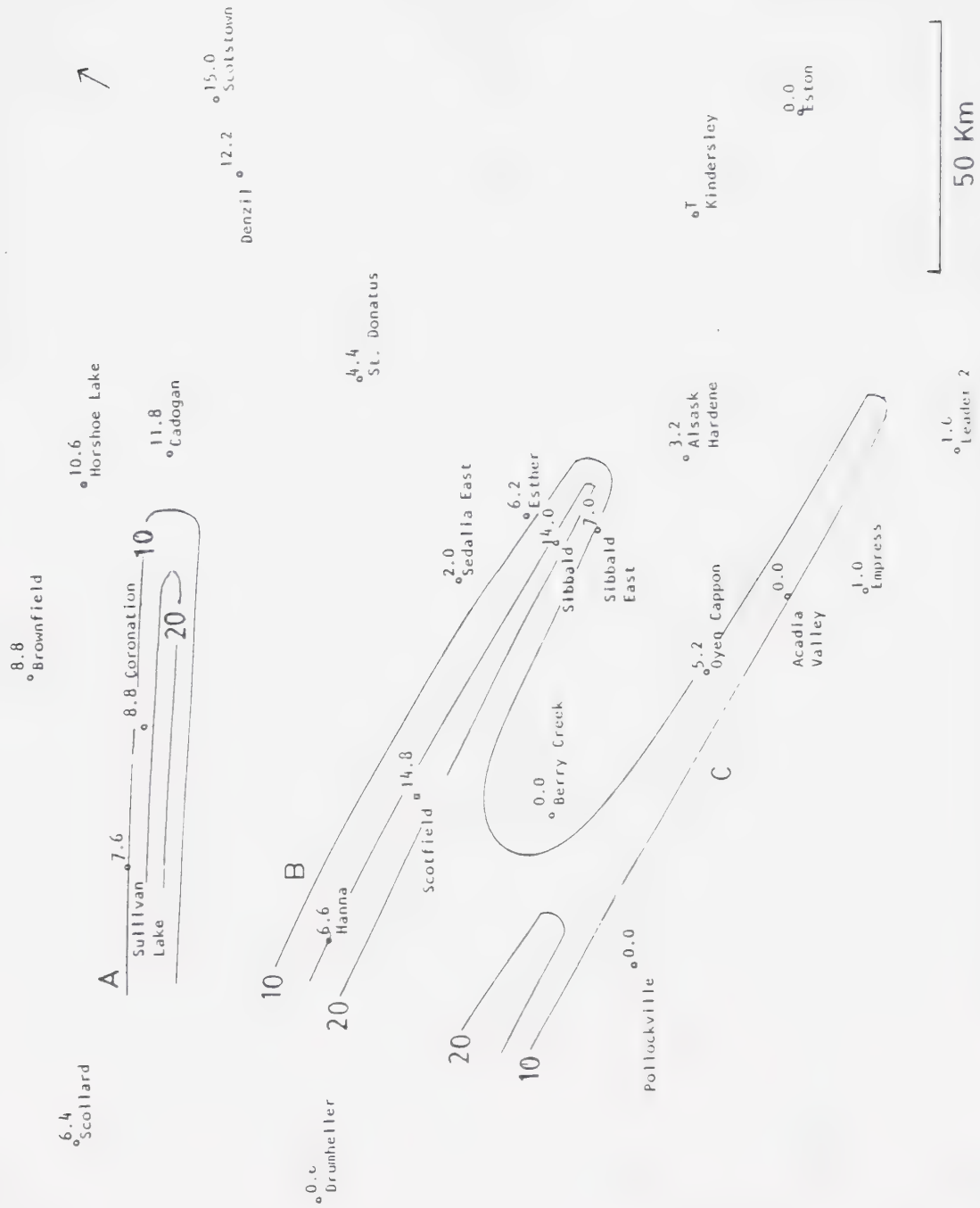
Figure 6.16a   As in Figure 6.2 except for June 22, 1982.

Figure 6.16b   As in Figure 6.16a except over southern Sakatchewan.
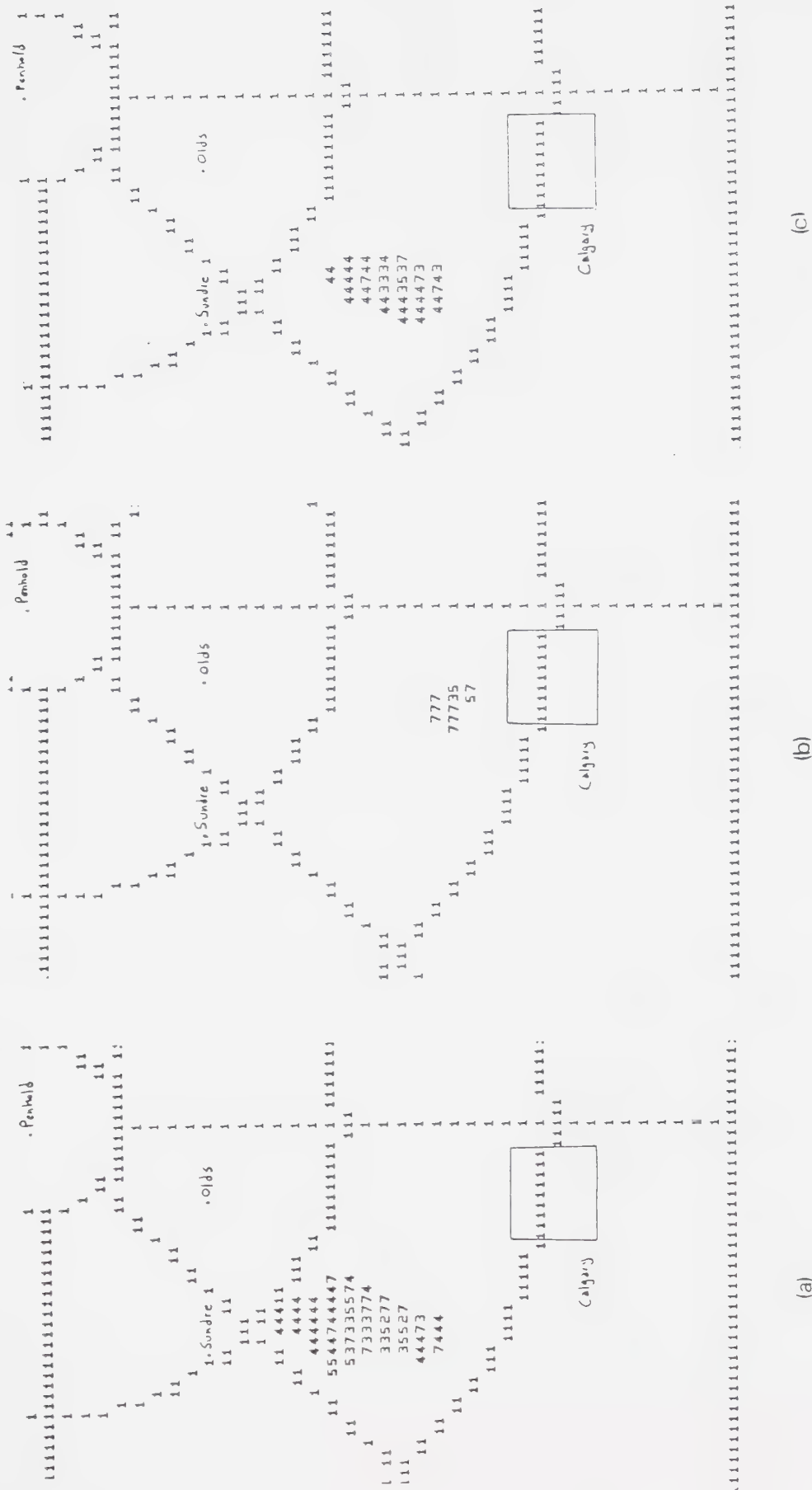
Table 6.3   SURFACE WEATHER OBSERVATIONS FOR JUNE 22, 1982

CORONATION

YCT SP 2005 40SCT E60BKN 90BKN 230OVC 15+T 3221G32
          CF1CB6ACC3CI1 SHWRS N QUAD PATCHS BD

YCT SP 2044 45SCT 60SCT E90BKN 15+ 3226G37 SC1CB4AS3CI1
                    OCNL LTGCG WNW HRZN SHWRS SE-S-W-N

YCT SA 2100 45SCT E60BKN 90BKN 230 BKN 15+ 3224G34
        SC1CB5AS2CI1 OCNL LTGCG SE-S-WNW HRZN SHWRS SE-S-W-N

YCT SP 2128 18SCT E60BKN 90BKN 230BKN 15+TRW- 3226G33
          CF1CB7AS2CI1 LTGCG S&W TSTM OVHD S AND W

YCT SA 2200 17SCT E55BKN 90BKN 230OVC 12TRW 3225G37
                    CF1CB7AS1CI1 FRQT LTGCG

YCT SP 2250 17SCT E55BKN 90BKN 220BKN 15TRW- 0126G36
                    CF1CB7AS1CI1 PRESFR

6.6.8 June 27 1982

The temperature contours for the single infrared image (at 21:15 GMT) available for this case is given in Figure 6.17. The attempt to map rainfall from this storm was approached with some hesitation. It is much larger than the other storms studied and may represent a different scale of development. The minimum cloud-top temperature is -71°C, far colder than any other cell investigated. Clearly, this storm is not the typical Cb that is common over Alberta and Saskatchewan. However, it was thought to be interesting to apply the rain-estimation technique to a variety of situations, so despite any possible misgivings, this case was included in the study.

Using Figure 5.4 as guidance, indicates maximum amounts of 30mm, corresponding to the very low temperatures. The size of the heavy rain area was drawn somewhat larger than usual, as a subjective response to the size and apparent intensity of the storm.

The rain contours are given in Figure 6.18 The arrow points toward the assumed direction of cloud motion based on the 700mb flow.

Estimated rainfalls do not match the observed amounts very well, but these are quite variable. Val-Marie, within the 20mm contour, received only 11.0mm. However, it is near the western edge of the cell and positioning errors could account for the discrepancy. A slight eastward shift of the rain pattern would put Val-Marie between the 10 and 20mm contours. Conditions further north cannot be explained so easily. Kincaid received only 2.2mm while slightly to the east 25.0mm fell on Lafleche. Generally, though, amounts in this area are near 10mm, consistent with the position of the 10mm contour. Accumulations > 20mm are common east of, and along the assumed storm track. However, these occurred well after the time of the satellite pass and considerable evolution of the storm could have taken place. Ormiston, for example, received its 26mm three hours after the time of the satellite image.

While this case is not a complete failure, as heavy rain amounts were reported, it is far from a success. As usual, more rain data would be helpful, especially in extreme southern Saskatchewan. The best that can be said is that the threat of heavy rain was properly predicted. However, with a storm of this intensity, even a novice meteorologist would have foreseen the possibility of associated severe weather.

Figure 6.17   As in Figure 6.1 except for June 27, 1982 at 2115 GMT.

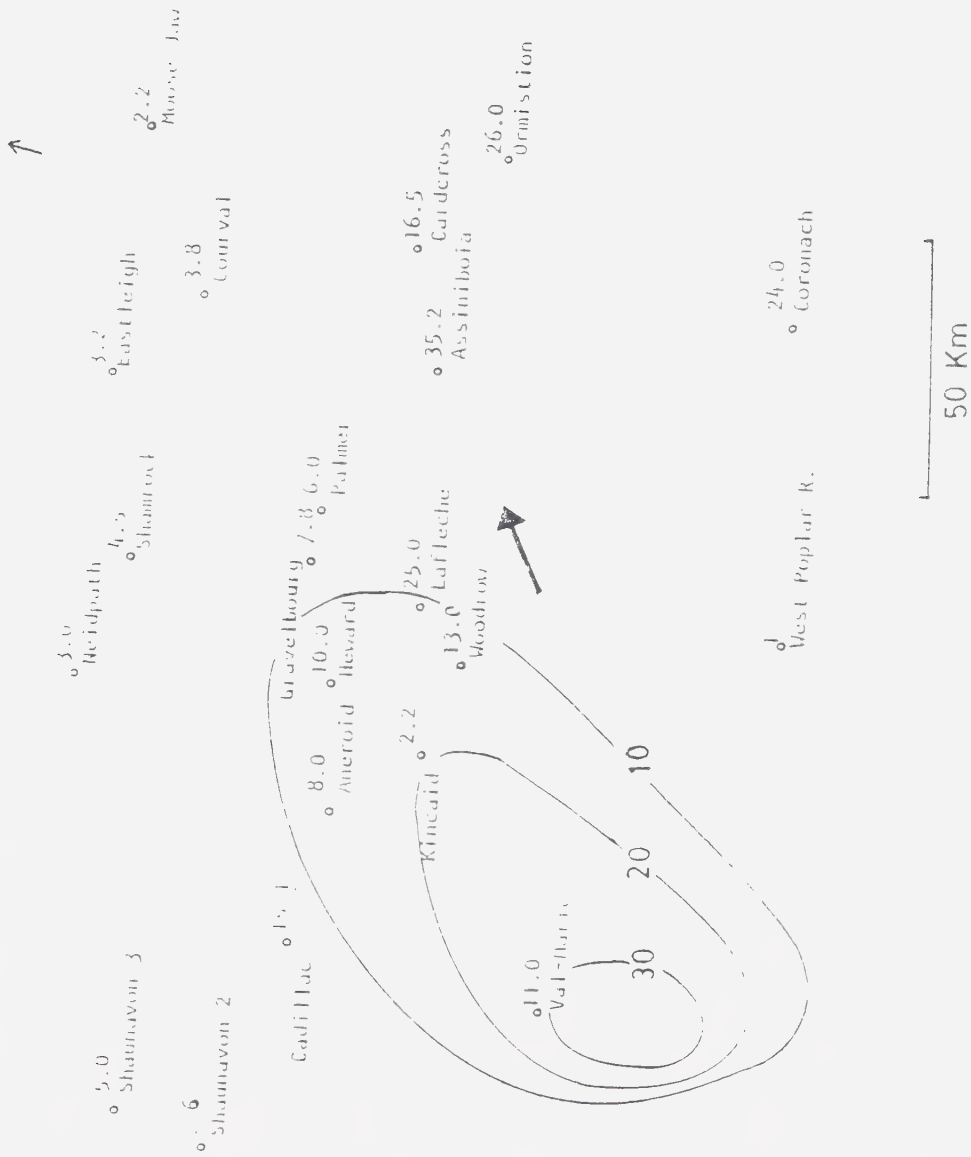Figure 6.18   As in Figure 6.2 except for June 27, 1982. The heavy arrow points in the direction of motion based on the 700mb winds.

6.6.9 July 29 1982

From the temperature contour maps at 20:00 GMT and 21:40 GMT, given in Figure 6.19, it is seen that there are many small cells that intensified between passes. This day was chosen for study as the majority of the cells appeared to be only borderline cases from the point of view of producing heavy rain amounts. As can be seen on the precipitation map given in Figure 6.20 the rain areas are quite small. Unfortunately, once again they lie mainly between, rather than over the climate stations. The largest area of inferred precipitation is just northwest of Edson, where a 20mm contour was drawn. Edson received only 4.1mm from 22-23 GMT. However, the weather reports, shown in Table 6.4, reveal that the storm was an intense one, giving heavy rain and hail. Also, as only 6/10 of the sky was covered by the Cb it is reasonable to assume that the storm did not pass directly overhead, and that amounts > 4mm could have fallen nearby. The area of greatest observed precipitation is near Rocky Mountain House. TBRG records show that this rain did not occur until 01-02 GMT and is possibly associated with the small 10mm contour to the southwest. This area has been denoted "forming" to indicate that a new cell appeared at this location on the second satellite image. New, in this case, means that the cell was not visible on the first image.

The 10mm contour east of Edmonton is associated with a small storm that intensified as it moved eastward through the Edmonton area. Rain amounts are light. Woodbend received 3.0mm while nearby stations reported less than 1mm. The cell was also seen by the ARC radar, but, unfortunately, not until 21:34 GMT. Figure 6.21a the rain intensity map for that time, shows that rates > 10mm/hr were occuring. However, the storm dissipated by 22:08 GMT and the rain accumulation map for 21:34 GMT to 22:08 GMT gives amounts less than 2.5mm. The weather reports for Edmonton International Airport are given in Table 6.4 and show that a heavy shower was seen east of the airport at 21:21 GMT.

Overall, no verification of the inferred rain amounts is possible, as the storms moved between climate stations. However, the lack of even one report of accumulations as large as predicted suggests that the inferred rain amounts are too large.

Figure 6.19   As in Figure 6.1 except for July 29, 1982 at a)2000 GMT and b) 2140 GMT.
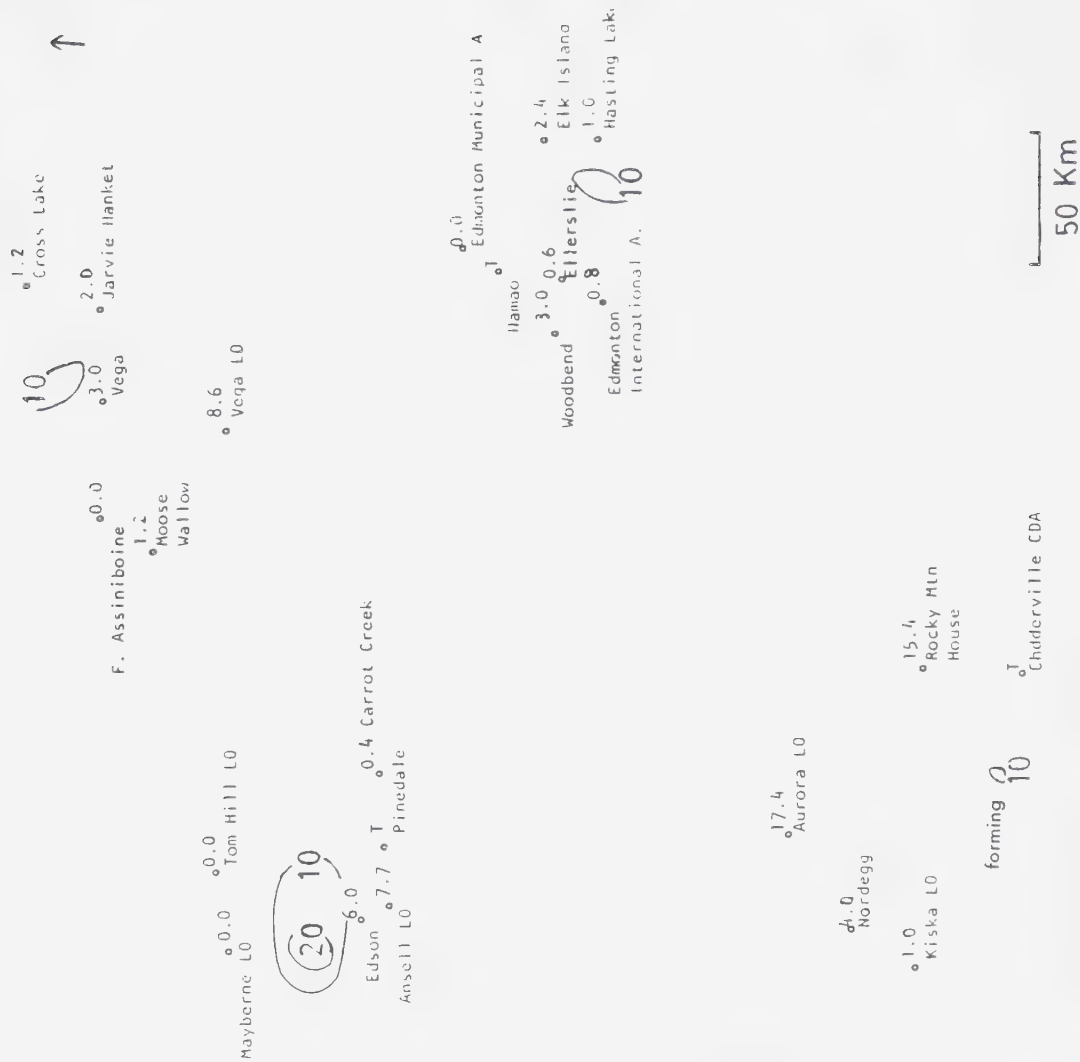
Figure 6.20   As in Figure 6.2 except for July 29, 1982.

(a)

(b)

(c)
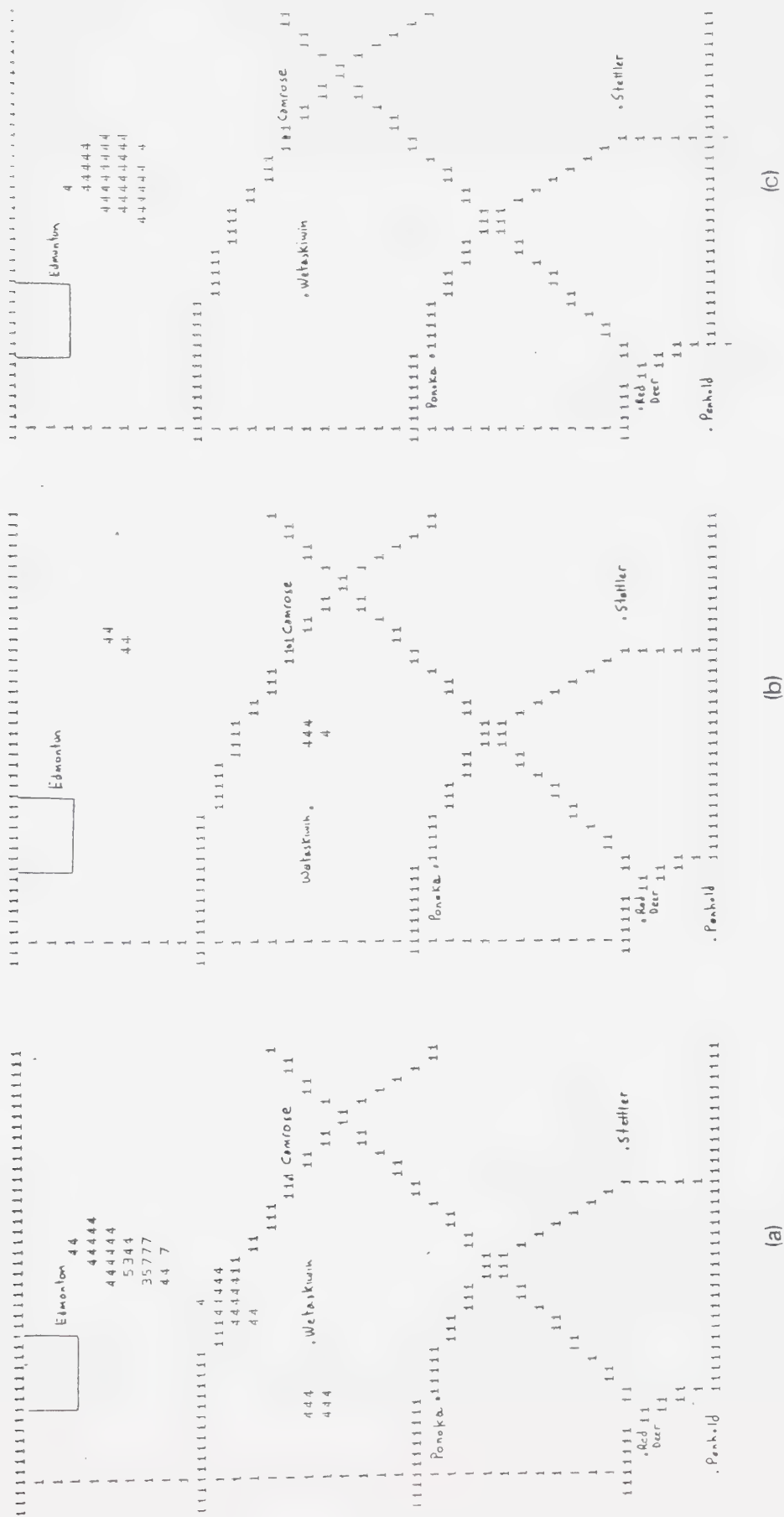
Figure 6.21   As in Figure 6.9 except for July 29, 1982 at a) 2135 GMT b) 2224 GMT
and c) 2135 - 2224 GMT.

.

Table 6.4   SURFACE WEATHER OBSERVATIONS FOR JULY 29, 1982

EDSON

YET SA 2100 70SCT 120SCT 30 CB2AC2 SHWRS N-NW

YET SP 2136 70SCT E120BKN 30T CB5AC1 LTGCG NW-SE

YET RS 2200 E70BKN 120BKN 5T+RW+A CB6 AC2 LTG ALL TYPES OVHD
                                                    A PEA SIZE

YET SP 2215 E70BKN 120BKN 15TRW- CB7 AC2 TSTM N-E MOVG SE
                                                    PRESFR

YET SA 2300 E60BKN 300BKN 30 CB6CI1 SHWRS ALQDS LTGCG E-SW

EDMONTON MUNICIPAL AIRPORT

YXD SA 2100 E60BKN 90BKN 15 TCU6AC2 K

YXD SA 2200 E80BKN 290BKN 15 AC6CI1 K CB EMBDD E

YXD SA 2300 90SCT 290-BKN 15 AC2CI2 K CB EMBDD E

EDMONTON INTERNATIONAL AIRPORT

YEG SA 2000 -X 40SCT E120BKN 300BKN 12 K1CU2AC4CI1

YEG SP 2044 -X E40BKN 120BKN 12T K1CB6AC1 LTGCG

YEG SA 2100 -X E40BKN 120BKN 12TRW-- K1CB7ACC1 LTGCG

YEG SP 2105 -X E40BKN 120 BKN 12TRW- K1CB6ACC1 LTGCG

YEG SP 2121 40SCT E100BKN 12 CB4ACC3 HVY SHWRS E

YEG SA 2200 40SCT 100SCT 12 CB4ACC1 K

YEG SA 2300 40SCT 300-BKN 12 CB2 CI CB TOPS W K

6.7 Discussion

Based on the cases studied some general comments can be made.

Inferred rain amounts and the position of the contours best represented the observed rainfall for isolated cells. Results were expectedly disappointing for cases involving merging cells, as large areas of obscuring cirrus debris from the merged anvils made it difficut to follow any given cloud area from one image to the next. Increased frequency of satellite images would aid in the solution to this problem. Even for isolated cells, the deduced track of the cell often differed from the actual path (based on the rain amounts) due to a combination of three errors:

1.   gridding uncertainties (10km)

2.   errors introduced when two images were overlaid (up to 30km)

3.   uncertainty in the position of the convective core within the cirrus anvil (error dependent on size of cloud area)

While precipitation amounts appear to be generally overestimated, this is to be expected. The rain contours drawn represent the maximum amounts associated with a cell passing directly overhead. As the cells studied here are generally smaller than the distance between climate stations, it is quite likely that, in many cases, the maximum rainfall occurred at some location between the stations. Radar-derived accumulations were obtained for three storms. Satellite estimates agreed on one occasion but were greater than the radar amounts for the other two. Results would have to be described as "mixed".

The observed rain amounts occasionally exhibited large variations over short distances (see discussion for June 14 and 15 for example). It is unknown if this was caused by a small rain area passing directly over one station while just grazing another, or the result of small-scale variations within a large precipitation element. The rain estimation method used here is not capable of discerning the latter situation.

One extremely intense storm was investigated. In general, intense storms are not expected to be well handled. The largest rain amount that can be predicted, for a storm moving at about 50km/hr, is 30mm (corresponding to a cloud-top temperature of -70°C). One-hour accumulations much greater than this are possible. For example, the storm of July 01, 1982 (see Chapter 4) gave 66mm to Lethbridge. Cloud-top temperatures at that

time are unknown, but were only -60°C one hour later. It may be that some feature other than temperature alone can be used to infer higher rain amounts. An example would be a storm exhibiting a "V" shaped cloud-top temperature structure. Prediction of the rain rates associated with such features will not be possible until they are first included in the development sample.

Finally, the question of "false alarm ratio" (the fraction of storms that are cold and bright but do not give heavy rain) has not been answered by the few case-studes investigated here. The cells over southern Saskatchewan on June 22, 1982 and near Moose Jaw on July 14, 1982 (see Chapter 4) were all bright and cold but little rain was reported. In the case of Moose Jaw, a thunderstorm is known to have occured and it is possible that the storm only grazed the city. However, the balance of cases strongly suggest that at least the threat of heavy rainfall somewhere along the storms path can be succesfully identified. With better time resolution of satellite images, the crude interpolation of temperature and brightness required to determine the beginning and end of rain areas would not be required. This should lead to much more accurate estimates of rain areas.

Overall, then, it is felt that "reasonable" estimates of rain amounts can be made using the TIROS satellite images. Complete accuracy is not obtainable as even the ground observed rain amounts can be in considerable error. Here, rain amounts were predicted only in very broad ranges. No doubt, more accurate and higher resolution satellite and rain data would result in a better rain estimation scheme, as would the inclusion of radar data. This, and other important improvements are the subject of the next and final chapter.

7. Conclusions and Future Work

7.1 Conclusions

Based on the development sample the following conclusions have been reached:

1. Given point rainfall amounts of $>$ 10mm, produced by the passage of a convective storm, the cloud top temperature is $<$ -49°C and the brightness is $>$145.

2. The amount of precipitation is inversely proportional to temperature.

3. Rain intensity is proportional to the temperature difference between the cloud top and the tropopause.

Result (3) is tentative as the sample size upon which it is based is small. However, it is potentially the most important, as the point rain accumulation, based on the storms studied here, rests mainly on the storm's rain rate.

When (1) and (2) were applied to a set of satellite images (in order to infer rain amounts) the estimates were comparable to observed accumulations for isolated cells. Results were poor for more complex situations such as merging cells, because individual cloud areas could not be tracked over two succesive images. Inferred rain ranges were large and the majority of observed rain accumulations were for 24 hours, so that comparisons are not completly reliable. Nonetheless, results are encouraging enough to warrant further investigation. Given in the next section are suggestions for extensions to the work done here that would, it is hoped, lead to a useful satellite rain estimation technique for the Canadian Prairies.

7.2 Future Work

7.2.1 Satellite

A basic step forward would be to use the HRPT visible and infrared images. Digital data for these are available from the Alberta Weather Centre in Edmonton. However, TBRG records may not be available until many months after the period they cover which requires that many months of satellite data be saved on magnetic tape until the days suitable for study are known. This could be a problem as tapes are not regularly archived

at the Weather Centre. The alternative is to produce temperature and brightness maps on a daily basis, however this too may not be feasible within the constraints of an operational weather office. Undoubtedly some compromise could be reached, such as saving only tapes of days which exhibit considerable convective activity.

Increased time resolution is also essential. GOES images are available every 30 minutes, but the resolution of the infrared images is only 16km over central Alberta. This is still useful as areal cloud growth could be monitored. Also relationships between temperature fields from co-incident GOES and TIROS images could be used to revise any incorrect values caused by the poor GOES resolution. At the very least, temperature changes could be obtained from the ½ hourly GOES pictures.

Duration of satellite coverage is important as well. The Weather Centre receives data from both the NOAA-7 and 8 satellites. At 2 passes / satellite this allows coverage for 5 hours. Of course, the use of GOES images makes continuous cloud monitoring possible. It would be interesting to determine if the correlation between satellite estimated and observed rain amounts increased with increasing duration of coverage.

Brightness values should be normalized for overhead illumination. This would allow better comparisons between different geographical areas, time of year, and other techniques developed by other investigators.

7.2.2 Radar

The most important improvement, next to better satellite data, is the introduction of radar data. The high temporal resolution would ensure that a radar map would be available at a time very close to that of the satellite pass. It would, therefore, no longer be necessary to correct and estimate cloud-top temperatures and brightness for time differences between the satellite picture and observation of rain. The wide areal coverage would allow correlation between echo strength or area to temperature and brightness throughout the cloud area. This is especially valuable as it would help define the position and size of the storm s convective core in relation to the overall cloud area and temperature structure. Furthermore, changes in the intensity of the rain rate could be easily monitored.

7.2.3 Rain

Even with radar data, there is still a pressing need for improved ground-truthing. It would be valuable to implement a dense network of high resolution rain gauges in an area frequented by convective storms, such as central Alberta. As a minimum, the actual traces from the existing TBRG network should be made available, rather than only the TAB31 charts which give only hourly amounts. This would allow accurate timing of the precipitation event, both in amount and intensity. These are available by special request from AES headquaters in Toronto, but only 8 months to a year after the date of the rain event.

7.2.4 Statistics

A much larger sample than was used here is required for proper statistical analysis. Also, all convective storms should be used in the development sample, independent of temperature, brightness or rainfall. Of course, this will result in a very large sample, but more importantly, it would avoid biasing the sample. This would eliminate one of the problems encountered here, namely that it is not known if the distribution of cloud-top temperatures for the "heavy rain" cases is different from that for all storms. Also the use of all cells would lead to a scheme that could predict smaller rain amounts (0-10mm), and allow an estimate to be made of the false alarm ratio for inferring heavy rain.

7.2.5 Further Suggestions

The shape of the cloud area or temperature structure could be used to infer the intensity of a storm. For example, a wedge-shaped anvil may indicate strong divergence aloft and hence a more intense storm (Scofield and Oliver, 1981).

Climatology should also be used to adjust rain estimates. If a geographical area is known to receive enhanced or diminished rainfalls, due to some topographical feature, this should be reflected in the predicted rain amounts.

Finally, all tests mentioned above or performed in this study could be applied to synoptic-scale rain events. A preliminary test was made for such a case that occurred on July 02, 1982. Considerable rainfall was found beneath an area with cloud-top temperatures near $-20^{\circ}C$ while almost no rain was reported under an area with extensive

cloud cover and temperatures near -45°C. Similar behavior was seen over Edson on July 14, 1982 (see Chapter 3). Clearly, the procedure used to infer synoptic rain amounts may be quite different than those for convective storms.

If all that is required is some means to identify areas were heavy rain is likely, then the simple technique presented in this study is a valuable tool. However, much work remains to be done. Given the experience of other investigators, there is little doubt that a method of estimating rain amounts, large or small, from satellites can be developed. It is hoped that the work presented here proves sufficiently encouraging to stimulate further reasearch, and that the suggestions given above will soon be acted upon.

Bibliography

Adler, R.F. and D.D. Fenn, 1979a: Thunderstorm intensity as determined from satellite data. *J. Appl. Meteorol.*, **18**, 502-517.

Adler, R.F. and D.D. Fenn, 1979b: Thunderstorm vertical velocities estimated from satellite data. *J. Atmos. Sci.*, **36**, 1747-1754.

Adler, R.F., A.J. Negri and D. Atlas, 1981: A simple basis for relating geosynchronous satellite infrared observation to thunderstorm rainfall. *Fourth Conference on Hydrometeorology, Oct. 7-9, Reno, Nevada*, American Meteorological Association, Boston, Mass., 121-128.

Adler, R.F. and M.J. Markus, 1983: Satellite severe thunderstorms detection: potential and limitations. *Thirteenth Conference on Severe Local Storms, Oct. 17-20, 1983, Tulsa, Oklahoma*, American Meteorological Society, Boston, Mass., J33-J36.

Atmospheric Environment Service of Canada, 1976: *Manual of Surface Observations*, Queen's Printer of Canada, Ottawa.

Augustine, J.A., J.G. Meitin, C.G. Griffith and W.L. Woodley, 1981: An objective evaluation of the the Griffith/Woodley rain estimation technique. *Fourth Conference on Hydrometeorology, Oct. 7-9, 1981, Reno Nevada*, American Meteorological Society, Boston, Mass., 134-140.

Barrett, E.C. and D.W. Martin, 1981: *The Use of Satellite Data in Rainfall Monitoring*, Academic Press, New York 340pp.

Curtis, W.R. and P.K. Roa, 1969: Gulf Stream thermal gradients from satellite, ship and aircraft observations. *Journal of Geophysical Research*, **74**, 6984-6990.

Doneaud, A.A., S. Ionescu-Niscov, D.L. Priegnitz and P.L. Smith, 1983: The area-time integral as an indicator for convective rain volumes. *Twenty-first Radar Conference, Sept. 19-23, 1983, Edmonton Alberta*, American Meteorological Society, Boston, Mass., 675-680.

Greaves, B.T., 1981: *Satellite Measured Changes in Thermal Fields of an Arctic Island*. MSc Thesis, University of Alberta, Edmonton, 189pp.

Griffith, C.G., W.L. Woodley, P.G. Grube, D.W. Martin, J. Stout and D.N. Sikdar, 1978: Rain estimation from geosynchronous satellite imagery - visible and infrared studies *Mon. Weather Rev.*, **106**, 1153-1171.

Griffith, C.G., J.A. Augustine and W.L. Woodley, 1981: Satellite rain estimation in the U.S. High Plains. *J. Appl. Meteorol.*, **20**, 53-56.

Hare, F.K. and M.K. Thomas, 1974: *Climate Canada.* Wiley Publishers of Canada, Toronto, 256pp.

Hymsfield, G.M., G. Szejwach, S. Schots and R.H. Blacmer Jr., 1983: Upper-level structure of Oklahoma tornadic storms on 2 May, 1979, II: proposed explanation of "V" pattern and internal warm region in infrared observations. *J. Atmos. Sci.*, **40**, 1756-1767.

Lauritson, L., G.J. Nelson and F.W. Porto, 1979: *Guide For Calibrating TIROS-N/NOAA Radiometers for Direct Readout Users (Draft).* NESS, Washington D.C. 90pp.

Lethbridge, M., 1967: Precipitation probability and satellite radiation data.   *Mon. Weather Rev.*, **95**, 487-490.

Lovejoy, S. and G.L. Austin, 1979a: The delineation of rain areas from visible and IR satellite data for GATE and mid-latitudes.   *Atmosphere Ocean,* **17**, 77-92.

Lovejoy, S. and G.L. Austin, 1979b: The sources of error in rain amount estimating schemes for GOES visible and IR satellite data.   *Mon. Weather Rev.*, **107**, 1048-1054.

Martin, D.W. and V.E. Suomi, 1972: A satellite study of cloud clusters over the tropical North Atlantic Ocean.   *Bull. Am. Meteorol. Soc.*, **53**, 135-156.

Negri, A.J. and R.F. Adler, 1981: Relation of satellite-based thunderstorm intensity to radar estimated rainfall.   *J. Appl. Meteorol.*, **20**, 288-300.

Reinelt, E.R., P. Hof, D. Oracheski and J. Broszkowski, 1975: *Research Studies of Numerical Enhancement of APT Scanning Radiometer Data for Application to Arctic Weather and Ice Prediction.*   Final Report, DDS(AES) Contract 0SV4-0183, University of Alberta, Edmonton, 204pp.

Schneider, S.R. and R.A. Scofield, 1980: Satellites and the Appalachin flash flooding of July 15, 1979.   *Second Conference on Flash Floods, March 18-20, 1980, Atlanta, Georgia*, American Meteorological Society, Boston, Mass., 91-96.

Schwalb, A., 1978: *The TIROS-N/NOAA A-G Satellite Series.*   NOAA Tech. Mem., NESS 95, Washingon, D.C., 75pp

Scofield, R.A., 1981: Satellite-derived rainfall estimates for the Bradys Bend, Pennsylvania flash flood.   *Fourth Conference of Hydrometeorology*, Oct. 7-9, 1981, Reno, Nevada, American Meteorological Society, Boston, Mass., 188-193.

Scofield, R.A. and V.J. Oliver, 1977: *A Scheme for Estimating Convective Rainfall from Satellite Imagery.* NOAA Tech. Mem., NESS 86, Washington, D.C., 47pp.

Scofield, R.A. and V.J. Oliver, 1980: Some improvements to the Scofield/Oliver Technique. *Second Conference on Flash Floods, March 18-20, 1980, Atlanta, Georgia,* American Meteorological Society, Boston, Mass., 115-122.

Scofield, R.A., V.J. Oliver and L. Spayd, 1980: Estimation rainfall from thunderstorms with warm tops in the infrared imagery. *Eighth Conference on Weather Forecasting and Analysis, June 10-13, 1980, Denver, Colorado,* American Meteorological Society, Boston, Mass., 85-92.

Stout, J.E., D.W. Martin and D.N. Sikdar, 1979: Estimating GATE rainfall with geosynchronous satellite images. *Mon. Weather Rev.,* **107**, 585-598.

Whitney, L.F. and S. Fritz, 1961: A toronado-producing cloud pattern seen from TIROS I. *Bull. Am. Meteorol. Soc.,* **42**, 603-614.

Woodley, W.L. and B. Sancho, 1971: A first step toward rainfall estimation from satellite cloud photographs, *Weather,***26**,279-289.

Wieler, J., 1981: *The Application of Satellite and Radar Data in Thunderstorm Research.* MSc Thesis, University of Alberta, Edmonton, 125pp.

Wiley, D.P. and D. Laitsch, 1983: The impact of different satellite data in rain-estimation schemes. *Journal of Climate and Applied Meteorology,* **22**, 1270-1281.

Zawadski, I.I., 1973: Statistical properties of precipitation patterns. *J. Appl. Meteorol.*, **12**, 459-472.

Appendix A

Infrared Calibration Equations

The step-by-step procedure used to convert the infrared radiance counts to equivalent black-body temperature has been described in section 2.1.2. Here, the coefficients and equations needed to apply those procedures are given.

A.1 Conversion of PRT Counts to Temperature

The equations used to convert the satellite counts from the four platinum resistor thermistors into temperature in ^oK are given in Table A.1. TMIRP are the digital counts. The factors of 4 and 16 are used to convert the received 8 bit number into a 10 bit number.

A.2 Conversion from Temperature to Black-body Radiation

The black-body radiation N(T) associated with temperature T is given by

$$N(T) = \int_{\nu_1}^{\nu_2} \beta(\nu,T)\hat{\phi}(\nu)d\nu \qquad (A.1)$$

where $\beta(\nu,T)$ is the Planck function, ν is the wavenumber (cm^{-1}) and $\hat{\phi}(\nu)$ is given by

$$\hat{\phi}(\nu) = \frac{\phi(\nu)}{\int_{\nu_1}^{\nu_2}\phi(\nu)d\nu} \qquad (A.2)$$

where ν_1 and ν_2 are the wavenumbers at the limit of the response function. Approximations of equations A.1 and A.2 are

$$N(T) = \sum_{i=1}^{n}(\nu_i,T)\hat{\phi}(\nu_i)\Delta\nu \qquad (A.3)$$

and

$$\hat{\phi}(\nu_i) = \frac{\phi(\nu_i)}{\sum_{j=1}^{n}\phi(\nu_j)\Delta\nu} \qquad (A.4)$$

155

The form of the Planck function used is

$$\beta(\nu_i, T) = c_1 \nu_i^3 / (\exp(c_2 \nu_i / T) - 1) \tag{A.5}$$

where the universal constants C1 and C2 are

$$C1 = 1.1910659 \times 10^{-5} \quad mw/(m^2 \text{ sterad } cm^{-4})$$

$$C2 = 1.438833 \text{ cm}^o K$$

Values of ν_{h+1}, $\Delta\nu$, n and $\phi(\nu_i)$ are given in Table A.2.

A.3 Correction for Non-Linearity of Space

As the output of the radiometer is not perfectly linear, a correction is applied at step 5 in section 2.1.2 by using a non-zero value for the radiance of space. The values used are -1.151 and -1.176 for TIROS-N and NOAA-7, respectively.

Table A.1   Conversion of satellite PRT digital counts(TMIRP)
                to Temperature (T) in °K

$T1=277.73+4*0.047752*TMIRP(1)+16*8.29E-6*TMIRP(1)**2$
$T2=277.41+4*0.046637*TMIRP(2)+16*11.01E-6*TMIRP(2)**2$
$T3=277.14+4*0.045188*TMIRP(3)+16*14.77E-6*TMIRP(3)**2$
$T4=277.42+4*0.046387*TMIRP(4)+16*10.59E-6*TMIRP(4)**2$

$T1=277.099+4*0.05048*TMIRP(1)+16*2.823E-6*TMIRP(1)**2$
$T2=276.734+4*0.05069*TMIRP(2)+16*2.493E-6*TMIRP(2)**2$
$T3=276.876+4*0.05148*TMIRP(3)+16*1.040E-6*TMIRP(3)**2$
$T4=276.160+4*0.05128*TMIRP(4)+16*1.414E-6*TMIRP(4)**2$

Table A.2   Values of ν , $\Delta\nu$, n and $\hat{\phi}(\nu_j)$ for
                        a) TIROS-N and b) NOAA-7
                used in determining the black body radiance

(a) ν_1 =837.6189 $\Delta\nu$ =2.41389   n =60

$\hat{\phi}_i$
0.0,0.33701E-4,0.73654E-4,0.10611E-3,0.14390E-3
0.24906E-3,0.50024E-3,0.95828E-3,0.15939E-2,0.23496E-2
0.31779E-2,0.40893E-2,0.51155E-2,0.62748E-3,0.74753E-2
0.85702E-2,0.94211E-2,0.10012E-1,0.10418E-1,0.10718E-1
0.10961E-1,0.11164E-1,0.11335E-1,0.11489E-1,0.11635E-1
0.11786E-1,0.11954E-1,0.12147E-1,0.12374E-1,0.12644E-1
0.12877E-1,0.12887E-1,0.12539E-1,0.12331E-1,0.12071E-1
0.11931E-1,0.11982E-1,0.12175E-1,0.12387E-1,0.12766E-1
0.13462E-1,0.14131E-1,0.14239E-1,0.13355E-1,0.11367E-1
0.87492E-2,0.60630E-2,0.38563E-2,0.23495E-2,0.13991E-2
0.84093E-1,0.51723E-3,0.33615E-3,0.24878E-3,0.20690E-3
0.16664E-3,0.11659E-3,0.59942E-4.0.61584E-8.0.0

(b) ν_1 =852.19552 $\Delta\nu$ =2.50516   n =60
$\hat{\phi}_i$
0.68434E-4,0.37976E-4,0.31403E-4,0.72602E-4,0.17647E-3
0.32774E-3,0.50486E-3,0.75401E-3,0.13345E-2,0.23817E-2
0.37972E-2,0.51690E-2,0.63215E-2,0.73632E-2,0.82421E-2
0.87867E-2,0.90399E-2,0.94533E-2,0.99801E-2,0.10065E-1
0.10489E-1,0.10624E-1,0.10989E-1,0.11130E-1,0.11457E-1
0.11626E-1,0.11927E-1,0.12171E-1,0.12519E-1,0.12767E-1
0.12932E-1,0.12948E-1,0.12944E-1,0.12901E-1,0.12917E-1
0.12998E-1,0.13105E-1,0.13329E-1,0.13504E-1,0.13687E-1
0.13440E-1,0.12832E-1,0.11237E-1,0.95630E-2,0.73611E-2
0.52078E-2,0.34448E-2,0.21374E-2,0.12548E-2,0.70548E-3
0.39308E-3,0.22416E-3,0.13631E-3,0.85331E-4,0.55726E-4
0.41953E-4,0.39776E-4,0.45328E-4,0.54746E-4,0.0

Appendix B

Calculation of Grid Positions

The position of townsites in terms of scan line and pixel number was determined by the point-by-point gridding procedure described by Reinelt et al. (1975, pp 135-141). Therefore, only a brief description is given here, following the summary given by Greaves (1981). Reference should be made to Reinelt et al. for further details.

The geometry of the satellite's orbital path, assuming a circular orbit and spherical earth, is given in Figure B.1. The satellite is assumed to start at the equator at ϕ_0, ϕ_0 where ϕ is the latitude and θ is the longtitude. The satellite moves along the arc "s" and scans a point on the ground at position ϕ_1, θ_1, an arc length Y radians from the satellite subpoint.

During the time that the satellite has moved over the arc s, the earth has rotated a distance given by

$$(s/2\pi)(2\pi L/360) = ks \tag{B.1}$$

where $k = L/360$ and L is the satellite's regression rate in degrees per orbit. The total longitudinal displacement that occurs between the time that the satellite crossed the equator and scanned position ϕ_1, θ_1 is, therefore, given by

$$\theta_0 - \theta_1 - ks \tag{B.2}$$

Spherical trigonometry is then used to determine a relationship between the arc length s and the position ϕ_1, θ_1. From Reinelt et al., this is given by

$$\begin{aligned} F(s) = \sin(s)\cos(\theta_0-\theta_1-ks)\cos(\phi_1) &- \cos(s)\sin(i)\sin(\phi_1) \\ &+ \cos(s)\sin(\theta_0-\theta_1-ks)\cos(i)\cos(\phi_1) = 0 \end{aligned} \tag{B.3}$$

This equation is solved by first taking its derivitive

$$\begin{aligned} F'(s) = \cos(s)\cos(\theta_0-\theta_1-ks)\cos(\phi_1) &+ k\sin(s)\sin(\theta_0-\theta_1-ks)\cos(\phi_1) \\ + \sin(s)\sin(i)\sin(\phi_1) &- \sin(s)\sin(\theta_0-\theta_1-ks)\cos(i)\cos(\phi_1) \\ - k\cos(s)\cos(\theta_0-\theta_1-ks)\cos(i)\cos(\phi_1) & \end{aligned} \tag{B.4}$$
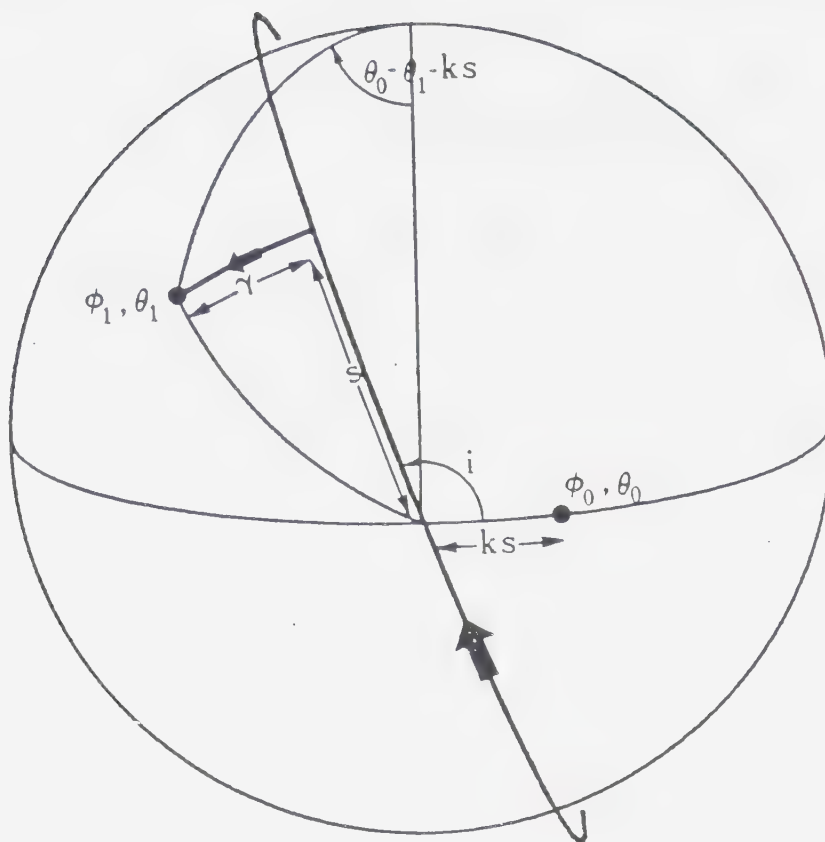
Figure B. 1   Geometry of a polar-orbiting satellite on a
non-rotating earth. See the text for explanation
of symbols. (After Reinelt et al., 1975).

then, using a first guess for s, performing the iterative procedure

$$s_{i+1} = s_i - F(s_i)/F'(s_i) \tag{B.5}$$

which converges to the root of equation B.3. The initial guess, s_0, is determined by re-writing equation B.3 as

$$\frac{\sin s_0}{\tan s_0} = \tan s_0 = \frac{\sin(i)\sin(\phi_1) - \sin(\theta_0-\theta_1-ks_0)\cos(i)\cos(\phi_1)}{\cos(\theta_0-\theta_1-ks_0)\cos(\phi_1)} \tag{B.6}$$

and setting $s_0 = \phi_1$ on the right hand side of equation B.6.

The number of the scan line which passes through ϕ_1,θ_1 (counting from the equator) is easily determine from

$$\# \text{ of scan lines} = (s)(P)(RPM)/2\pi \tag{B.7}$$

where P is the orbital period in minutes and RPM is the rotation rate of the scanning radiometer.

The position along the scan line from the subpoint to ϕ_1,θ_1 is found by relatiing the arc length γ along the ground, given by

$$\sin\gamma = \sin(\theta_0-\theta_1-ks)\sin(i)\cos(\phi_1) + \cos(i)\sin(\phi_1) \tag{B.8}$$

to the rotation of the scanning radiometer η (see Figure B.2) found from

$$\tan\eta = R\sin\gamma/(H+R(1-\cos\gamma)) \tag{B.9}$$

where R is the radius of the earth, and H is the height of the satellite above the ground. The arc length η is then converted to a pixel along the scan line using

$$(\eta)(DIGF)(60)/((2\pi)(RPM)) \tag{B.10}$$

where DIGF is the digitizing frequency in values per second.
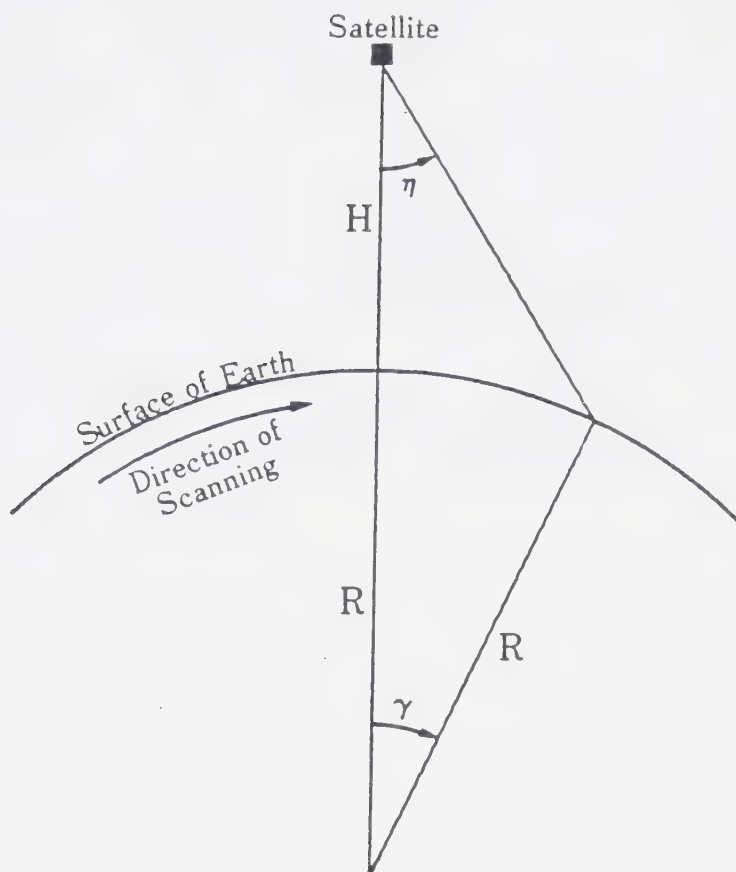
Figure B.2   Geometry of the scanning radiometer as it views the earth.
See the text for explanation of symbols.
(After Reinelt et al., 1975)

Appendix C

Surface Weather Observations

Following are the surface weather observations for the dependent sample discussed in chapter 4. The format is as follows:

1. three letter station identifier
2. type of report
3. time of report (GMT)
4. cloud heights (hundreths of feet) and amounts (tenths)
5. visibility (statute miles)
6. weather and obstructions to vision
7. winds (in tens degrees and knots, included only if > 15 Kts)
8. cloud type and opacities
9. remarks

Table C.1   SURFACE WEATHER OBSERVATIONS FOR JULY 07, 1979

EDSON

```
YET RS 1900 E200VC 6TRW--A CB10 LTGCG ALQDS

YET SP 1920 E300VC 15TRW-  CB10 LTGCG ALQDS

YET SA 2000 E300VC 15TRW-  CB10 LTGCG ALQDS

YET SP 2005 E200VC 2TRW+F  CB10 LTGCG ALQDS

YET SP 2040 E25BKN 15TRW-  CB9

YET SA 2100 E25BKN 20TRW-  CB9 LTGCG

YET SA 2200 E30BKN 30RW-   CB9 LTGCG NE
```

Table C.2   SURFACE WEATHER OBSERVATIONS FOR JULY 10, 1979

EDSON

YET SP 2040 E20OVC 15TRW CB10 LTGCG ALQDS VSBY W 1 MI

YET SA 2100 E20OVC 20TRW- CB10 LTGCG ALQDS TSTM MVG E
                                   MAMA

YET SA 2200 E20BKN 50OVC 10TRW SC6CB4 TSTM NE MVG NE

SASKATOON

YXE SA 2100 20SCT 70SCT E100BKN 270BKN 15 3022G30 CF1CB4A
                                        SQUALL LINE N-S

YXE SP 2103 20SCT E70BKN 100BKN 1TRW+ 2435G44 CF2CB7ACC1

YXE SP 2118 E70BKN 100BKN 2TRW+ 3212 CB7ACC1

YXE SP 2126 70SCT E100BKN 270BKN 12T 3412 CB5ACC2CI1
                                          HVY SHWRS E

YXE SA 2200 70SCT E100BKN 270BKN 15 CB5ACC2CI1
                              LTNG N-SE SHWRS NE

NORTH BATTLEFORD

YQW SA 1900 80SCT E100BKN 300BKN 15 ACC3AC3CI1
                                      SHWRS W-S

YQW SP 1926 50SCT E80BKN 300BKN 15T CB3ACC4CI1
                              HVY SHWRS SW LTGCG W

YQW SP 1945 E50BKN 80BKN 300OVC 12TRW- CB6ACC2CI1
                         HVY SHWRS SW-W-NW LTGCG W

YQW SP 1952 E40BKN 80OVC 2TRW+F CB8ACC1 LTGCG

YQW RS 2000 E40BKN 80OVC 10TRW- CB7ACC3 LTGCG

YQW SP 2045 E40BKN 90OVC 10TRW- CB6ACC4 HVY SHWRS SW-E

Table C.3   SURFACE WEATHER OBSERVATIONS FOR JULY 11, 1979

EDMONTON MUNICIPAL AIRPORT

YXD RS 2200 5SCT E15BKN 40OVC 8RW CF4SC5SC1

YXD SP 2044 -X E5BKN 15OVC 1/4RW+F F5CB4SC1 VIS E-SW 1/8

YXD RS 2100 4SCT E8BKN 70BKN 12RW- CF1TCU8AC1 VIS E-S 5

YXD SP 2126 E4BKN 10OVC 1TRW+F CF6CB4 VIS LWRNG FRM W

YXD SP 2132 4SCT E22BKN 10TRW- CF4CB5 RW+ N-ESE LTGCG S

YXD SA 2200 7SCT E20OVC 10TRW- CF3CB7 RW+ E

NAMAO

YED SP 2027 3SCT E15BKN 100BKN 15RW- SF2TCU5AC2 CB S
                              HVY SHWRS E-SW

YED RS 2100 8SCT E18BKN 100BKN 15 SF2TCU6AC1 CB SE
                              HVY SHWRS SE-SW

YED SP 2137 10SCT E20BKN 15T CB5TCU4 VERY HVY SHWRS SE-S
                              LTNG S

YED RS 2200 E10BKN 20 BKN 100BKN 8RW+ CB6TCU2AC1
                              HVY SHWRS SE

YED SP 2210 E10BKN 20BKN 100BKN 10TRW- CB6TCU2AC1
                              SHWRS ALQDS

EDMONTON INTERNATIONAL AIRPORT

YEG SA 2100 E18BKN 35BKN 15+ CU6SC2 HVY SHWR N

YEG SA 2200 E18BKN 15+RW- TCU9 CB ASOCT N HVY SHWRS N

Table C.4   SURFACE WEATHER OBSERVATIONS FOR JULY 14, 1979

KINDERSLEY

```
WKY SA 2100 8SCT 30SCT E90BKN 15 SF1CB4AC1 SHWRS W-SW

WKY SP 2110 8SCT E30BKN 90BKN 15RW- SF1CB6AC1

WKY SP 2120 E30BKN 15 CB8 SHWR N-NW

WKY SP 2130 E20BKN 90OVC 1RWF CB9AC1

WKY SP 2140 E20OVC 15RW- CB10

WKY RS 2200 8SCT E20BKN 90OVC 15RW- SF1SC8AC1
```

Table C.5   SURFACE WEATHER OBSERVATIONS FOR AUGUST 21, 1979

LETHBRIDGE

```
YQL SA 2000 60SCT 120SCT E250 BKN 15 TCU2AC3CI2

YQL SA 2100 E60BKN 120BKN 250OVC 15T CB6AC2CI1 SHWRS ALQDS

YQL SP 2114 E60BKN 120BKN 250BKN 12TRW- CB6AC2CI

YQL SA 2200 E50BKN 120BKN 250BKN 12TRW- CB6AC2CI1

YQL SP 2244 50SCT E100BKN 250BKN 152 CB4AC3CI2 SHWRS ALQDS
```

Table C.6   SURFACE WEATHER OBSERVATIONS FOR JULY 10, 1982

CORONATION

YCT SP 2215 E50BKN 15+TRW- CB7 LTGCG VCNTY

YCT SP 2240 E50BKN 6TRWA CB8 FQT LTNG ALQDS

YCT SA 2300 E50BKN 4TRW+A CB8 FQT LTNG ALQDS

YCT SP 2301 E50BKN 15TRW-A CB8 FQT LTNG ALQDS

YCT SP 2310 E50BKN 15+T CB8 TSTM LTGCG HVY SHWRS E QUAD

Table C.7   SURFACE WEATHER OBSERVATIONS FOR JULY 14, 1982

GRANDE PRAIRIE

reporting TR or TR+ since 15:31Z

YQU SA 2000 -X E5BKN 20 OVC 3TRF R1SF7CB2 LTNG ALL TYPES

YQU SA 2100 -X E5OVC 3TRW+ F1SF9 LTNG ALL TYPES

YQU SA 2200 5-BKN E10OVC 6TRWF SF5CB5 LTGCG ALL QUADS

YQU SP 2232 5SCT E12BKN 70OVC 10RW- SF2SC5AC3
                            CB EMBDD HVY SHWRS ALQDS

YQU SA 2300 5-SCT E14BKN 8RW- SF2TCU8 HVY SHWRS ALQDS

EDSON

YET SA 2000 B3BKN 20OVC 10R- SF7NS3 CIG RGD F

YET SA 2100 E3BKN 20OVC 3R+F SF6NS4 CIF RGD

YET SA 2200 E3BKN 20OVC 3RF SF6SC4

YET SP 2224 3SCT E20OVC 5R- SF4SC6

YET SP 2240 3SCT E10BKN 20OVC 5RW- SF2TCU7SC1

YET RS 2300 3SCT E10BKN 3RW-F SF4TCU6

MOOSE JAW

YMJ SA 2100 28SCT E70BKN 120BKN 12RW- SC4AC4AS1 CB EMBDD

YMJ SP 2112 28SCT E70BKN 120BKN 12TRW- SC3AC5AC1 CB EMBDD

YMJ RS 2200 10SCT 20SCT E28BKN 70BKN 12TRW- CF1CB4SC1AS3
                            OCNL LTGICCG MAMA PRESRR

YMJ SA 2300 12SCT 25SCT E75BKN 15 CF1CB2TCU1AC3 CB SE+NW

Table C.8   SURFACE WEATHER OBSERVATIONS FOR JULY 16, 1982

REGINA

```
YQR SP 1920 20SCT E35OVC 12TRW- SF3SC7 CB EMBDD
                                      HVY SHWRS S

YQR SA 2000 24SCT E35OVC 10TRW- SF3CB7

YQR SP 2037 E24BKN 35OVC 8RW SF6CB4

YQR SA 2100 E25BKN 35BKN 80OVC 10RW- SC6CB2AC1
                                  HVY SHWRS N-SE

YQR SP 2124 20SCT 35SCT E49BKN 30OOVC 10 SF1SC3CB3CI2
                                    HVY SHWRS N-SE
```

Table C.9   SURFACE WEATHER OBSERVATIONS FOR JULY 18, 1982

COLD LAKE

YOD SA 1900 30SCT E70BKN 100BKN 280OVC 15TRW- CU1ACC8AC1CI1
                                              CB EMBDD

YOD SP 1919 20SCT E70BKN 100OVC 5RWF CU1ACC6AC4

YOD SP 1933 -X E70BKN 100OVC 4TRW-F R2ACC5AC3 CB EMBDD

YOD SP 2005 14SCT E60OVC 2TRW+F SC4SC6 CB EMBDD

YOD SP 2011 7SCT E60OVC 2TRW+F SF5SC5 CB EMBDD
                            OCNL LTGCG VSBY SE 1

YOD SP 2035 15SCT E80OVC 2RWF SF4ACC6

YOD SP 2044 7SCT E90OVC 3RWF SF1ACC9

YOD SA 2100 7SCT 20SCT E90OVC 5RW-F SF1SC1ACC8

YOD SP 2133 M6BKN 20BKN 900VC 12RW- SF6CU1AC3

YOD RS 2200 7SCT 20SCT E90OVC 12RW- SF4CU1AC5 ACC ASOCTD E

YOD SP 2233 7SCT 25SCT E100BKN 15 SF2CU1AC7

NORTH BATTLEFORD

YQW SA 2100 20SCT E40BKN 80BKN 250OVC CB2SC4AC2CI1
                              SHWRS SW-W-NW

YQW SP 2103 20SCT E40BKN 80BKN 250OVC 15T CB3SC3AC2CI1
                              SHWRS SW-W-NW

YQW SP 2132 E20BKN 250OVC 3TRW CB9CI1 LTGICCG

YQW SA 2200 E25BKN 100OVC 10TRW- CB9AC1 LTGIC OVHD LTGCG E

Table C.10   SURFACE WEATHER OBSERVATIONS FOR AUGUST 11, 1982

ROCKY MOUNTAIN HOUSE

YRM SA 2000 E50 BKN 90BKN 40 TCU8AC1 CB EMBDD TSTM W-NW

YRM SP 2017 E50BKN 90OVC 40TRW- CB2 AC2 TSTM OVHD
                                    VSBY LWR NW

YRM SP 2020 E50BKN 3/4 TRWA CB10 TSTM OVHD
                HAIL GRAPE TO WALNUT SIZE

YRM SP 2026 E50BKN 6TRW- CB10 TSTM MOVG E CLRNG W

YRM SP 2042 30SCT E50BKN 300OVC 40TRW-- CF2CB6CI1
                            TSTM E LTGIC E

B30400